DETERMINATION OF PARTICULATE EMISSIONS FROM CONFINED ANIMAL HOUSING

BY

JOSHUA WAYNE MCCLURE

DISSERTATION

Submitted in partial fulfillment of the requirements
for the degree of Doctor of Philosophy in Agricultural and Biological Engineering
in the Graduate College of the
University of Illinois at Urbana-Champaign, 2009

Urbana, Illinois

Doctoral Committee:

Professor Yuanhui Zhang, Chair
Extension Specialist Ted L. Funk
Associate Professor Xinlei Wang
Professor Richard S. Gates
Professor Gerald L. Riskowski, Texas A&M University

ABSTRACT

Determining particulate emission from mechanically ventilated confined animal feeding buildings is a challenging undertaking. This is due to the relatively large particle sizes involved, wide size range and difficulties in measurement of the ventilation rate of the building. This study seeks to address these issues by looking at the three critical measurements used in determining particulate emissions: total suspended particulates (TSP), particle size and ventilation rate. A new TSP sampling system was developed and tested in a controlled environment. This system appeared to perform as expected based on existing literature. It was fairly easy to use and its low cost suggests that further study is warranted. Measurement of particle size for agricultural particles is difficult since most of the instrumentation is designed for laboratory work or for particles smaller than those encountered in these settings. Several instruments were used to measure particle sizes. As expected many of the samplers designed for ambient sampling failed due to clogged nozzles or overloaded impactors. The final results focused on three instruments: the TSI APS, TSI Aerosizer DSP and the Coulter Multisizer. While the relative performance of each instrument was generally as expected, none appeared to have a distinct edge. The effective particle size range of the Coulter and the APS can limit their usefulness in many animal environments. Based on the experience during this study, it seems future research is needed for collecting particle samples in the field and measuring their size in the laboratory For ventilation rate measurement a small vane anemometer was tested on three common fan sizes. Results showed reasonable performance but the need for field calibration and the need to examine environmental impacts on the long-term usefulness of these anemometers. This study highlighted a number of problems with sampling particles above 10 μm. Agreement within the research community is needed for developing a functional definition of TSP so that an appropriate sampling method can be established for confined animal buildings.

In memory of my Grandpa.

ACKNOWLEDGEMENTS

I would like to thank all of those who have helped me with this research. In particular I would like to thank Sheryll Jerez for her help with data collection and interpretation. I would also like to thank the faculty and staff at the now dissolved Silsoe Research Institute in the United Kingdom for lending me their time and facilities, especially Theo Demmers. A special thanks to Dr. Zhang for sticking with me for so long.

TABLE OF CONTENTS

LIST OF SYMBOLS, ABBREVIATIONS AND NOMENCLATURE

SYMBOL	DEFINITION
APS	Aerodynamic Particle Sizer
DSP	Aerosizer DSP
FANS	Fan Assessment Numeration System
GCMD	Geometric Count Mean Diameter
GCSD	Geometric Count Standard Deviation
GMD	Geometric Mean Diameter
GSD	Geometric Standard Deviation
GMMD	Geometric Mass Mean Diameter
GMSD	Geometric Mass Standard Deviation
SAPRA	State Air Pollution Regulatory Agency
TSP	Total Suspended Particulates
USDA	United States Department of Agriculture
USEPA	Unites States Environmental Protection Agency

CHAPTER ONE: **INTRODUCTION**

Historically, agricultural air pollution emissions have not been heavily regulated. When they have, it was mostly from a nuisance perspective concerning odors and occasionally dust. As the size of the confined animal feeding buildings (CAFB) facilities has grown and urban populations have moved closer to these areas, the desire for increased regulatory involvement has grown.

This drive for greater regulatory involvement has been led by the U.S. Environmental Protection Agency (USEPA). In recent years they have begun a nationwide study of confined animal feeding operations (CAFO) emissions, including CAFB, through the voluntary Animal Feeding Operations Consent Agreement (US FR, 2005). This agreement allowed for CAFO to sign up for emission monitoring, while paying a penalty for any past non compliance. In exchange they would have immunity from future legal action concerning past emissions. In addition, these operations would help fund emission measurements to assess the extent of the emissions and determine how best to shape regulations directed at animal feeding operations. Similar consent agreements and studies have been conducted by individual producers (Burns et al., 2007a and 2007b).

Although the U.S. Clean Air Act and other environmental regulations have always applied to CAFB, the various regulatory agencies have not always taken an active interest in enforcing it. This is in part due to a lack of reliable data on emission rates. Without this data, it can be difficult to assess whether a facility is in compliance, or whether there is even a need to be concerned with the operation.

Before the Consent Agreement, the USEPA and the United States Department of Agriculture (USDA) commissioned a study by the National Science Foundation (National Research Council, 2002 and 2003) to determine the amount and quality of the existing data on agricultural air quality. The study found that there were substantial variations in the methods, quality and results of estimated aerial pollutants from confined animal buildings.

In addition to potential regulatory concerns there are general scientific and health concerns. Dust can act as a carrier for a number of gases and odor, resulting in longer range transport (Bottcher, 2001; Takai et al., 1998). It also acts as a nuisance to nearby neighbors. Inside the buildings it presents a health risk to both the animals and the workers. Additionally,

there is the risk of the dust particles acting as a carrier for biological agents. There have been a number of studies in Europe concerning worker health and biological activity associated with agricultural aerosols (Chang et al., 2001; Seedorf et al., 1998; Takai et al., 1998). With the increased concern in recent years on biosecurity, dust could prove to be an important carrier for animal diseases.

Measuring emissions from animal buildings can be difficult for a number of reasons. The biggest problem is probably the number of emission points, which can number as many as 100. Each point is nothing more than a wall mounted fan with no ductwork. This makes traditional particulate sampling difficult. In addition, the environment can be hostile to many electronic instruments due to the high moisture, NH_3 and H_2S concentrations. All of this makes many existing methods unfeasible.

When determining emissions of a pollutant from a mechanically ventilated facility, the most common method used is to measure the concentration and multiply it by the exhaust flow rate. This gives the total emission rate. In the case of animal buildings there are at least two sets of measurements: the concentration of the pollutant and the ventilation rate of the building. When dealing with particles, there are also concerns of the size of the particles. This can greatly influence the health effects and behavior of the particles. This study seeks to improve the methodology associated with the measurement of particle emissions from mechanically ventilated CAFB.

1.1 Existing Methodology

One of the reasons that there are few consistent regulations involving agriculture is that there is relatively little data concerning these emissions and what is available is very inconsistent. Researchers involved in agricultural air quality have utilized a wide variety of samplers, often based on factors other than whether the sampler is the best or most reliable method. The mass samplers used are frequently either ambient samplers or industrial hygiene samplers.

In the U.S. many studies have utilized ambient samplers including High-Vol TSP, various models of PM_{10} and $PM_{2.5}$, TEOMs and cascade impactors (Jacobson et al., 2003; Lacey et al., 2003). In Europe there tends to be a greater use of respirable and inhalable samplers (Hinz and Linke, 1998; Phillips et al., 1998; Takai et al., 1998; Wathes et al., 1997; Wathes et al.,

1998) although TEOMs and impactors are also used. When particle size is measured, it seems that laser particle counters are used most frequently, although time-of-flight instruments are used occasionally (Demmers et al., 2000). Occasionally instruments such as the Coulter Multisizer (Beckman Coulter, Inc., Fullerton, CA) and more advanced instruments are utilized depending on the availability at a particular institution (Lacy et al., 2003; Parnell et al., 1986; Schneider et al., 2001; Sweeten et al., 1988).

Many of these instruments are not intended for use on larger particles or in such hostile environments. While some of the practical limitation can be overcome, there is often not adequate attention paid to the instrument's proper use and limitations, including proper calibration, sampling efficiency, and data interpretation. It is common to simply take whatever sampling device is on hand or that can be borrowed and collect samples with little regard for whether the device measures the parameter of interest, whether it has been properly calibrated, or whether it has been properly operated.

The primary reason for these problems is that the interest of the researcher does not lie in the sampling method but in the goal of the project, such as investigating control methods. In addition there has traditionally been little training or education concerning aerosol behavior or sampling. Couple this with the never ending task of finding an ideal sampler, even for lifelong experts in the field, and it is not surprising that many agricultural air quality researchers have not focused on this topic.

Another factor that cannot be overlooked is the relative lack of standardization in the U.S. when it comes to particulate sampling in general and in agriculture in particular. In Europe there have been a number of attempts to standardize many of the methods associated with air sampling, including agriculture. This has led to an increased standardization of equipment and methods amongst the major European researchers (Hinz and Linke, 1998; Phillips et al., 1998; Takai et al., 1998; Wathes et al., 1998). Previously this trend has begun to take place in the U.S. on a more voluntary basis with the undertaking of a couple of multi-institution studies of emissions from CAFBs, which are funded by the USDA with technical oversight from the USEPA (Gates, et al., 2001; Jacobson et al., 2003; Heber et al., 2006a and 2006b). Some of the particle sampling equipment for the project was designed by this author and is discussed in Chapter 3. While this project was a major step forward for standardization, it still utilized some,

as yet, unproven methodology. The USPEA Compliance Agreement discussed earlier seeks to further this process by using consistent methodology throughout the nationwide study.

Measurement of ventilation rate is problematic due to the large number of fans in a given building and the nature of the fans. Most agricultural fans have been tested at the University of Illinois Bioenvironmental and Structural Systems (BESS) Laboratory and the results are published showing the relationship between voltage, static pressure and ventilation rate (AMCA 1999). This data can be used to estimate emissions but can be problematic as fans age, especially if they are not properly maintained. The Fan Assessment Numeration System (FANS) has been developed and shown to give accurate results for spot checks of ventilation rate and in-situ calibration (Casey et al., 2007 and 2008; Gates et al., 2002 and 2004). This calibration curve can be used to accurately determine flow rate from single speed fans with continuous measurement of fan status and building static pressure. It is not as useful for variable speed fans since there are many such calibration curves and reliable monitoring of all parameters becomes more challenging.

1.2 Justification

Agricultural air quality studies have often times suffered from a poor understanding of sampling methods and their proper use. As discussed above, this is especially true of dust sampling. The goal of this study is to improve the knowledge and methodology of particulate emissions from mechanically ventilated confined animal feeding operations. To accomplish this it is necessary to sample TSP because the size of agricultural particles are relatively large compared to those that are intended to be sampled by ambient or personal samplers. In addition to total concentration, it is necessary to know the particle size distribution, which determines health effects and transport distance, as well as the best abatement methods. Particular emphasis has been placed on methods that cover most if not all of the particle size range for animal buildings, particularly the APS, Aerosizer DSP and the Coulter Multisizer.

To calculate emissions it is necessary to measure ventilation rate in addition to concentration. Because of the large numbers of fans and their nature, whole building ventilation rate can be difficult to measure. This study will examine two methods to accomplish this.

1.3 Objectives

The overall objective of this study is to improve the knowledge and methodology of particulate emissions from confined animal feeding operations. To accomplish this, the sampling literature was reviewed to determine what the sampling needs of the industry are as well as what methods would be best used for sampling in mechanically ventilated CAFB. Based on this analysis the following individual objectives will need to be addressed.

1. TSP - Design and test a new TSP sampler to evaluate its performance in animal environments and its consistency with existing knowledge and theory.
2. Particle Size - Compare the performance of various particle sizing instruments and size selective samplers to assess their relative performance, as well as their practical usefulness, in several different CAFB.
3. Ventilation Rate - Test a single vane anemometer in the laboratory to determine its potential for continuous measurement of fan ventilation rate.
4. Future Research Needs - Use the findings from these studies to assess the direction for future research in particulate emissions measurements from CAFB.

CHAPTER TWO: **LITERATURE REVIEW**

2.1 Introduction

When reviewing the air quality literature of confined animal feeding buildings (CAFBs), it becomes evident that there are nearly as many sampling methods employed as there are researchers using them. This results in a wide variety of results that can be difficult to compare. The reasons for this are many. One main reason is that historically there has been little enforcement of regulations, and therefore, no need to standardize methodology. In addition, most agricultural researchers have had little interest in the sampling procedures themselves and have, therefore, spent little time considering them.

To help remedy this problem this study will examine the existing methodology and lay out a way forward. Before delving into the existing methodology, a brief discussion of aerosol science and sampling principles is necessary to establish a common framework for examining the various methods. This framework will also be referenced throughout this study.

2.2 Aerosol Science

When dealing with dust, it is important to understand the behavior of aerosols and the important definitions. An aerosol is a volume of air and all of the particles within it. The individual particles do not make up an aerosol alone and are often discussed separately. The following discussion will provide only a very basic discussion of the theory and formulas used in aerosol science. Hinds (1999) should be consulted for a more thorough coverage of the topic. Most of the equations used here are taken from Hinds (1999) and his original equation number will be provided along with this author's own.

Particles come in a wide variety of shapes, sizes and materials. A question that rapidly arises when studying particles and aerosols is how to define their size. When studying aerosol behavior, what really want to know is whether the particles are likely to be collected in a control device or enter the respiratory system. The terminal settling velocity of a particle is frequently used as a proxy for this, since it indicates how the particle moves through the air. The following equation can be used to calculate the terminal settling velocity (Hinds, 1999):

$$V_{TS} = \frac{\rho_p d_e^2 g C_C}{18\eta\chi} \tag{2-1}$$

Where ρ_p is the particle density in kg/m^3. The equivalent diameter (d_e) is found using the volume of the particle and is in meters. Acceleration of gravity (g) is assumed to be a constant 9.81 m/s^2. The viscosity of air (η) at the given temperature and pressure with units in Pa·s and can be found in physical tables. C_C is the Cunningham correction factor, which adjusts the settling velocity for smaller particles (<5 to 10 μm) to account for the mean free path between air molecules. This factor becomes important as the size of the particle begins approaching the distance between molecules. The following formula can be used to determine this factor for a given particle size (d) in μm and absolute pressure (P) in kPa (Hinds, 1999).

$$C_C 1 + \frac{1}{Pd}\left[15.60 + 7.00\exp\left(-0.059Pd\right)\right] \tag{2-2}$$

χ is the dynamic shape factor, which is generally found experimentally. Table 2.1, adapted from Hinds (1999), shows examples of dynamic shape factors. As expected, the shape factor varies greatly, indicating that the terminal settling velocity of particles with varying shapes will also vary greatly. The importance of this will show up later when looking at systems that measure only particle volume.

Table 2.1. Dynamic shape factors (χ) from Hinds (1999).

	Dynamic Shape Factors, χ			
		Axial Ratio		
Shape		2	5	10
Sphere	1.00			
Cubes	1.08			
Cylinder				
Vertical Axis		1.01	1.06	1.20
Horizontal Axis		1.14	1.34	1.58
Averaged		1.09	1.23	1.43
Straight Chain		1.10	1.35	1.68
Compact Cluster				
Three Spheres	1.15			
Four Spheres	1.17			
Bituminous Coal Dust	1.05-1.11			
Quartz Dust	1.36			
Sand	1.57			
Talc	1.88			

These equations show that the particle behavior in air will vary greatly depending on its volume, density and shape. To simplify comparison and analysis of particles, we use the

aerodynamic diameter, which is defined as the diameter of a unit density sphere that falls at the same rate as the particle of interest. By equating the terminal settling velocity of an ideal particle (ρ_0 = 1.0 g/ml and χ = 1.0) to that of the actual particle in question we can use the following formula to determine the aerodynamic diameter (d_a).

$$d_a = d_e\left(\frac{\rho_p}{\rho_0\chi}\right)^{1/2}\left(\frac{C_C(d_e)}{C_C(d_a)}\right)^{1/2} = d_e\left(\frac{SG}{\chi}\right)^{1/2}\left(\frac{C_C(d_e)}{C_C(d_a)}\right)^{1/2} \quad (2\text{-}3)$$

The Cunningham correction factor is negligible above 5-10 µm, which simplifies the analysis for larger particles.

2.2.1 Particle Size Distributions

When dealing with aerosols, we are rarely interested in a single particle or even a single size of particle. In agriculture we often see high concentrations of particles (thousands/cm^3) with sizes ranging from less than 1 µm to above 100 µm. Figure 2.1 shows a hypothetical dataset in the form of a histogram. In this case it is the number of particles in each size bin. This is a common way of receiving data from particle counters. The first thing to note is that the bin sizes vary. This means that you cannot directly compare one bin to another because they sample different ranges of particles.

To rectify this problem the number of particles can be divided by the width of the bin as seen in Figure 2.2. This basically assumes that the particles are equally spaced throughout the size range. It then spreads them out equally, thus reducing the bias associated within varying bin widths. The result is a more uniform distribution.

While this representation is smoother than the first, it is still dependent on the number of particles. This makes it difficult to compare different sized samples or results from different instruments. To create a common form of comparison the number of particles can be divided by the total to get the fraction of particles within that bin. The results can be seen in Figure 2.3. In this figure the histogram representation has also been dropped for a line connecting the points. This form of particle size data is known as a frequency distribution, or a probability density function. By characterizing the data in this manner it may be possible to mathematically interpret

it. Comparison to other data is also made easier because bias from samples sizes and bin sizes is eliminated.

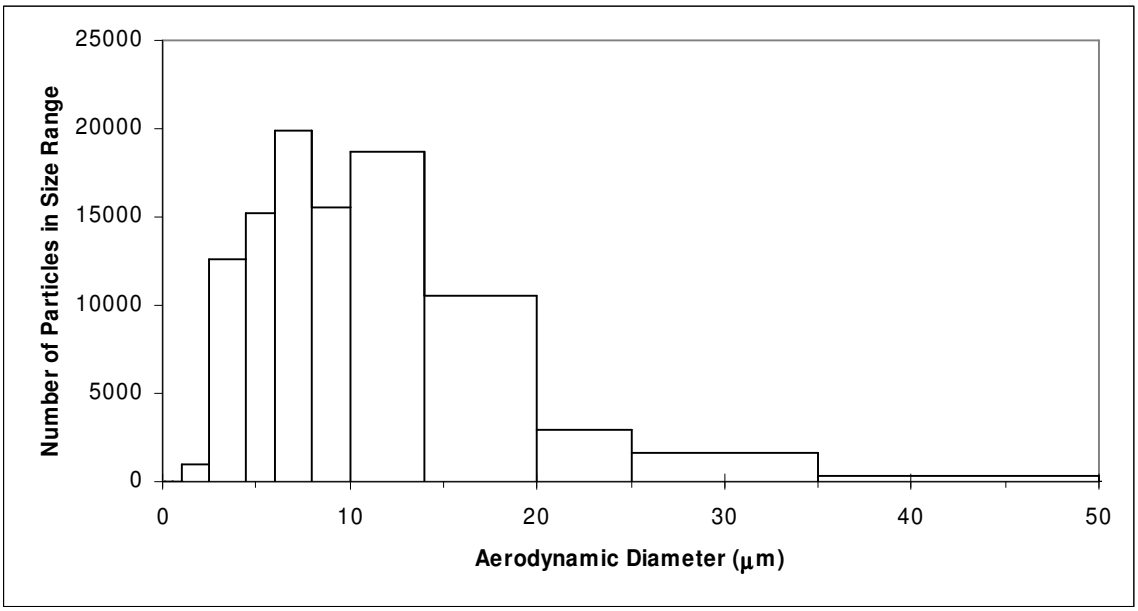

Figure 2.1 Hypothetical particle size histogram showing number of particles within size range.

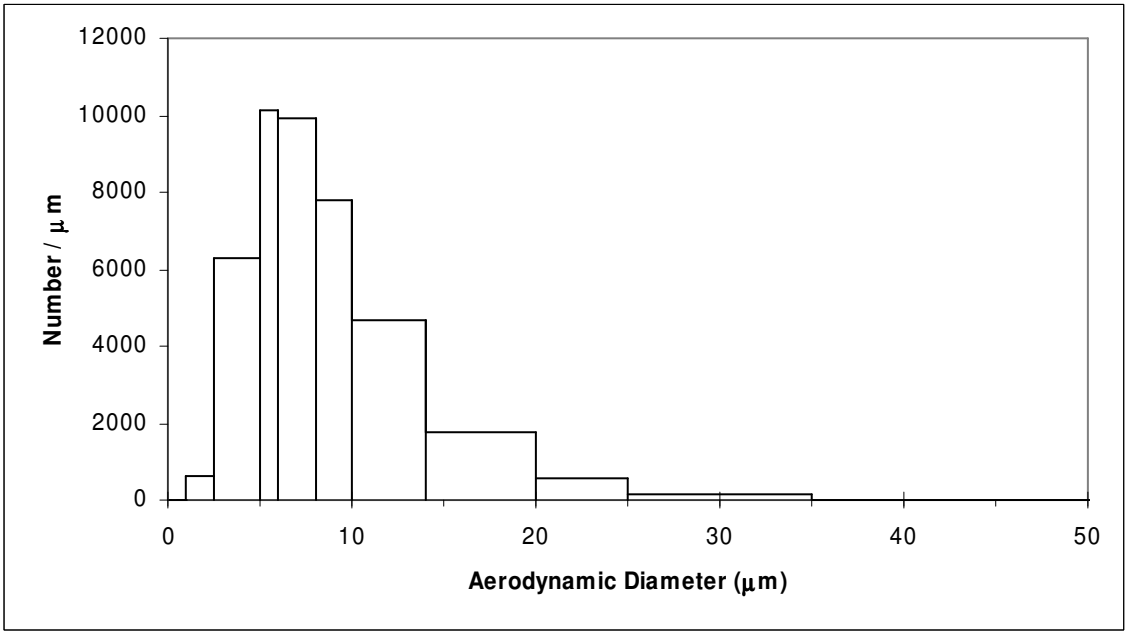

Figure 2.2 Hypothetical particle size histogram showing number of particles within size range divided by the width of the size bin.

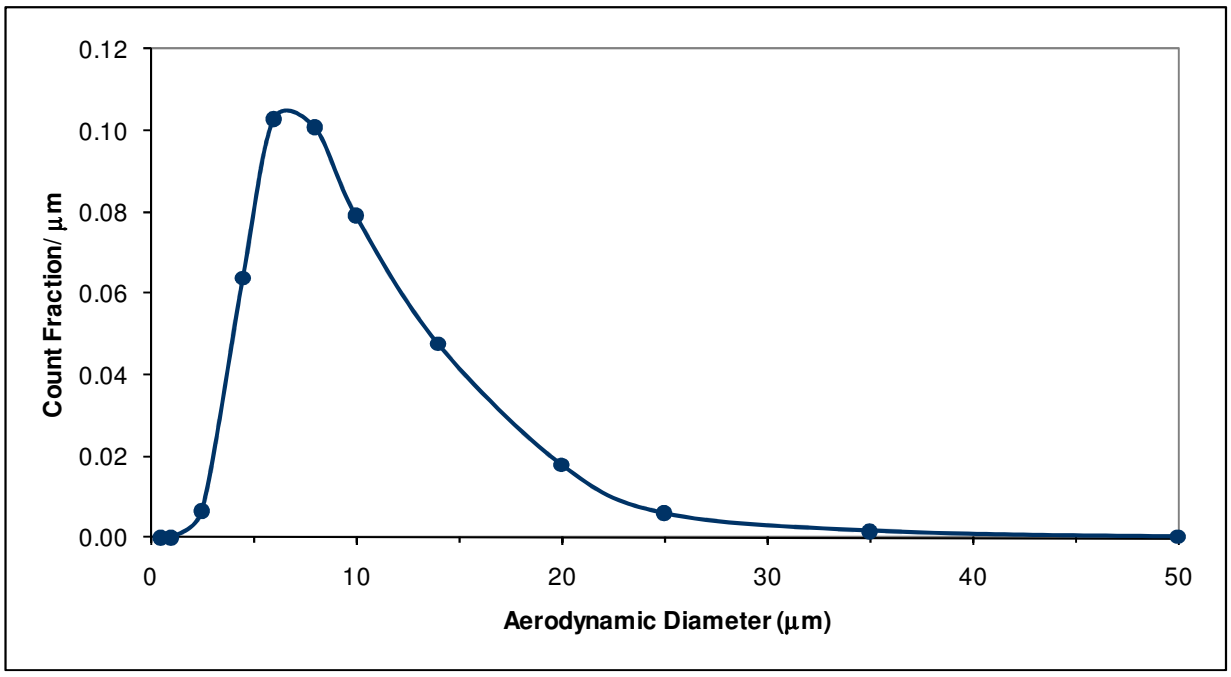

Figure 2.3 Count frequency distribution curve for the histogram data presented in Figure 2.2.

2.2.1.1 Log-Normal Count Distribution

The shape of the distribution shown in Figure 2.3 is typical of many aerosols. It is a long tail to the right with a short tail to the left. This type of distribution is known as the Log-Normal distribution (also referred to as the lognormal or log normal distribution). The reason becomes evident when the same distribution is plotted with the particle size on a log axis as shown in Figure 2.4. By taking the log of the particle diameter, the frequency distribution is transformed into a normal distribution. Although a natural logarithm or a base 10 logarithm can be used, it is typical to use the natural logarithm. This will be the case throughout this study.

The log-normal distribution can be described with two variables, the geometric mean diameter (GMD) and the geometric standard deviation (GSD). These are analogous to the mean and standard deviation of the normal distribution. For the number distribution these parameters can be described using the following equations.

$$\ln CGMD = \frac{\sum n_i \ln D_i}{N} \tag{2-4}$$

$$\ln CGSD = \left(\frac{\sum n_i \left(\ln D_i - \ln CGMD \right)^2}{N-1} \right)^{1/2} \tag{2-5}$$

Where n is the number of particles in each size range, N is the total number of particles and D is particle diameter. For the example distribution shown in Figure 2.4, the CGMD is calculated to be 8.07 µm and the CGSD is 1.75.

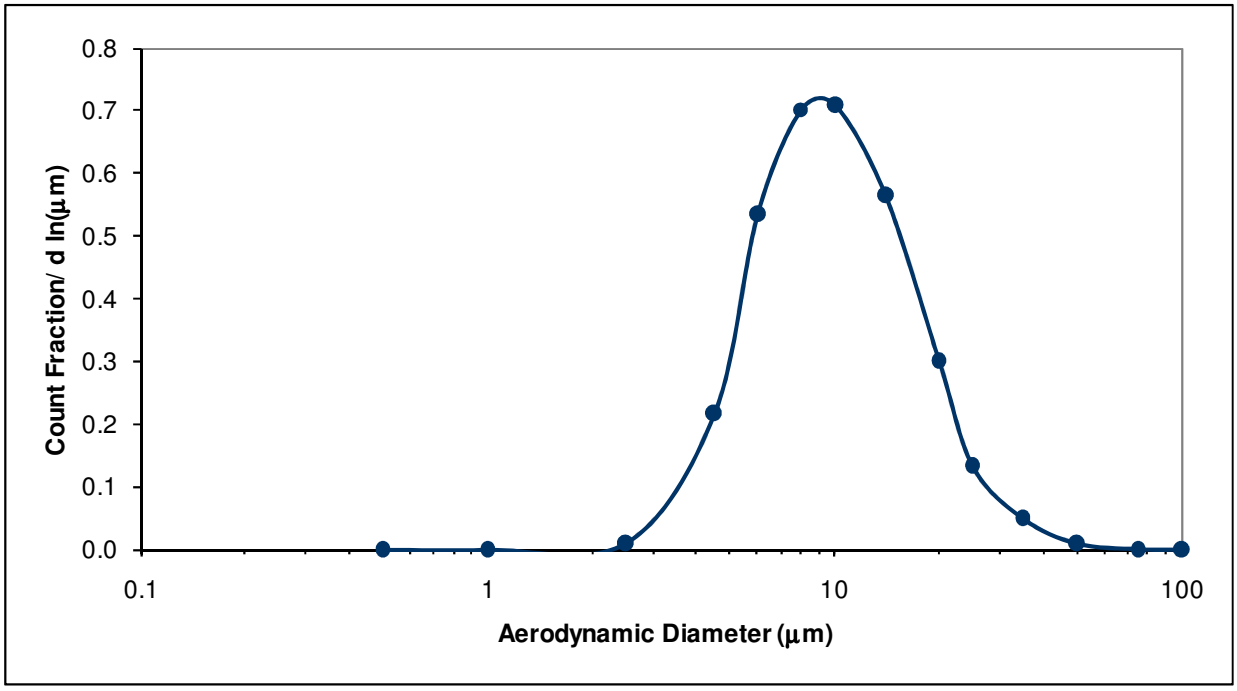

Figure 2.4 Count frequency distribution plotted on a log-normal graph.

It should be noted, that the GMD is not the same as the mode. The relationship between the mean, median and mode for the log-normal distribution is Mean>Median=GMD>Mode. The GMD being equal to the median is an important feature. This relationship is evident when the data is viewed as a cumulative distribution as shown in Figure 2.5, where the distribution clearly crosses 0.5 (the median value) at about 8 µm. The importance of this relationship will become more evident when the particle mass distribution is examined below.

Thus far the discussion has centered on the count size distribution. Typically this is of little interest for emission studies. Interest is usually focused on the mass distribution, which gives a more tangible measure of the amount of emissions. If a distribution is log-normal then the mass distribution can be easily obtained by multiplying the number of particles in each bin by the average volume of a particle in that bin. Once the values have been normalized by converting

to mass fraction per d ln(D_p), the result is an identical particle size distribution shifted to the right as shown in Figure 2.6. In this case the mass distribution is not a perfect match of the count distribution due to random variations in the raw data and the number of bins. As will be evident in the results of Chapters 3 and 4, it is rare to measure a perfectly log-normal distribution.

To determine a representative diameter (D_{avg}) for each bin, for plotting and calculating volumes, the following formula is used for log-normal distributions:

$$D_{avg} = \sqrt{D_U \times D_L} \tag{2-6}$$

Where D_U and D_L are the upper and lower particle sizes for the bin.

While there are methods for transforming count size distributions to mass size distributions using only the CGMD and CGSD (Hinds, 1999), these methods will not be used in this study due to the differences between the actual and ideal distributions. The following section will detail the methods used for determining the mass distribution properties.

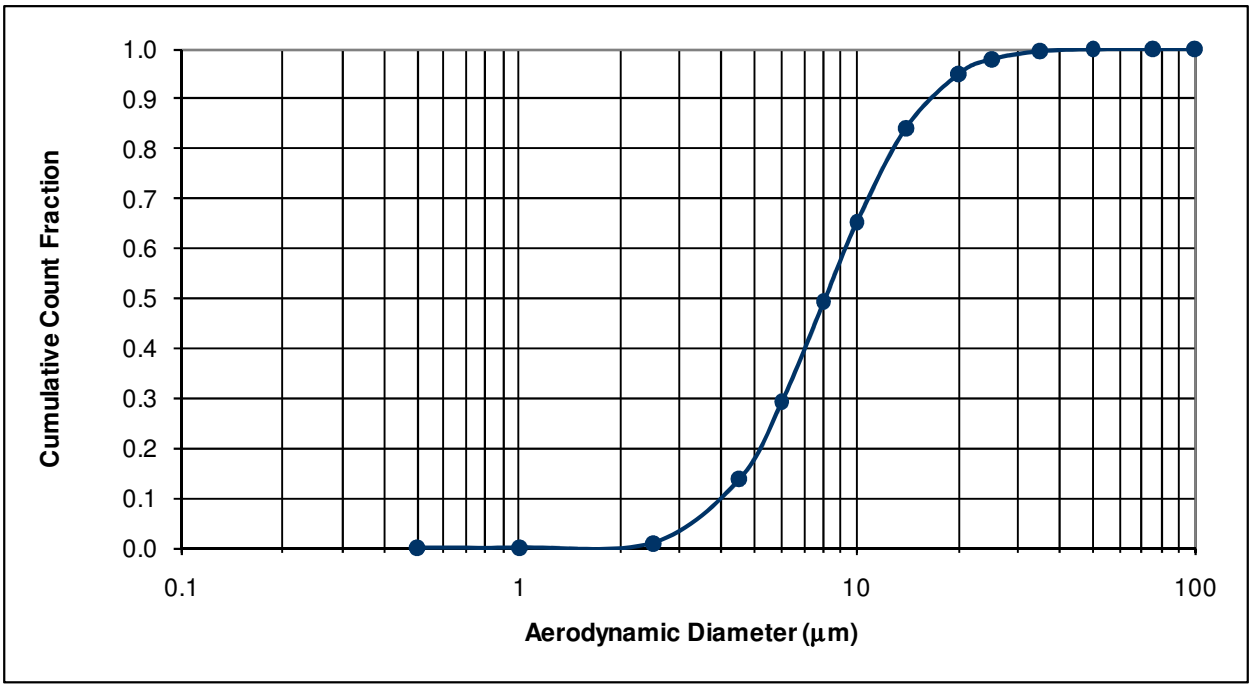

Figure 2.5 Cumulative count distribution of synthetic particle size data.

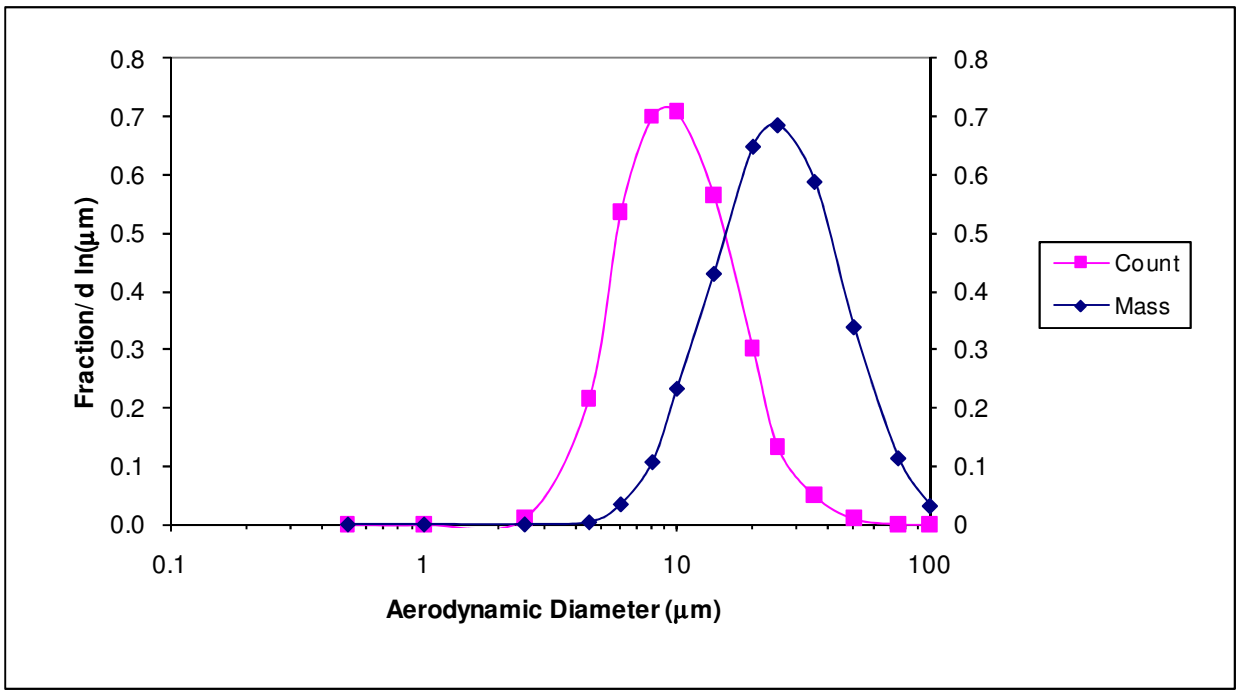

Figure 2.6 Count and mass particle size distributions based on the same synthetic particle size data.

2.2.1.2 Log-Normal Mass Size Distribution

Under ideal circumstances the count distribution statistics could be used to easily determine the mass distribution statistics. In real world scenarios the actual mass distributions are rarely perfectly log-normal. This can be because of inadequate sample size, poor bin spacing, or that the data is not actually log-normal. The goal of this study is not to determine the best particle size distribution for the aerosols sampled, but rather to compare the performance of the instruments used. Therefore this section will discuss the methods and statistics used to analyze the particle size distribution obtained from the various instruments.

The particle size instruments used during this study provide either count or volume (mass) distributions. When a count distribution is received it is converted to a mass distribution by using the following formula for each size bin.

$$m = n \times D_{avtg}^{3} \tag{2-7}$$

This formula deliberately omits the density and other aspects of determining the actual mass of particles. The reason for this is that they only scale the distribution vertically and will be factored out later when the distribution is normalized.

Once the particle mass has been calculated for each bin it needs to be converted to a frequency distribution as was done with the count distribution. This is done by converting the particle mass in each bin to a fraction of the total mass (thus eliminating density, etc.) and then dividing by the width of the bin (d ln D_p). Doing this standardizes the distribution so that data from different sources can be compared. Figure 2.7 shows the result of this process for the artificial size distribution previously discussed.

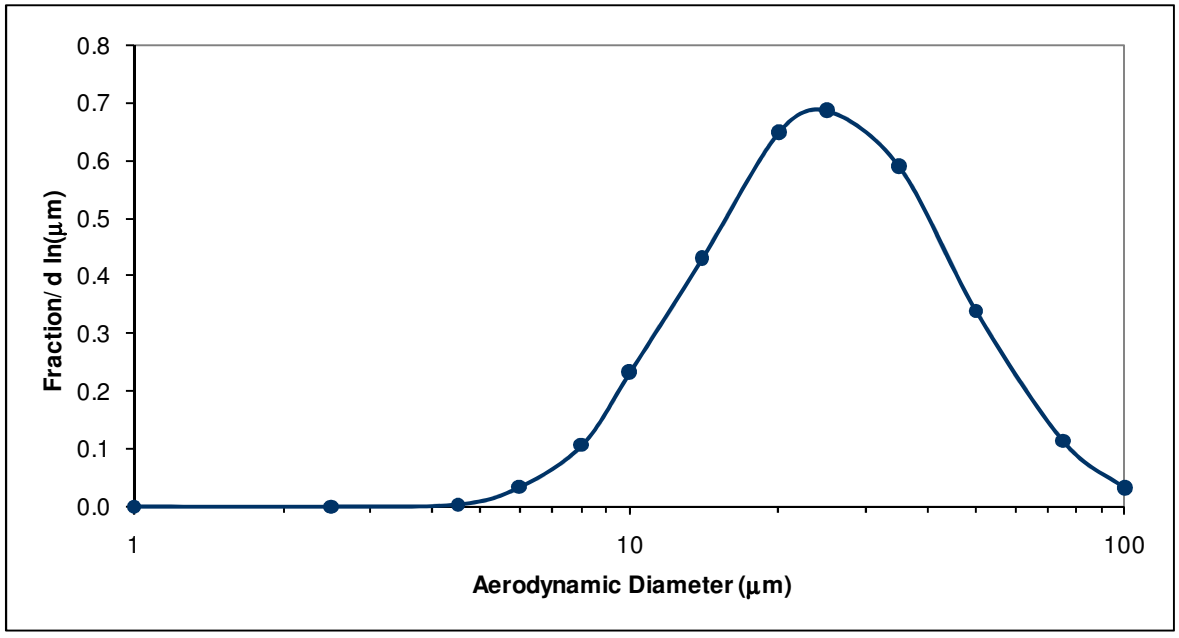

Figure 2.7 Normalized mass size distribution.

While normalizing the data is useful for displaying the frequency distribution, it can only give qualitative answers about the distribution, to get quantitative results, the cumulative distribution must be analyzed. The cumulative distribution shows the mass fraction (or percent) of particles below each size. When generating the upper limit of each bin is used to determine the total mass fraction below that point. The resulting cumulative mass distribution for the artificial data is shown in Figure 2.8.

Like the log-normal count distribution, the mass geometric mean diameter (MGMD) is the median, or 50% point in the cumulative distribution. To determine the mass geometric standard deviation (MGSD), Formula 2-8 can be used.

$$MGSD = \left(\frac{D_{84}}{D_{16}} \right)^{1/2} = \frac{D_{84}}{D_{50}} = \frac{D_{50}}{D_{16}} \tag{2-8}$$

This equality requires an ideal log-normal distribution. In reality, the three different calculations will vary depending on how close to log-normal the distribution is. During most analysis in this study, all three values will be calculated as well as an average of the three.

While the cumulative plot is useful, it is difficult to tell just how close the distribution is to log-normal. To aid in this analysis, the data can be plotted on a log-normal probability graph as shown in Figure 2.9. A perfectly log-normal distribution would be a straight line, crossing the 50% point at the GMD. In this case there are obvious points at the ends that deviate from a straight line fit. This is typical for the tails of a distribution where there may not be enough particles to create a smooth distribution or where there may be outliers. Hinds (1999), recommends removing or ignoring this data when determining fit. Generally, the tail will be removed when it becomes less than 0.01% of the entire distribution. This will help ensure that minimal amounts of fringe data do not dominate the curve fitting.

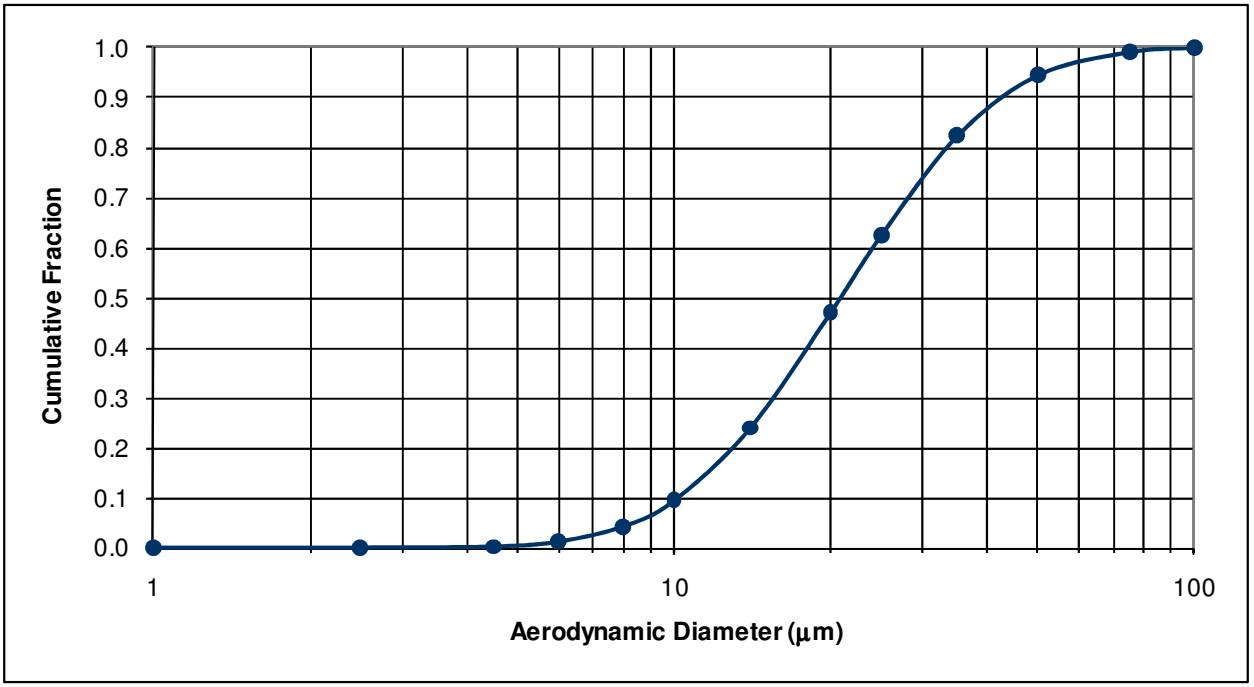

Figure 2.8 Cumulative mass particle size distribution of artificial data.

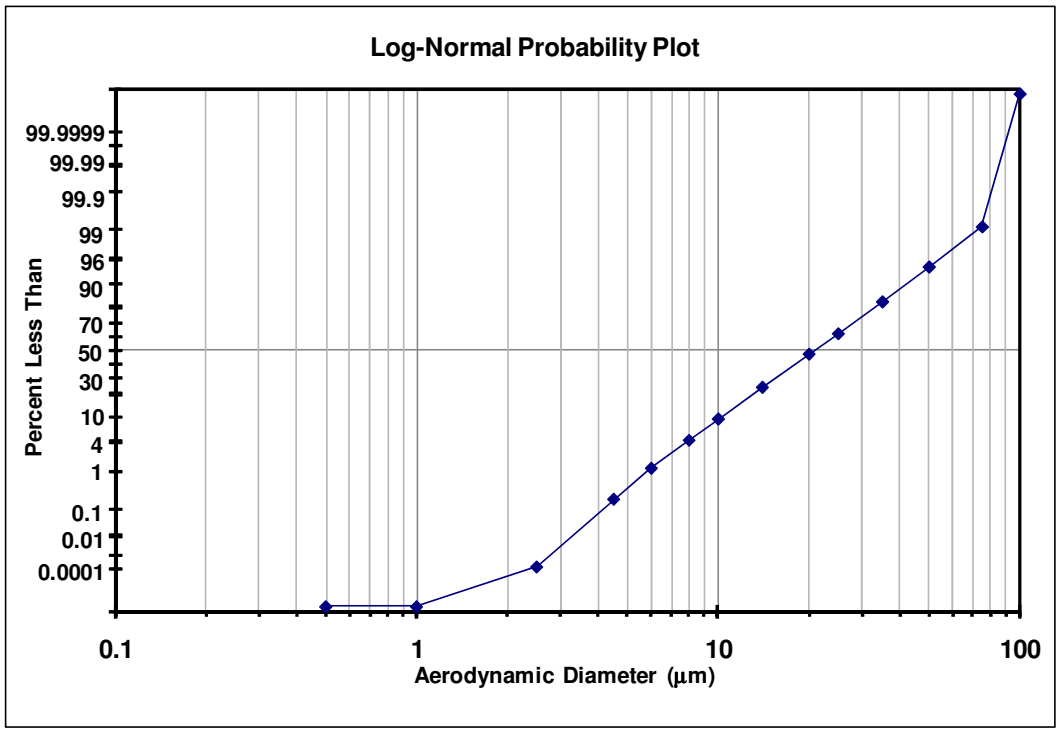

Figure 2.9 Log-normal probability plot of mass distribution.

The effects of removing these points can be seen in Figure 2.10. It is evident that this data is lognormal with a very high R^2 value of 0.9998. Using the fitted line you can determine the MGMD by seeing where the line crosses 50%. The D_{84} and D_{16} can be read from the graph as well for calculating the MGSD using Eq. 2.8. The specific methods for determining the probability plots are discussed in the next section.

2.2.1.3 Log-Normal Curve Fitting Techniques

The log-normal probability plots shown in Figure 2.9 and Figure 2.10 were actually generated using the standard normal cumulative density function in Excel. Each probability on the y-axis has a corresponding point on the cumulative density function. Using Excel's statistical functions, a probit is generated for each probability. Every one probit is equivalent to one standard deviation from the standard mean of zero.

Table 2.2 shows probit values for the standard normal distribution. There are three important probit values when calculating statistics for the log-normal distribution: -1, 0 and 1. These correspond roughly to the 16%, 50% and 84% points on the distribution. With these three points the GMD and GSD can be calculated using the raw data or the fitted line. The log-normal

probability plots can also use the probits along the y-axis to achieve the same straight line. The probabilities are shown only to make the plot more easily understood.

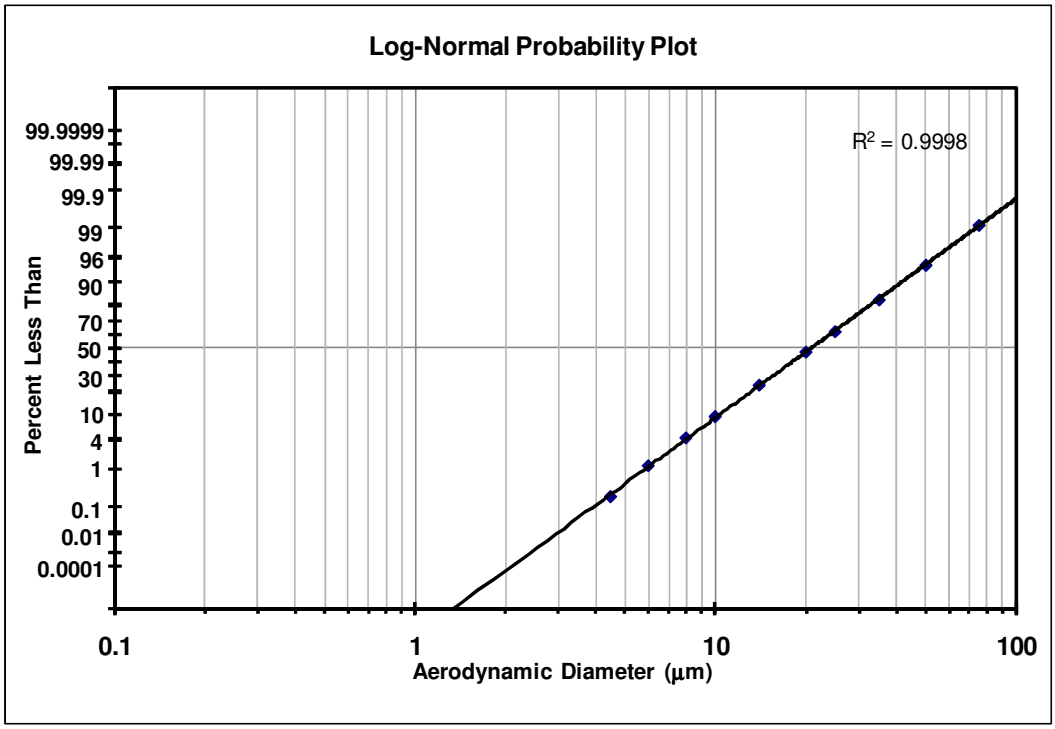

Figure 2.10 Log-normal probability plot with tails removed and line fitted.

Table 2.2 Probit values for the cumulative standard normal distribution.

Cumulative Distribution		Probit
Percent	Fraction	(# of σ)
0.00	0.0000	-4.900*
0.01	0.0001	-3.719
0.10	0.0010	-3.090
1.00	0.0100	-2.326
5.00	0.0500	-1.645
15.87	0.1587	-1.000
25.00	0.2500	-0.674
50.00	0.5000	0.000
75.00	0.7500	0.674
84.13	0.8413	1.000
95.00	0.9500	1.645
99.00	0.9900	2.326
99.90	0.9990	3.090
99.99	0.9999	3.719
100.00	1.0000	4.900*

* Values is assumed because the normal distribution goes to infinity in either direction.

When particle size distributions are discussed in the following chapters this curve fitting technique will be used to determine a best log-normal fit for the data. The log-normal parameters (GMD and GSD) calculated from this data will be compared with those determined using the raw data as discussed Section 2.2.1.2. The curve fitting will also be used to qualitatively describe the goodness of fit. As will be evident later, specific statistics will not be needed for this process.

2.2.2 Sampling Efficiency

The inertia of particles is often employed to separate particles by aerodynamic diameter. Instruments utilizing this technique will be discussed later. This same inertia can cause major problems when trying to sample larger particles. Sampling efficiency is defined as the concentration of particles collected compared to the concentration of particles in the aerosol of interest. This section will focus on the models used to predict sampling efficiency. These models are discussed in much greater detail by Baron and Willeke (2001) in their book "Aerosol Measurement." Their formula numbers will be provided along with my own to make determining the source easier.

There are a number of places where particles losses, and sometimes gains, can occur. The first place where inefficiency occurs is at the entrance of the sampling nozzle. The ideal case here is isokinetic sampling, as shown in Figure 2.11. Here the velocity inside the sampling nozzle matches the air velocity, in both magnitude and direction. As a result the concentration of particles entering the nozzle is the same as the free airstream for all sizes.

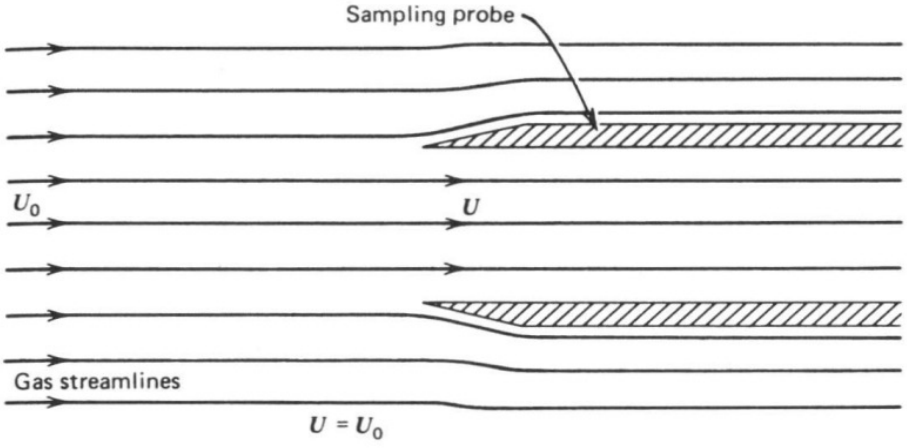

Figure 2.11 Isokinetic sampling condition (Hinds, 1999).

When the flows and/or angles are not the same then the condition is known as anisokinetic sampling. The three basic anisokinetic sampling conditions are shown in Figure 2.12. When the nozzle is misaligned, the momentum of the larger particles can cause them to overshoot the sampler, thus reducing the concentration of these particles in the sampler. Superisokinetic sampling occurs when the velocity in the sampler is higher than outside of the sampler. In this case larger particles cannot make the turn into the sampler, thus reducing their concentration within the sampler. The last scenario is subisokinetic sampling, where the velocity within the sampling nozzle is less than the surrounding air. In this case, the momentum of the larger particles carries them into the sampling nozzle, which increases their concentration in the sampler.

These conditions affect the aspiration efficiency (η_{asp}) of a sampler, which is the efficiency that a certain size of particles will penetrate into the sampling nozzle. Once inside, there are additional transmission losses as the particles move through the sampling system before being filtered or counted. Although a particle may enter the nozzle, its inertia can cause it to impact the inside wall, thus reducing its inertial deposition transport efficiency ($\eta_{trans,\ inert}$). As the particles move along the sampling system, they experience gravitational settling, which will lower the gravitational settling transmission efficiency ($\eta_{trans,\ inert}$).

The following two sections cover the models used to estimate sampling efficiency in moving air. The first covers isoaxial sampling where the nozzle is aligned with the flow, while the second covers anisoaxial samplers. Later discussion will involve sampling in low flow or calm air conditions, which deserve special treatment.

2.2.2.1 Isoaxial Sampling

For the isoaxial scenario, one of the most frequently used models for estimating aspiration efficiency is presented in the following formulas (Baron and Willeke, 2001). This relationship was established by Belyaev and Levin (1972, 1974), and has been confirmed by a number of authors as summarized by Baron and Willeke (2001).

$$\eta_{asp} = 1 + \left(\frac{U_0}{U} - 1\right)\left(1 - \frac{1}{1 + k \cdot Stk}\right) \tag{2-9}$$

$$Stk = \frac{\tau U_0}{d} \tag{2-10}$$

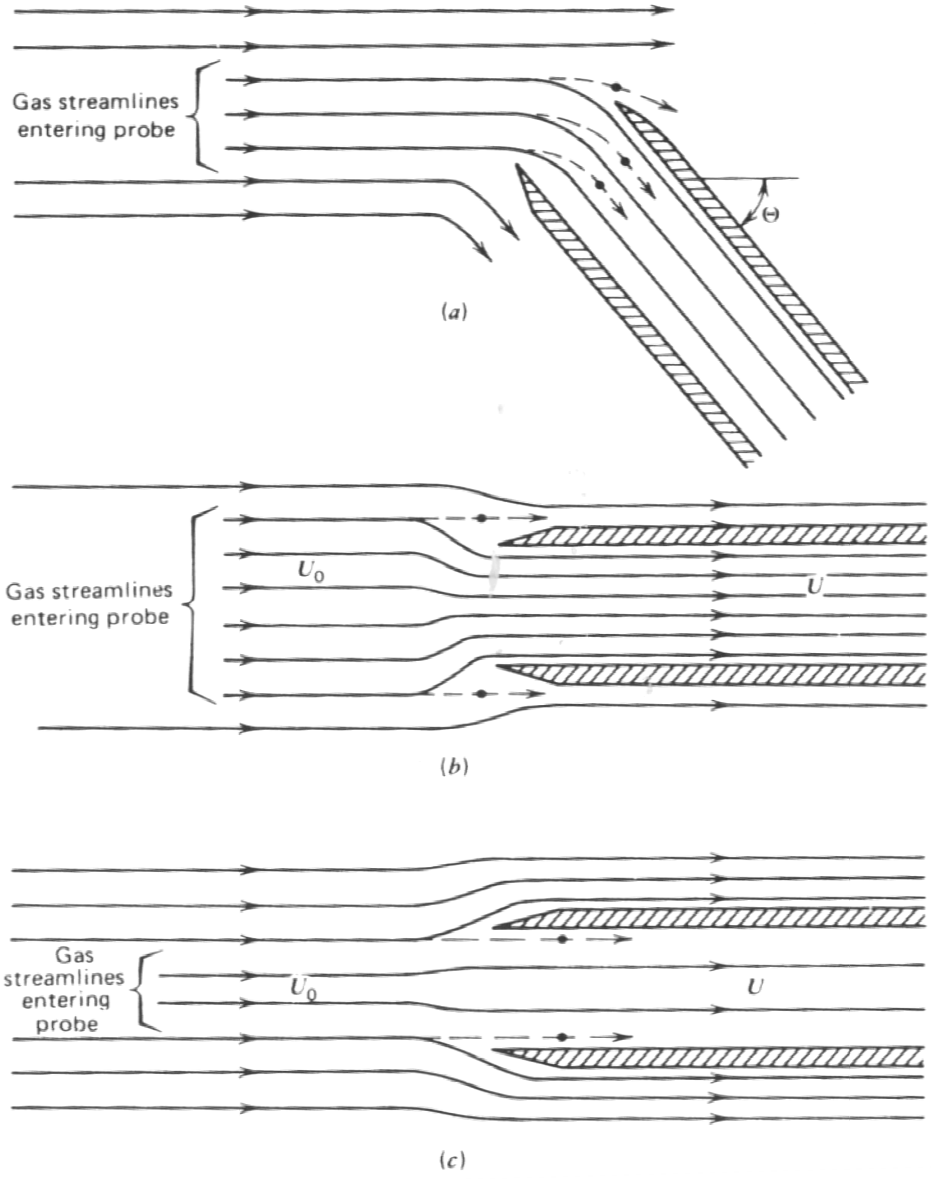

Figure 2.12 Anisokinetic sampling conditions: (a) Anisoaxial (misalignment); (b) Superisokinetic, U>U0; (c) Subisokinetic, U<U0. (Hinds, 1999).

$$k = 2 + 0.617\left(\frac{U_0}{U}\right)^{-1} \tag{2-11}$$

Where *d* is the nozzle diameter. The relaxation time (τ) is an indication of how quickly a particle can respond to a change in flow direction or speed, and can be found using Eq. 2-12 (Baron and Willeke, 2001).

$$\tau = \frac{\rho_p D_p^2}{18\eta} \tag{2-12}$$

The effects of inlet gravitational effects are calculated using the following formulas (Baron and Willeke, 2001), which are based on work by Okazaki (1987a, b).

$$\eta_{trans,grav} = \exp\left(-4.7K^{0.75}\right) \tag{2-13}$$

$$K = Z^{1/2} Stk^{1/2} \,\mathrm{Re}^{-1/4} \tag{2-14}$$

$$Z = \frac{L}{d}\frac{V_{ts}}{U} \tag{2-15}$$

Inertial losses vary depending on whether sampling is subisokinetic or superisokinetic. Lui et al. (1989) provide the following formula (Baron and Willeke, 2001) for inertial transmission efficiency under subisokinetic sampling.

$$\eta_{trans,inert} = \frac{1 + \left(\frac{U_0}{U} - 1\right) \Big/ \left(1 + \frac{2.66}{Stk^{2/3}}\right)}{1 + \left(\frac{U_0}{U} - 1\right) \Big/ \left(1 + \frac{0.418}{Stk^{2/3}}\right)} \tag{2-16}$$

For superisokinetic sampling, Hangal and Willeke (1990) provide the following formula (Baron and Willeke, 2001) for inertial transmission efficiency.

$$\eta_{trans,inert} = \exp\left(-75I_v^2\right) \tag{2-17}$$

$$I_v = 0.09\left(Stk\frac{U - U_0}{U_0}\right)^{0.3} \tag{2-18}$$

Baron and Willeke (2001) discuss that there is some disagreement in the literature concerning the effects of inertial deposition. This would seem especially true for solid particles, which would seem less likely to stick to the sampler walls than liquid particles.

The total sampling efficiency (η) is then determined by multiplying the individual efficiencies as shown in the following formula.

$$\eta = \eta_{asp} \times \eta_{trans,inert} \times \eta_{trans,grav} \tag{2-19}$$

2.2.2.2 Anisoaxial Sampling

Hangal and Willeke (1990) have modified the formulas for aspiration efficiency and gravitational settling to account for the sampler being angled vertically relative to the airflow. The following formula for aspiration efficiency is valid for angles ranging from 0 to 60°. This covers the range of interest in this study.

$$\eta_{asp} = 1 + I_a I_b \left[\frac{1 - \left(1 + \left(2 + 0.617(U/U_0)\right)Stk'\right)^{-1}}{1 - \left(1 + 2.617Stk'\right)^{-1}} \right] \tag{2-20}$$

$$I_a = \left(\frac{U_0}{U}\right)\cos\theta - 1 \tag{2-21}$$

$$I_b = 1 - \left[1 + 0.55Stk'\exp\left(0.25Stk'\right)\right]^{-1} \tag{2-22}$$

$$Stk' = Stk\exp\left(0.022\theta\right) \tag{2-23}$$

Gravitational losses are calculated using a modified version of equations 2-13 and 2-14 (Baron and Willeke, 2001).

$$\eta_{trans,grav} = \exp\left(-4.7K_\theta^{0.75}\right) \tag{2-24}$$

$$K_\theta = K\cos\theta = Z^{1/2}Stk^{1/2}\,\mathrm{Re}^{-1/4}\cos\theta \tag{2-25}$$

It should be noted that the angle in this formula is the angle of the nozzle relative to level, not necessarily the angle of nozzle relative to the air movement. The other formulas for isoaxial sampling are applicable for either scenario.

The inertial transmission efficiency is dependent on the direction of airflow into the sampler (upward or downward). Since this study is only concerned with downward sampling (nozzle facing upward relative to the air movement), the following formulas are used (Baron and Willeke, 2001).

$$\eta_{trans,inert} = \exp\left(-75\left(I_v + I_w\right)^2\right) \tag{2-26}$$

I_v is the *vena contract* term, which is zero for subisokinetic sampling and for superisokinetic sampling is defined as

$$I_v = 0.09\left(Stk\cos\theta\frac{U-U_0}{U_0}\right)^{0.3} \quad (2\text{-}27)$$

The wall impaction term (I_w) is the following for downward sampling.

$$I_w = Stk\left(\frac{U_0}{U}\right)^{1/2}\left[\sin(\theta-\alpha)\sin\left(\frac{\theta-\alpha}{2}\right)\right] \quad (2\text{-}28)$$

$$\alpha = 12\left[\left(1-\frac{\theta}{90}\right)-\exp(-\theta)\right] \quad (2\text{-}29)$$

2.2.2.3 Calm Air Sampling

Calm air sampling is a special condition where the air velocity is very low and the particle settling velocity becomes more relevant. Before calculating sampling efficiencies in this environment, it is first necessary to determine what "calm air" is. Baron and Willeke (2001) recommend the use of criteria provided by Grinshpun et al. (1993), which provides criteria for the relationship between the inlet size and flow for greater than 95% sampling efficiency.

$$\frac{U^2}{g\cdot d}\le 1 \quad (2\text{-}30)$$

or

$$\frac{4Q}{\pi d^{2.5}\sqrt{g}}\le 1 \quad (2\text{-}31)$$

These criteria are based on the calm air aspiration efficiency formula, also provided by Grishpun et al. (1993).

$$\eta_{asp,calm\ air} = \frac{V_{ts}}{U}\cos\varphi + \exp\left(-\frac{4Stk_i^{1+\sqrt{\frac{V_{TS}}{U}}}}{1+2Stk_i}\right) \quad (2\text{-}32)$$

This formula is applicable for any angle between horizontal and vertical.

2.2.2.4 Sampling in Low Velocity Air

Slow moving air provides a particularly difficult sampling scenario. This is because the settling velocity of the particles is still relevant, but the aerosol is moving sufficiently fast that the inertial effects are also significant. Grishpun et al. (1993, 1994) have developed equations

that combine the moving and calm air efficiencies by weighting the two depending on a ratio of the sampling to air velocities.

2.2.2.5 Sampling Efficiency Summary

The sampling efficiencies discussed above are specific to a particular sampler, flow rate, air speed and particle size. To determine the overall efficiency of a particular sampler in a particular situation, it is first necessary to calculate the sampling efficiency for each particle size in the range of expected results. Normally these sizes would be chosen to correspond to the bins of a particle sizing instrument.

Once the sampling efficiency for each particle size has been determined, it must be multiplied by the particle size distribution. If, as suggested above, a sampling efficiency for each bin has been calculated, this task is fairly straightforward. The overall sampling efficiency for that aerosol can then be determined by comparing the mass of particles that penetrate the sampling nozzle to the total mass in the original size distribution. This process will be demonstrated in Chapter 3.

As evident by the number of formulas discussed above, there are numerous calculations involved in determining the efficiency of a sampler. When combined with a distribution consisting of over a hundred bins, the task can be daunting. To aid in this process, Baron (2001) has provided a series of spreadsheets in a package called *Aerosol Calculator* (Aerocalc), which is available from a several websites (http://www.tsi.com, http://www.bgiusa.com). The primary spreadsheet provides calculations for most of the formulas in Baron and Willeke (2001), along with references and indicators to ensure that the formulas are being applied within their useful ranges. Most of the sampling efficiency calculations in this study utilize the *Aerosol Calculator* (Baron, 2001) as their basis.

2.3 Sampling Methods

Generally speaking, dust sampling methods fall into two general categories, real-time and integrated sampling methods. Electronic instruments typically give real-time results whereas mass samplers typically give time-averaged, or integrated, results. The type of particles sampled is also important, whether it is total suspended particles (TSP), a specific size range or the entire particle size distribution.

2.4 Time-Averaged

Most gravimetric methods fall into the time-averaged category. This is due to the relatively large amount of time required to collect enough dust mass to weigh. The substrate that the particles are collected on is typically a filter, although impaction plates can also be used. The most common types of integrated samplers are TSP samplers, impactors and personal samplers.

2.4.1 TSP

TSP samplers can be as simple as a filter attached to a pump or can be substantially more complex involving nozzles, filter holders and elaborate flow control methods. The general idea is to obtain a "total" dust sample, which is vaguely defined since it does not indicate any upper size limit and could theoretically include any floating "particle," including feathers. Because of this ambiguity it is difficult to design and compare TSP samplers, which explain why many researchers and regulatory agencies have gone towards samplers designed to measure particular particle sizes of interest. This study is still interested in TSP in order to have a better understanding of the entire particle size distribution and not just particles below a certain size. Additionally agricultural particles tend to be larger than ambient particles and, therefore, ambient samplers could misrepresent the actual amount of dust in the air. Therefore, this study will further evaluate TSP samplers. There are generally three styles of TSP samplers used: ambient, isokinetic and open faced.

2.4.1.1 Ambient

Ambient TSP samplers used for USEPA sampling have traditionally been relatively high volume samplers with flow rates greater than 1 m^3/min (US CFR, 1983). They basically consist of a filter, a pump and a basic flow measurement/control device. There was a simple metal hood to protect from rain and non-dust objects such as insects, hairs, feathers, etc. Personal experience has shown that these hoods were not necessarily effective at preventing some of these things from becoming collected on the filter. The hood also caused the air to have to change directions as it entered the sampler and as a result some larger particles were lost. The extent of this is highly variable with the wind speed and direction but measurements of the cut-point have ranged from 20 to 40 µm (McFarland et al., 1980; Wedding et al., 1977).

2.4.1.2 Isokinetic

Another common TSP sampler is the isokinetic sampler typically used for stack sampling (Baron and Willeke, 2001; ACGIH, 2001). The most basic versions of these consist of a nozzle chosen to match the duct velocity, tubing, a filter holder, and then a flow control device. Many systems consist of complex flow control devices whereas newer systems have simpler electronic controls(Baron and Willeke, 2001; ACGIH, 2001). These systems require significant stretches of steady airflow and are, therefore, not practical for use in buildings that have wall mounted fans with no stacks or ductwork. Because of the length and shape of the nozzles and tubing there can be substantial particle losses along the length of the tubing requiring that the tubing be washed with an appropriate solvent and the solution dried and weighed in addition to the filter (Baron and Willeke, 2001; ACGIH, 2001).. This can be both time consuming and impractical for large numbers of samples.

2.4.1.3 Open Faced

A third type of TSP sampler has been called a number of things, including calm air and open faced samplers. These samplers are similar to the ambient TSP sampler except that they do not generally have a hood. The lack of hood tends to make them behave more predictably in calm-air conditions. This limits the use of these samplers to areas of very little air movement since they can be sensitive to changes in air velocity, this will be discussed further below. The lack of a hood means that there is a possibility of larger objects being collected on the filter, but this is almost unavoidable for TSP samplers. It is not uncommon to construct a shroud made from coarse screen to filter out these larger objects. The problem with this method is that the screen can quickly become clogged and begin filtering the particles of interest. Probably the most common filters used for these samplers are 37 and 47 mm filters with open faced plastic filter holders with sampling flows ranging from 2 to 100 lpm (Baron and Willeke, 2001; Hinds, 1999; Vincent, 1989).

The sampling efficiency of these samplers has been examined in a number of studies and have been summarized by several authors (Baron and Willeke, 2001; Hinds, 1999; Vincent, 1989). Davies (1968) established a much cited criteria for determining the conditions under which calm air sampling could be conducted. These criteria indicated the maximum velocity for calm air sampling given a certain entrance size and flow rate or vice versa. These criteria have

been noted to be very strict since it allows for sampling at any orientation. Generally, sampling at a non-vertical angle (filter not facing upward) can lead to a variable sampling efficiency due to changes in direction of the air movement, even when it is low. Baron and Willeke (2001) recommend a more liberal criterion for sampling with a vertical orientation that is adapted from several studies.

2.4.2 Impactors

Impactors utilize the inertia of larger particles to separate a sample by size. A typical design involves accelerating the airflow through a hole to form a jet that then impacts a plate. As the jet rapidly changes direction, particles above a certain size impact onto the plate and are assumed to adhere to the plate while the smaller particles continue to move with the airstream. The smaller particles can then be captured on a filter and weighed. One of the most common uses of impactors is as a sampling head to remove larger particles to give a single cut before further sizing is to occur.

Cascade impactors take this principle further by cascading several impactors so that each one cuts at a progressively smaller size. The plate from each stage can then be weighed to determine the mass in each size range.

The most common problem with impactors is particle bounce and re-entrainment, which results in larger particles continuing on to lower stages or to the filter. This problem has been recognized since the impactor was invented in the 1950's. It has been well documented in the literature with several authors giving good summaries of these studies (ACGIH, 2001; Baron and Willeke, 2001; Hinds, 1999; Vincent, 1989). To reduce this error it is generally recommended that the impaction surface be coated with a grease to help trap particles. Baron and Willeke (2001) discuss the best greases to use as does the ACGIH Air Sampling Instruments book (2001). Of course the grease is only effective so long as particles do not build-up so that the new particles begin bouncing off of the collected particles. This can be a problem in CAFBs due to the high concentration and large particle size as the first stages of a cascade impactor quickly becomes overloaded.

To remedy the particle bounce problem, virtual impactors replace the plate with a probe that samples at a relatively low rate. This effectively acts as an impactor since most of the air

must change direction, but there is no plate from which particles can bounce. The low flow subsample is then collected on a filter. These samplers generally cut fairly sharp on the upper end but the lower end of the cut is affected by the flow rate of the minor flow (Baron and Willeke, 2001). A major problem that can exist with these samplers is internal particle losses due to improper design or operation. Baron and Willeke offer a number of studies that detail these problems. For the most part this problem can be overcome with proper design and operation.

2.4.3 Personal or Industrial Hygiene Samplers

Personal or industrial hygiene samplers are similar to the samplers discussed already, except that they attempt to mimic various aspects of the respiratory system. A variety of these samplers exist, including open faced samplers as discussed above, but the most common seen in agricultural research use a cyclone as a pre-separator (Chang et al., 2001; Phillips et al., 1998; Takai et al., 1998). The cyclone used is typically intended to mimic particle size distribution that makes it past the nose (inhalable) or that will make it into the lung (respirable). There are a number of manufacturers of such devices, which use a variety of materials and designs. Studies have shown a large variation in performance of such devices (Görner et al., 2001; Li et al., 2000). In the U.S. there are a variety of laws for different industries, which often result with a single company trying to use the same device to meet all of them. This is beginning to change, but there is still relatively little conformity of performance. On the other hand the European Union has standardized the desired performance, but standardization of results has yet to materialize.

2.5 Real-Time Methods

A number of real or near real-time methods exist for measuring particle concentration and/or size. Some of these instruments utilize the same basic principle of gravimetric samplers while others do not collect particles at all but instead measure various properties while they are in flight.

2.5.1 Collective Methods

Several instruments exist that utilize the basic principles of impaction and filtration to collect particles, but these particles are then weighed in near real-time. A variety of techniques

are used to measure the particles, the basic requirement being that the technique has to be very sensitive to very low changes in weight. Some of the methods that have been successfully used for ambient particles have been beta attenuation and vibration dampening. Of these, the Tapered Element Oscillating Microbalance (TEOM) has the greatest potential for use in agriculture. It basically functions the same as a typical sampler with an impaction inlet and a filter, the exception being that the filter is mounted on a vibrating element. The variations in the vibrations are used to determine the change in mass of the filter. Several problems exist with this instrument though. The first is that it is necessary to heat the sample to ensure that only the particle mass is being weighed and not water. During this process, volatile compounds can be lost. In addition, at elevated temperatures and humidity the reliability of the drying process is questionable. The second problem is that the filter can become overloaded relatively quickly so for longer samples the filter may have to be changed fairly frequently.

2.5.2 Light Scattering

A common method for measuring particle size is to measure the amount of light scattered as a particle passes through a light source, such as a laser. These instruments are quite popular because they are relatively cheap and easy to use, but they have some significant limitations. The primary problem with such instruments is that their calibration depends not only on the size of the particle but also on its shape and composition. As a result, using it to measure particles for which it was not calibrated can lead to significant error. It is common to use such instruments in agricultural studies, but the data is only useful as a qualitative indication of trends in concentration, not an absolute measure of particle size.

2.5.3 Time of Flight

Time of flight instruments combine light scattering with a particle's aerodynamic behavior to yield a more accurate measure of aerodynamic particle size. Essentially the sampled flow is accelerated through a nozzle. At the exit of the nozzle the flow crosses two laser beams. The nozzle serves to concentrate the flow into a single line or beam of particles, which can then be detected by the laser beams. The velocity of the particles in the area of the beams is related to the mass of the particle as well as the particle drag. Based on this data these instruments can approximate the true aerodynamic behavior of the particle.

Several problems exist with these instruments when used to measure particles other than those they were calibrated with. Because the instruments are calibrated with spherical particles of a known density, variations in the behavior of other measured particles are not always well accounted for. These instruments operate well outside of the Stokesian velocity and pressure range in which the aerodynamic diameter was defined. As a result, the measured aerodynamic behavior may be very different from what would be expected in the Stokes' region. Therefore, particles with large densities and extreme shapes are not sized well. Coincidence errors can also result in particles being mis-sized or not counted when two particles cross the laser beam simultaneously. Another common problem is sampling efficiency and particle losses in the instrumentation, which can be quite significant. Due to poor sampling efficiency, coincidence error, etc., the concentration data from these instruments cannot be relied on, but the general shape of the distribution is generally reliable assuming the particles can be delivered to the instrument accurately. The two most common time of flight instruments, both made by TSI (Shoreview, MN), are discussed below.

2.5.3.1 APS 3320/21

The APS has been used in a variety of situations where rapid sizing of a relatively wide range of particles is desired. In addition to the errors associated with density and shape discussed above, it has a low sampling efficiency. Baron and Willeke (2001) discuss a number of internal losses in the APS. In addition to these are the sampling losses associated with the inlet if it is used to sample in relatively calm air (Chen at al., 1998; Peters and Leith, 2003).

Older APS models including the APS 3320 had noted problems with detecting large "phantom" particles due to coincidence and particle recirculation in the detection region (Peters and Leith, 2003). The upgraded APS 3321 has a newly redesigned nozzle and software that is supposed to fix this problem. Early indications are that is has been successful (Peters and Leith, 2003).

There are two primary limitations to the use of the APS in CAFB. The first is that the size range has an upper limit of about 20 μm, which cuts off much of the size distribution seen in animal buildings. In practicality the instrument is intended for laboratory use and great care must be taken in using it in a CAFB. In addition to these problems, the errors already discussed apply to agricultural dusts since it is common to see irregular shapes, if not high densities.

2.5.3.2 Aerosizer DSP

The Aerosizer operates on the same basic principle as the APS, except that the detection chamber is partially evacuated. As a result, the velocities in that region reach the sonic range. This can expound some of the sizing errors discussed earlier. As with the APS there can be significant losses of particles in the plumbing of the system and smaller particles can pass through undetected (Baron and Willeke, 2001).

TSI purchased the Aerosizer in 1999 from API and at the time of this study had done little with it. As a result, the Aerosizer DSP model is housed in a large heavy container, has a separate pump and requires a dedicated desktop computer. This makes it very difficult to use for any kind of field use. A new model was scheduled to be released, which is supposed to improve the instrument and condenses it and the pump into a smaller package that can be operated with a laptop computer. Due to the unavailability and cost, this new model it will not be considered in this study.

2.6 Summary of Particle Measurement Literature

There is a multitude of particle sizing instruments available. In agriculture we are generally only interested in particles larger than 1 µm. This study is primarily concerned with the emissions of particles from CAFB and not with any particular aspect of the particle with the exception of size. This chapter has given a basic survey of the instrumentation that is or could be used for sampling in a CAFB environment. This discussion has been limited primarily to commercially available instrumentation with only limited discussion of specific brands.

It is evident that there are a variety of instruments that can be used for measuring both mass and particle size in CAFB, but few if any that are well suited. The most common reasons are either due to the limited size range of the instrument, inability to handle large concentrations or sensitivity to hostile environments. These findings, along with personal experience, have led to this study to examine a new method of sampling TSP emissions from CAFB and to compare the use of a variety of particle sizing instruments in various CAFBs.

2.7 Ventilation Rate

Confined animal buildings present a unique challenge when trying to estimate the emission rates of airborne pollutants. Each building or room represents an enclosed area source, with

several exhaust fans representing point source emissions. These fans generally have little or no duct work and can range in size from about 30 to 120 cm in diameter. In addition, the flow rate can vary drastically over short time periods due to external wind speed fluctuations, doors opening and closing as well as fan adjustments in response to temperature changes. All of this makes it difficult to quantify the flow rates needed to calculate the emission rates of the various pollutants.

Because agricultural fans have no ducts, traditional methods used for measurement of stack flow rates cannot be used. While there are devices for measuring the flow rates of air conditioning and heating vents, these are not able to handle the relatively high flow rate of agricultural fans or the harsh environment created by the dust and gasses present. Often times, estimates of the ventilation rate are made based on laboratory produced fan curves and the building static pressure.

There are standard methods for determining the flow rate of agricultural fans (AMCA, 1999). While these give accurate measurements for the fan flow rate in the lab, it is common for the performance to change substantially after some time in the field. This can be due to power differences, wind blowing against the fan exhaust, worn belts and motors, and blockage due to dust and feathers. The previously mentioned factors make using the laboratory produced fan curves for actual ventilations rates questionable.

There are some methods for obtaining accurate fan performance in the field. The FANS unit consists of an open ended box that is placed in front of (or behind if necessary) a fan. It has a row of five vane anemometers that are traversed vertically across the entrance of the fan. This basically gives a velocity map across the box that is used to calculate the flow rate entering (or leaving) the fan (Casey et al., 2007 and 2008; Gates et al., 2002 and 2004). It gives good results when compared simultaneously with the AMCA standard fan test chamber. In practice, the FANS is used to develop in-situ calibration curves for each fan against building static pressure. Continuous monitoring of building static pressure and fan operation (on/off) can then yield continuous measurement of fan flow rate. This is useful for single speed fans, but not as much for variable speed fans where each fan can be operated at different speeds, thus requiring a potentially large number of calibration curves.

Several options exist for continuous measurement of flow rate, although the accuracy and ease of use vary. One method is the use of a tracer gas (Demmers et al., 2003). It involves feeding a tracer gas at a known rate and sampling the concentration of the exhaust. This method suffers from inaccuracy when there is incomplete mixing and is very instrument intensive. Another option for measuring flow rate is using a frictionless anemometer that is just smaller than the fan size (Maghirang et al., 2003; Berckmans et al., 2001). This method showed good results for smaller fans below 41 cm, but pressure drop became a problem as it was scaled up and it requires the installation of a small duct section upstream of the fan, which could be problematic in many facilities.

Most of these methods can involve significant changes to the ventilation system and/or involve substantial capital cost. Another option is the use of a relatively small commercially available vane anemometer for continuous measurement of fan flow rate at a single point on a fan (Heber, 2003). With this method, continuous measurement of the ventilation rate can be made on multiple fans without substantially altering the existing facilities. This study evaluated the performance of such an anemometer for measuring the ventilation rate and addresses the effects of anemometer location and fan size.

CHAPTER THREE: **TOTAL SUSPENDED PARTICULATE SAMPLING**

3.1 Objectives

The primary objective of this portion of the study was to develop a simple, inexpensive TSP sampler for mechanically ventilated confinement animal buildings. Specifically, the objectives are to:

1. Design the sampler(s) based on existing theories;
2. Evaluate the sampler performance versus the theoretical predictions; and
3. Determine the number of samplers needed for typical sampling at an exhaust fan.

3.2 Sampler System Design

Confined animal buildings typically have multiple fans and one or more inlets along the length of the building. These inlets are commonly located along the ridge or ceiling of the room and can result in downward airflow toward the wall mounted fans. This makes sampling difficult because traditional isokinetic sampling procedures cannot be used when the air speeds and directions vary. A simplified isokinetic procedure was developed that takes these problems into consideration.

Figure 3.1 shows the basic sampler set-up and Figure 3.2 shows a more detailed view of the sampler components. Whenever possible, common commercially available parts were used to simplify the assembly of the samplers and reduce the costs. The sampler consists of a conical nozzle that is inserted into a common 37 mm plastic filter holder. Downstream of the sampling head the flow is controlled by a critical venturi that operates similar to more commonplace critical orifices, but with a lower critical pressure of about 10 kPa. The critical venturi has been described by Wang and Zhang (1999). This system has the advantage in that a single pump can operate several sampling heads and no adjustment of the system is necessary under normal operating conditions.

3.3 Sampling Probe Design

The probes used in this study were designed to achieve isokinetic sampling in mechanically ventilated animal buildings. When designing an isokinetic sampling probe there are many factors involved including the flow rate, sampling velocity, collection media, cost and accuracy.

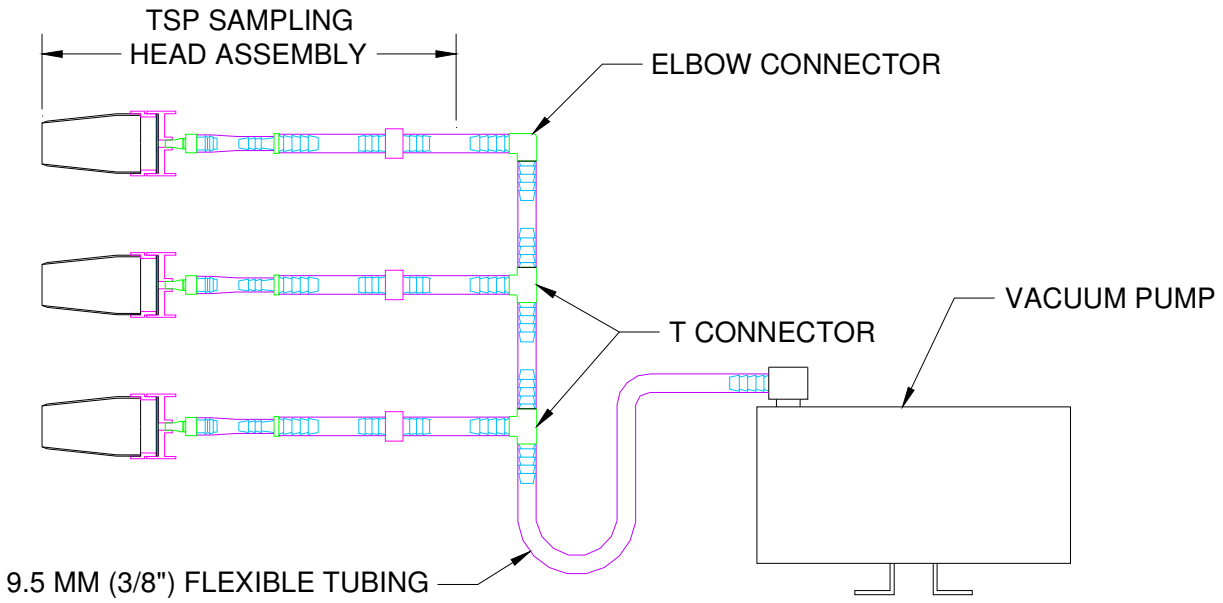

Figure 3.1 TSP sampling system example assembly.

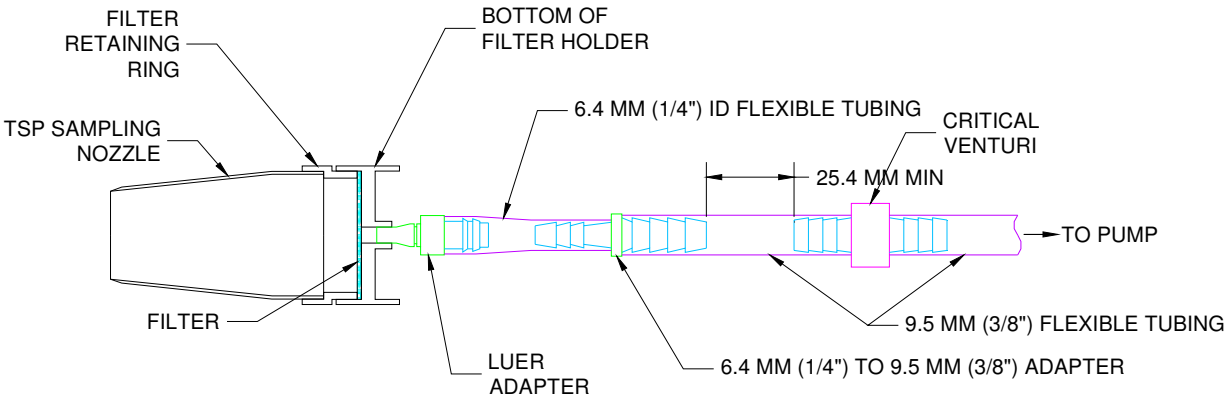

Figure 3.2 Details of the TSP sampling head assembly.

Due to the availability and simplicity of the critical venturis discussed above, these were used as the basis for the flow control. This fixed the sampling flow rate at 20 lpm. The second factor affecting the nozzle size is the desired sampling velocity. The areas in front of a wall mounted fan typically have velocities ranging from 1-3 m/s. Higher velocities are experienced in the fan, but physical restraints do not allow sampling this close to the fan. Considering this, nozzles were designed for 1, 2 and 3 m/s sampling velocities.

Figure 3.3 and Table 3.1 show the dimensions of three nozzle sizes that were used in this study. The nozzle entrance diameters of 12.0, 14.6 and 21.1 mm correspond to 3, 2 and 1 m/s sampling velocities at 20 lpm. Most of the existing models in the literature are for velocities above 3 m/s or for calm air conditions below 1 m/s (Baron and Willeke, 2001; Vincent, 1989). While there are a few studies that consider the intermediate range, they are basically methods for merging the models produced in other studies (Baron and Willeke, 2001).

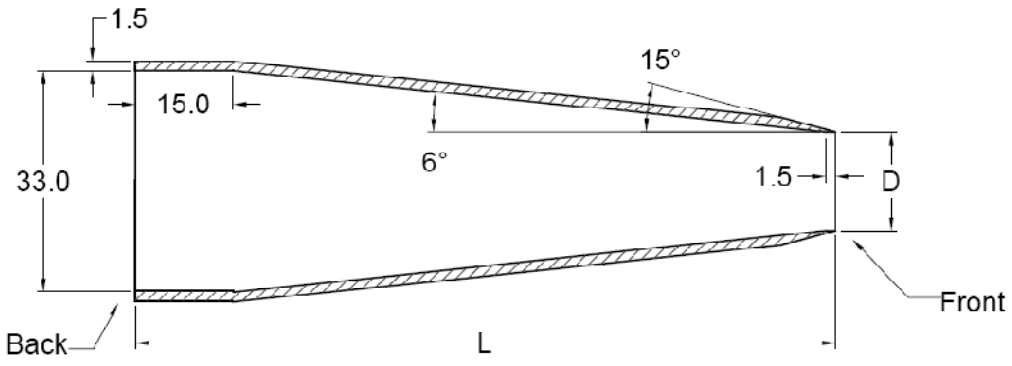

Figure 3.3 TSP nozzle details (All dimensions in mm).

Table 3.1 TSP nozzle dimensions.

Sampling Velocity	D (mm)	L (mm)
1 m/s	21.1	73
2 m/s	14.6	104
3 m/s	12.0	116

The entrance area of the nozzles was modeled after EPA Method 201A PM10 sampling nozzles where the 15° taper is considered sufficient for the sharp edged criteria of an ideal isokinetic sampler. In practice, the nozzle has to be blunted slightly at the tip to prevent it from curling or being easily damaged. The angle of the expansion was chosen as 6°, which fit in the 3-6° range of many EPA isokinetic sampler designs. The rear of the probe was designed to fit into Millipore 37mm Aerosol Analysis Monitors (Millipore, Billerica, MA). These are plastic filter cassettes that have a filter holding base, a removable ring that keeps the filter in place and removable cover as shown in Figure 3.2. The dimensions shown are approximate, the actual size and shape will depend on the filter holders used. These were chosen because of their ease of use, low cost and because they are frequently used for indoor aerosol studies. Glass fiber filters were used in the 37 mm holders.

Unlike traditional isokinetic systems used for stack monitoring, this system was designed so that the entire sampling apparatus can sit in the airflow. This reduces particle losses in the transport system, which can be very significant for traditional isokinetic systems (Baron and Willeke, 2001).

3.4 Performance Modeling

The formulas used to determine the overall sampling efficiency of these nozzles were discussed in detail in Chapter 2. These will be referenced throughout this section. Each of the three sampling scenarios will be discussed below.

3.4.1 Isokinetic – Isoaxial

Isokinetic sampling occurs when the velocity within the nozzle is the same as the air stream from which it is sampling. Isoxial means that the nozzle is aligned with the airflow. In this scenario, as shown in Figure 2.11, the air streamlines enter the nozzle smoothly with no transitions to cause vena contracta or inertial impacts. This means that the aspiration efficiency is 100%, as is the inertial and vena contracta and inertial transmission efficiencies. Equations 2-9, 2-16 and 2-17 confirm this since each goes to one for $U_0/U = 1$ (Isokinetic). Although these losses are minimal, the gravitational losses are still significant (Equation 2-13). The effects of the gravitational losses can be seen in Figure 3.4, which shows the total efficiency of each sampler at

its design velocity. Again, the total efficiency for an isokinetic sampler is the same as its gravitational efficiency since all other efficiencies are one.

Although all of the particles enter the sampler without a problem, the larger particles can quickly settle out. The efficiency for the samplers with lower velocities is higher because they are shorter (see Table 3.1), and thus have less opportunity for settling. These calculations assume that there is no re-entrainment of the particles, which is unlikely if a significant amount build up on the nozzle walls.

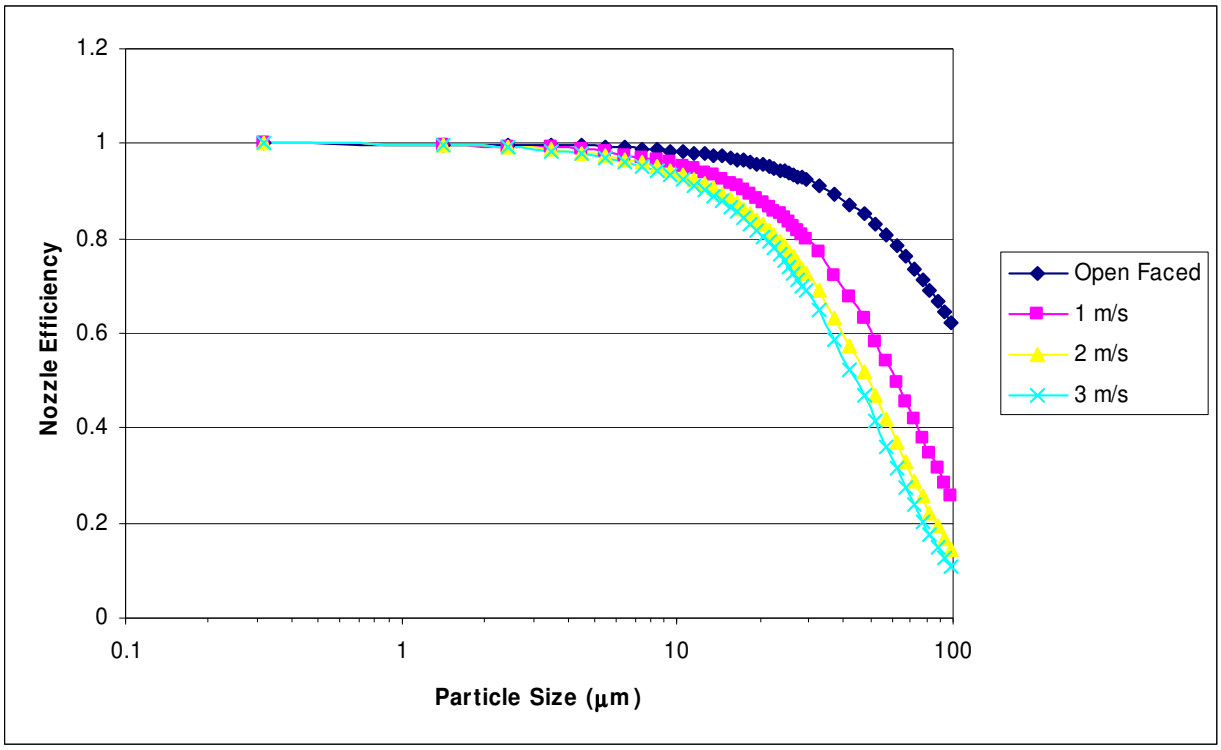

Figure 3.4 Isokinetic sampling efficiency of each nozzle and an open faced sampler.

3.4.2 Anisokinetic - Isoaxial

When the sampling velocity differs from the surrounding air flow, it is known as anisokinetic. When the sampling velocity (U) is less than the air velocity (U_0) then the sampling condition is subisokinetic. Under this scenario, the aspiration efficiency is above one because the momentum of the particles causes them to enter the sampler, as shown in Figure 2.11c. In addition, the change in trajectory causes some of the particles that enter the sampler to impact onto the walls. Gravitational forces also cause particles losses. The equations to describe these

are the same as those used for isokinetic conditions. Figure 3.5 shows the effects of these issues on the sampling efficiency of the nozzle.

The gains caused by subisokinetic aspiration efficiency are significant. The inertial losses are significant for mid and large sized particles. Again, the gravitational losses are most significant, with nearly 90% of the 100 µm particles lost. Overall the sampling efficiency of a subisokinetic sampler is higher than that of an isokinetic sampler due to the increased aspiration efficiency.

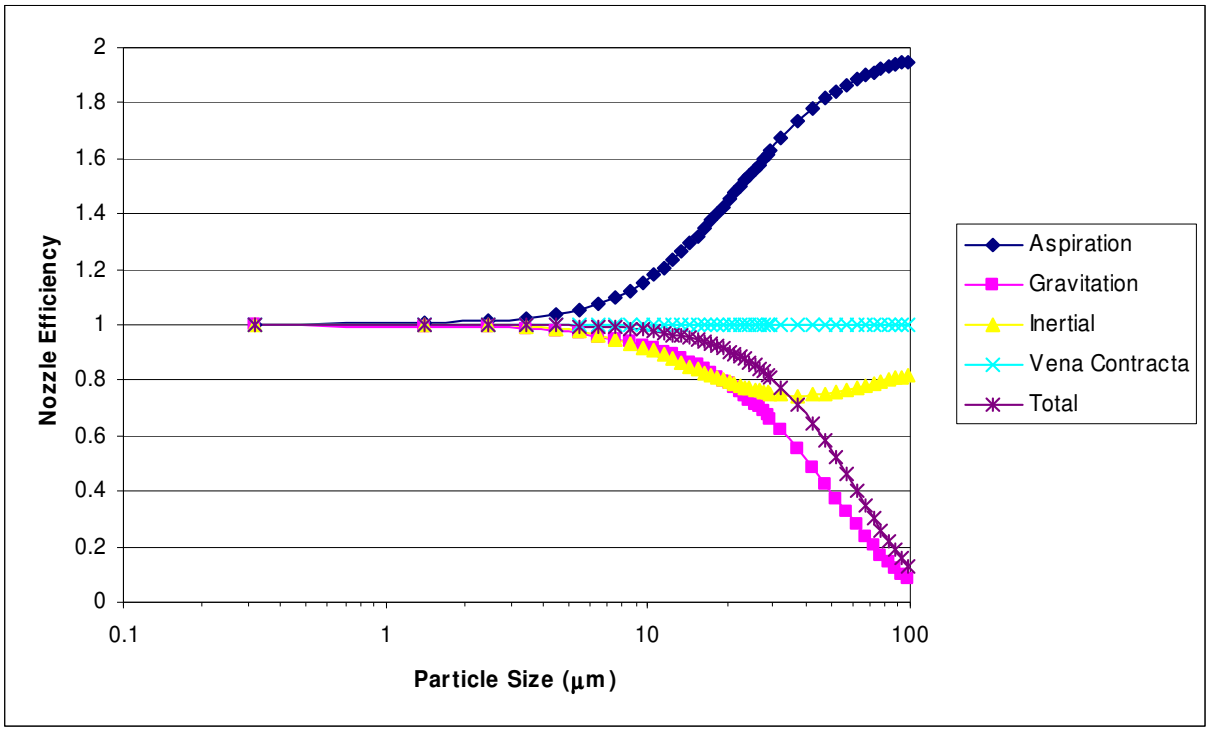

Figure 3.5 Subisokinetic ($U_0/U = 2$) sampling efficiency with the 2 m/s nozzle.

Superisokinetic sampling occurs when the sampling velocity is higher than the velocity of the surrounding air. In this case, the air must change directions to enter the nozzle. Larger particles that cannot make the turn are lost. This was visualized in Figure 2.12b. In addition to lowering the aspiration efficiency, a vena contracta forms at the entrance of the nozzle, which can trap particles and cause them to impact the nozzle wall. The affects of this can be seen in Figure 3.6, which shows the sampling efficiency of the 2 m/s nozzle under superisokinetic

conditions. The losses as the particles enter the nozzle (aspiration) are significant, but the losses from vena contracta and gravitational losses dominate.

3.4.3 Anisoaxial Sampling

Anisoaxial sampling means that the sampling nozzle is not aligned with the surrounding airflow. As a result, particles can overshoot the sampler because the air has to change direction to enter the nozzle. Figure 2.12a, shows a schematic of this scenario. This causes the aspiration efficiency to decrease as described by Eq. 2-20. The same forces that cause the particles to overshoot the sampler can also cause some particles to impact the inside wall of the sampler. In addition, a vena contracta can form inside the nozzle, thus causing additional impaction. The inertial losses caused by these two issues are described in Eq. 2-26. The gravitational losses are described using Eq. 2-24.

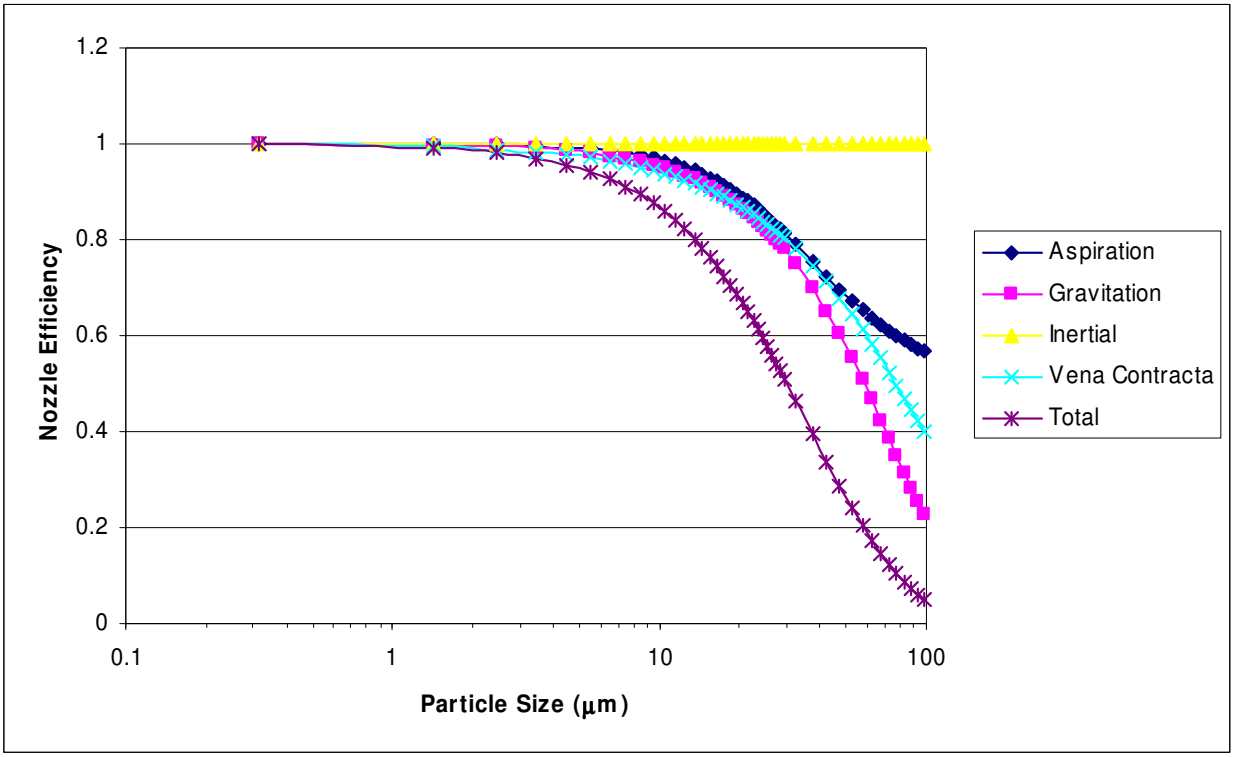

Figure 3.6 Superisokinetic ($U_0/U = 0.5$) sampling efficiency of the 2 m/s nozzle.

Under normal circumstances, the nozzles used in this study would be installed horizontally. The anisoxial condition would be caused by air flow lines that are angled relative to the samplers. This is typical when close to fan as the air changes direction to enter the fan. This means, that for the gravitational losses, the angle is zero since the nozzle is level. As a result, the gravitational losses for anisoaxial sampling are the same as those of isoaxial. For calculating the aspirational and inertial efficiencies, the nozzle is considered angled and θ is the angle between the two. Figure 3.7 shows the magnitude of each loss for the 2 m/s nozzle, angled 45° to the air flow. Again, the aspiration losses are significant, but they are dwarfed by the inertial and gravitational losses.

Figure 3.8 shows the effect of the angle on overall sampling efficiency. At 15°, the effect is minimal, but increases rapidly from there. This indicates that minimal misalignment should not greatly impact the sampler performance, although larger angles could be problematic.

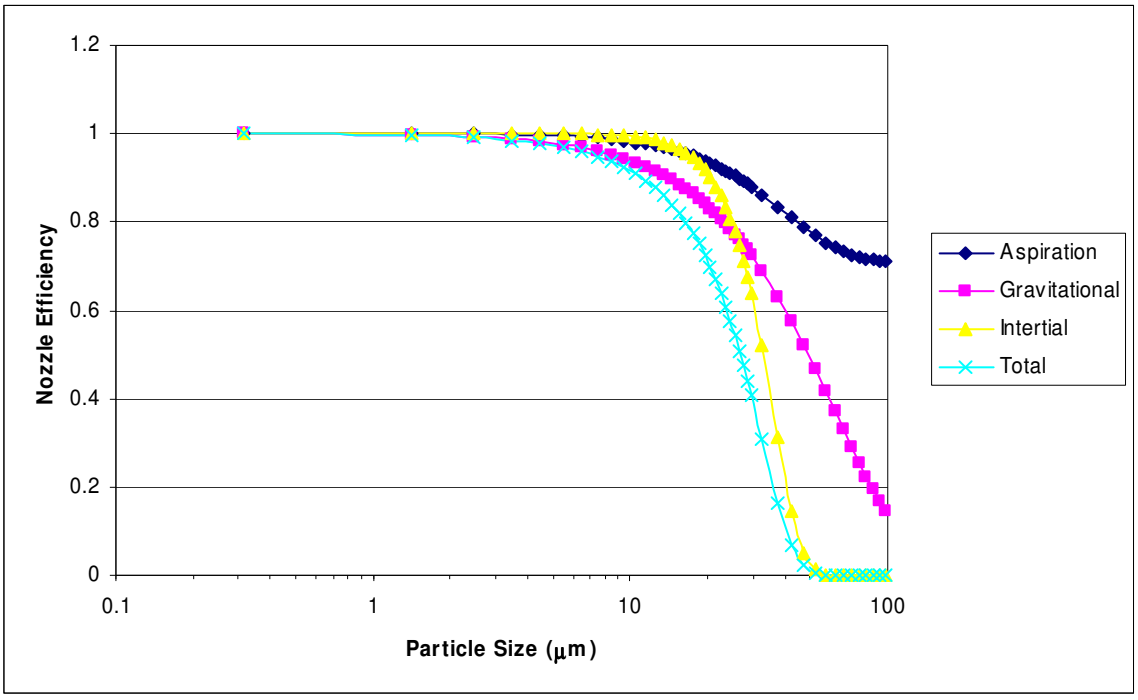

Figure 3.7 Anisoaxial (θ = 45°) sampling efficiency of the 2-m/s nozzle under isokinetic conditions.

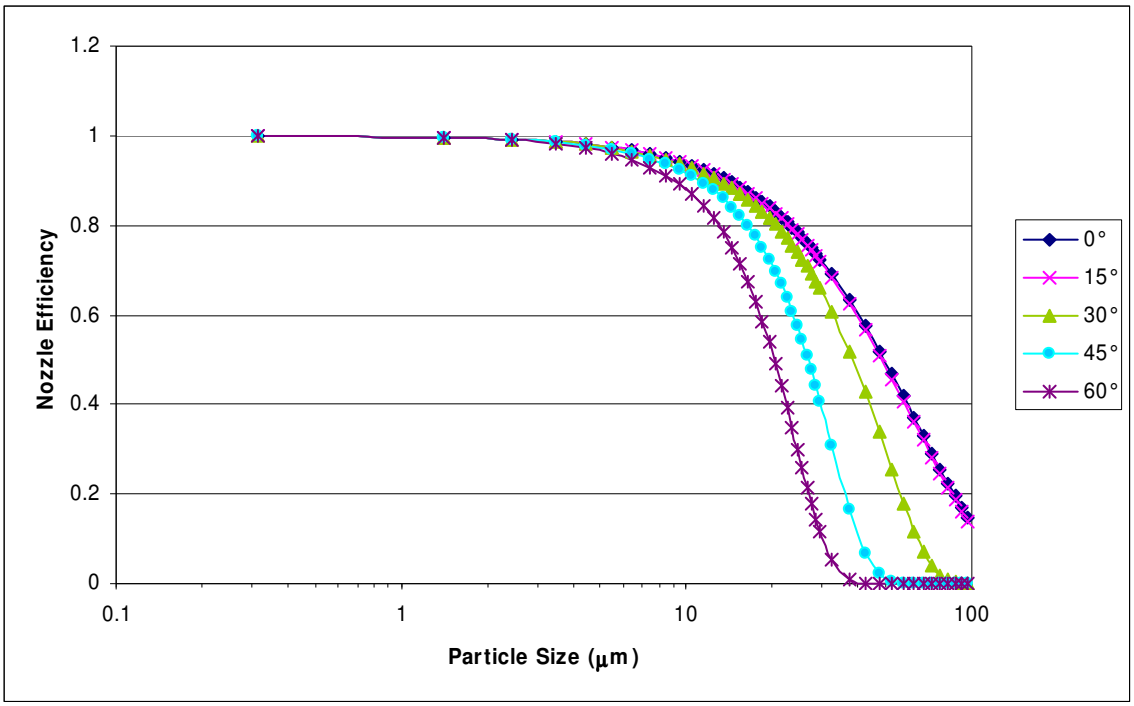

Figure 3.8 Anisoaxial sampling efficiency at various angles for the 2 m/s nozzle under isokinetic conditions.

3.5 Experimental Facility and Materials

To compare the actual performance to the modeled results discussed above, it was necessary to test the sampler in a real world scenario. Despite this, control of many parameters is necessary to reduce the amount of experimental error. Silsoe Research Institute, in the United Kingdom, had a model swine building section for this kind of testing. This facility was described by Harral and Boone (1997) and Demmers et al. (2000). Figure 3.9 shows the layout of the facility. With the "Left Fan" being in the upper left corner of the drawing, while the "Right Fan" is in the lower right corner. The total maximum flow from the two fans is approximately 4800 m^3/h.

This building section was designed to simulate a small section of a European swine housing unit. The fans were 45 cm axial fans and were recessed into the walls so that there was a duct section of about 1 m. This was done so that a vane anemometer could be used upstream for measurement of flow rate. The ridge vent along the top of the room is where the air entered and it could be adjusted, along with the fan speed, to obtain the desired ventilation rate. The room

facility was equipped with sensors and dataloggers to monitor temperature, pressure, flow rate and other parameters. The room had previously been used for a study of air flow in a swine building (Harral and Boone, 1997). Their results showed that the velocity in front of the fan was about 2 m/s. This was tested in more detail as discussed in the next section.

Other than sampling equipment, there are none of the typical obstructions found in a swine building. Since there are no animals, there is also less air disturbance and heat generation. For the purpose of this study, a constant air velocity and flow pattern are desired. This may not be likely in situations where there are animals or obstructions near the fans. Because the goal of this study is not to assess the extent of these variations, this idealized section is considered adequate.

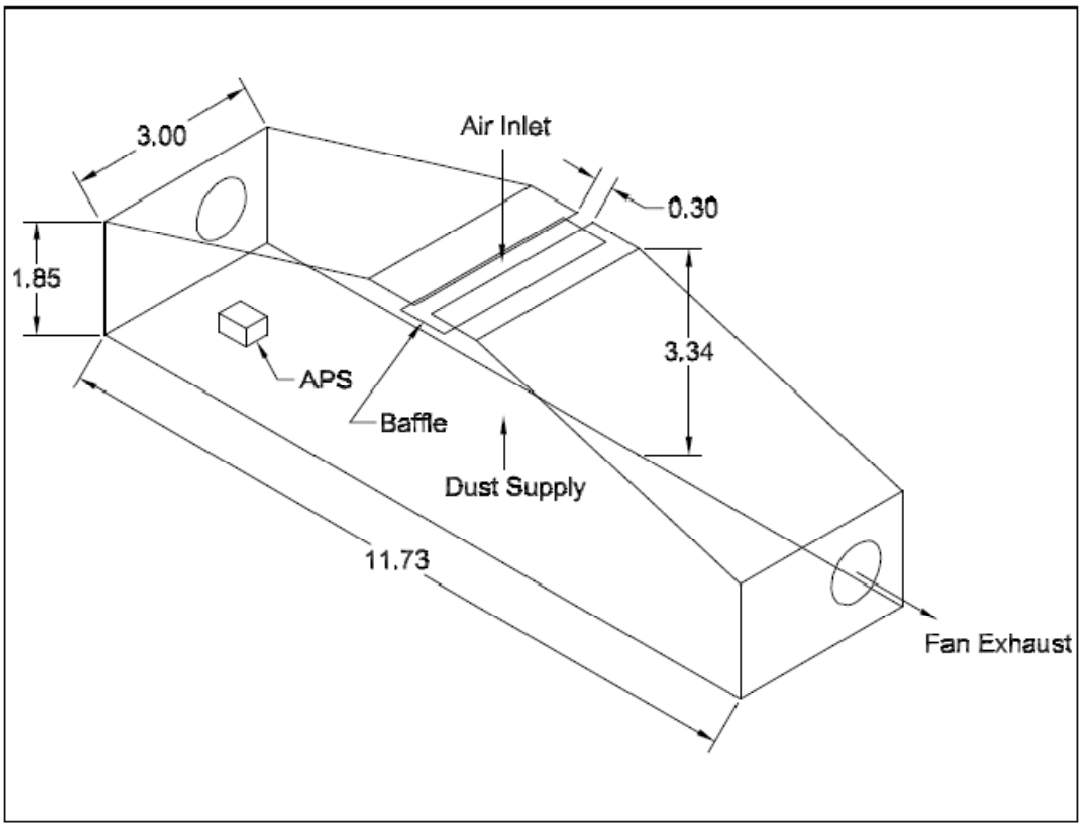

Figure 3.9 Experimental swine housing room section located at Silsoe Research Institute, United Kingdom (All measurements are in meters).

3.5.1 Dust Supply

Dust was supplied for the tests using a venturi feeder with an agitated, auger driven hopper (Demmers et al., 2000). The compressed air flow rate of the aerosolized PM supply was 100 lpm and fed directly into the center of the room where it mixed with the incoming air supply. It was expected that mixing would not be complete or uniform. The maximum feed rate of the PM feeder was 14 g/h, which is where the supply was operated for these experiments to obtain as high a concentration in the room as possible, thus reducing the required sampling time.

The dust used was an artificial swine dust created for previous experiments and has been previously described by Demmers et al. (2000). It was composed of similar materials as typical swine dust, including fecal matter, feed, and straw, and was ground to the desired size range. Using an electrical sensing zone method (volumetric results), they measured the GMMD to be about 23 µm. Once aerosolized, the dust was shown to have a GMMD of 13.1±0.9 µm and a MGSD of 1.89±0.04, measured using a TSI Aerodynamic Particle Sizer (Demmers et al., 2000).

3.6 Methods for All Tests

3.6.1 Fan Flow Patterns

In order to accurately determine sampler flow conditions, it was first necessary to establish the flow pattern in front of the fans. The fans were set at their maximum speed, as they were for all other tests. A Gill sonic anemometer (Gill Instruments, Lymington, Hampshire, England) was used to measure the velocity and direction of flow on a 3-D grid in front of the fan. The sonic anemometer measures the 3-D flow, providing the velocity magnitude in each of the three principle directions.

The anemometer was placed in the desired position and then the room was sealed. Once the fans were started the flow was allowed to stabilize for three minutes Anemometer data was then collected for three minutes. Once the data collection was completed the anemometer data collection was stopped and the fans shut off. The anemometer was then moved to the next location on the grid. This process was repeated for both fans. The sample grid and specific anemometer locations are shown in Figure 3.10.

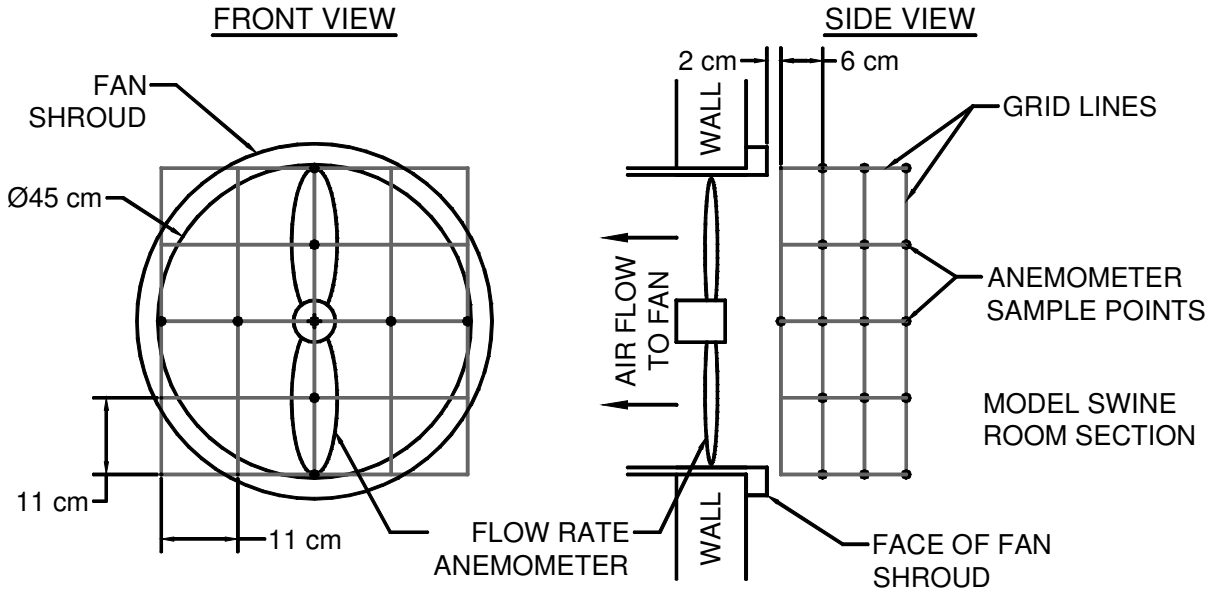

Figure 3.10 Anemometer sampling points for fan velocity study.

This raw data was then transformed to provide the actual magnitude and direction of the velocity vectors. Figure 3.11 and Figure 3.12 show the resulting flow pattern, where the lengths of the arrows are proportional to the magnitude of the air velocity. Distances are taken from the face of the fan shroud. They show the higher downward flow coming from the ceiling inlet and the lower, more level flow entering from the lower half of the fan. The velocities range from 0.5 to 3 m/s, although in the area where sampling could occur the velocity is about 2 m/s. Since the fans were already operating at maximum capacity, it was decided to conduct all tests at these conditions. A contour map of the velocity vectors was developed and used to determine the location for placement of the samplers. All samplers, regardless of design velocity, were placed such that their nozzle tips were in an area where the magnitude of the velocity was 2 m/s. This allowed for isokinetic sampling with the 2 m/s nozzle, superisokinetic sampling for the 3 m/s nozzle and subisokinetic sampling for the 1 m/s and open faced samplers.

3.6.2 Particle Size

As discussed in Chapter 2, knowing the particle size distribution is a critical part of estimating overall sampler efficiency. To measure particle size during the testing, a TSI APS 3320 was used. It was placed on the floor in an area of relatively calm air, about half way between the center and if the room and left fan. During testing, samples were collected every ten

minutes for 30 seconds each. The results for each bin were then summed to get an average result. The methods used to determine the MGMD and MGSD are discussed in Section 2.2. The APS has an upper size range of about 20 µm. Since the actual distribution probably extends beyond this point, an ideal log-normal distribution was developed using the MGMD and MGSD.

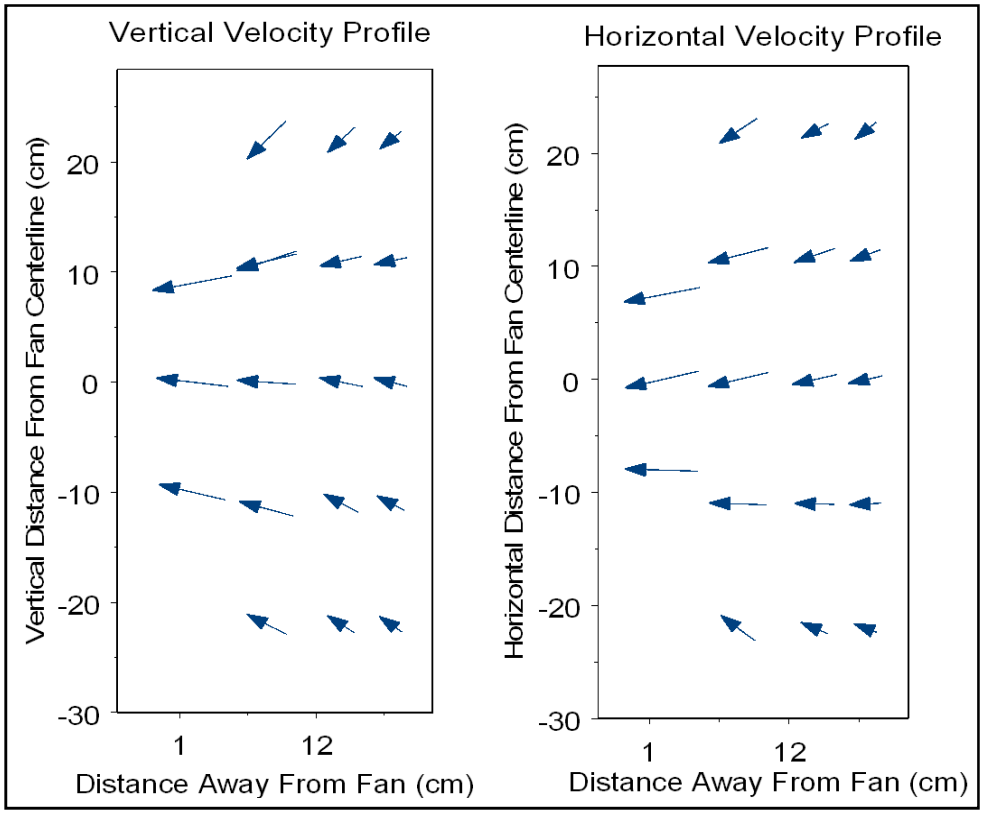

Figure 3.11 Velocity profile of the left fan in the vertical and horizontal (looking down) directions.

3.6.3 Filter Handling

Before weighing, the filters were conditioned at 25°C and 50% humidity for at least 24 hours with their plugs removed to allow the filters to equilibrate with the surrounding air. The filters were weighed in their holder with the lids removed using a microbalance. The total weight of the filter holder and filter was about 13 g, while the accuracy of the microbalance was 10 µg. The data was recorded to the nearest 100 µg.

There were a total of 8 weighing blanks and 6 field blanks collected. The weighing blanks went through the weighing process, but were left in the weighing room. Field blanks were

treated exactly like filters used for sampling, but the pumps were not turned on. These would be taken into the model room and installed at a sampling point with the nozzle. The nozzle would then be removed, the cap reinstalled and the closed filter holder placed back in the storage box.

The data from these blanks was used to determine handling problems and detect possible bias. The weighing blanks indicated no bias, with an average change in weight of -0.1 ± 0.4 mg. The field blanks indicated potential bias with an average change in weight of -1.2 ± 0.8 mg. All of the field blanks showed a net loss. The reason is not clear, although it is possible that there is some loss of materials when the aluminum nozzles are inserted into the plastic filter holder. Because the loss was so consistent, it was decided to add the average field blank loss of 1.2 mg to all filters tested.

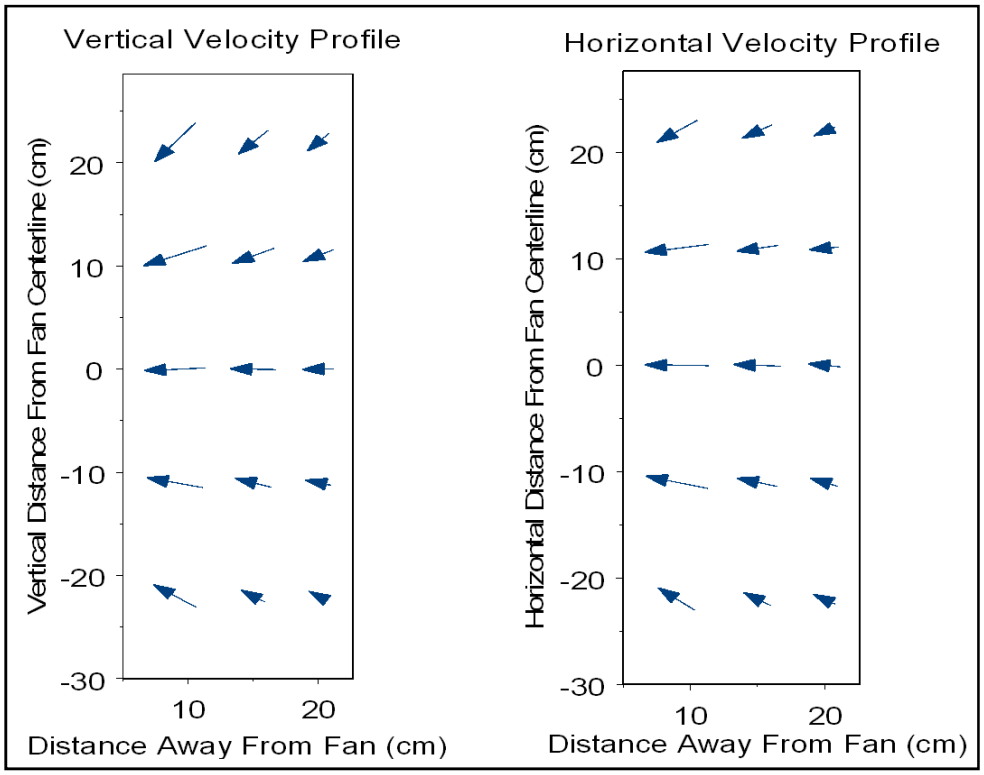

Figure 3.12 Velocity profile of the right fan in the vertical and horizontal (looking down) directions.

3.7 Experimental Design – Sampler Performance

To test the sampler performance, two each of the 1, 2 and 3 m/s samplers were tested, as well as open faced filters, two facing up and two facing into the air stream (away from the fan). Five sampler positions were established in front of each fan. One at the center and four located at each axis around the center, at a distance of 16 cm from the center (about 70% of the radius). Again, the tip of each nozzle was located so that the average velocity was 2 m/s based on the sonic anemometer results discussed earlier. Figure 3.13 shows the general layout of the nozzle locations in front of the fans. The samplers were held in place using chemistry ring stand type clamps. The pumps were placed on the floor and were connected to outlets that could be turned on outside of the model room.

A latin square design was used, with a total of five tests, such that each nozzle type was located at each position once. The order was randomized to minimize temporal effects. This arrangement was done for both fans, and samples were collected simultaneously for each. This gave a total of ten samples collected for each run, for a total of 50 samples.

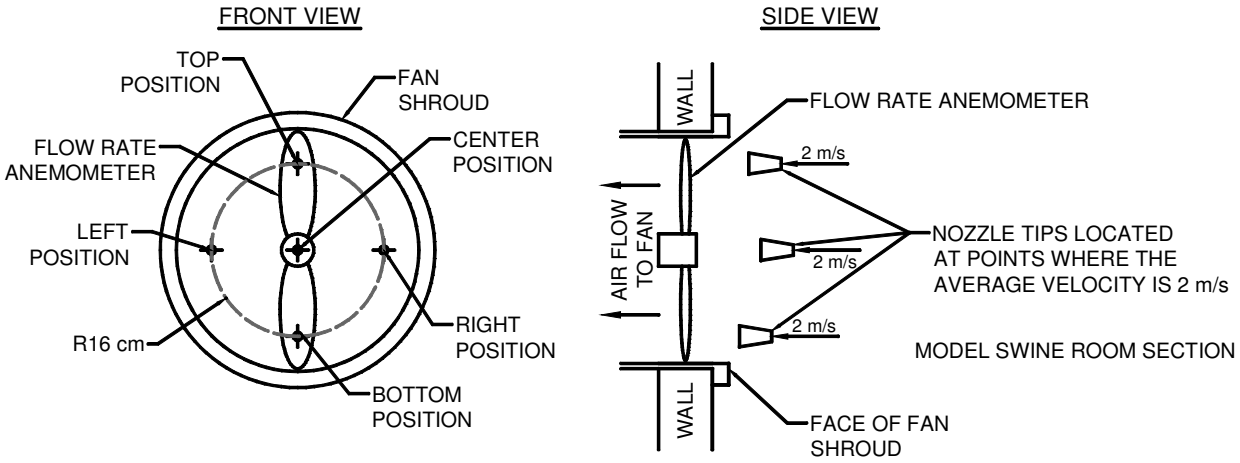

Figure 3.13 General nozzle layout in front of the 45 cm fan opening.

At the beginning of the tests, the fans and PM generator were started and allowed to run for about 24 hours to obtain a stable flow field and PM concentration. For each test the filter holders and sampling heads were installed and the positions adjusted to ensure that the nozzle entrance was at the proper location. The room air flow was then allowed to stabilize again for about 15-20 minutes before the pumps were remotely actuated. To end the test, the pumps were

stopped remotely, the filter holders removed and the nozzles brushed clean for the next test. During the tests, a datalogger recorded all of the room parameters and the APS was used to measure the particle size distribution.

3.8 Results – Sampler Performance

3.8.1 Dust Concentration

During the five tests, the fan and dust supply were left at their highest levels. The dust supply rate is fixed at 14 g/hr, while the ventilation rate can vary slightly. The ventilation rates and estimated dust concentrations can be seen Table 3.2.

Table 3.2 Average room ventilation rate and dust concentration over the five tests for sampler performance.

	Flow Rate (m^3/hr)			Dust Conc.
Test	Average	Std. Dev.	Std. Dev. (%)	(mg/m^3)
1	4731	66.5	1.41	2.96
2	4800	73.7	1.54	2.92
3	4791	71.0	1.48	2.92
4	4804	74.4	1.55	2.91
5	4806	76.4	1.59	2.91
Average	4786	72.4	1.51	2.93

This dust concentration is based purely on the feed rate and ventilation rate. In reality the there will be incomplete mixing, settling and other factors that will affect the actual concentration at each sampler. For these tests, these factors are assumed to be negligible. Although there are likely errors in the average dust concentration, it will be used as the baseline for comparison. At a minimum, this should provide a basis for comparing the trends between modeled and actual performance.

3.8.2 Particle Size Distribution

The particle size distribution was measured using a TSI APS 3320. Table 3.3 shows the count particle size statistics as provided by the APS. It shows the average and standard deviation of the 18 samples collected during each 3 hr test. There is very good consistency during and between tests.

Table 3.3 Count particle size statistics as provided by the APS.

	Count Geometric Mean Diameter			Count Geometric Standard Deviation		
Test	Average	Std. Dev.	Std. Dev (%)	Average	Std. Dev.	Std. Dev (%)
1	1.572	0.006	0.390	1.618	0.005	0.307
2	1.623	0.007	0.453	1.604	0.005	0.291
3	1.631	0.008	0.495	1.603	0.006	0.368
4	1.624	0.011	0.691	1.608	0.006	0.361
5	1.608	0.006	0.394	1.606	0.004	0.274
Avg	1.612	0.008	0.484	1.608	0.005	0.320

To determine the mass particle size statistics the methods discussed in Chapter 2 were used. A representative volume for each bin was found and multiplied by the number of particles in that bin. This was converted to a mass fraction, which was used to generate a cumulative probability distribution. A line was fit through this cumulative probability curve, the equation for which was used to determine the MGMD and the MGSD. These parameters were also calculated using the raw data, where the 50% point is the GMMD and MGSD can be found using Eq. 2-8 provided the 16% and 84% points in the cumulative distribution. The results from this are shown in Table 3.4. These numbers show good consistency with a deviation of ±1.3% for the best fit data and ±0.8% using the raw data.

Although there is small difference (<10%) between the two answers, this is expected since curve fitting takes into account all points in the distribution. Both the actual and fitted distributions can be seen in Figure 3.14. The GMMD of the fitted distribution is higher for the raw data because it contains more particles at the higher end than an ideal log-normal distribution. Overall it appears to be a reasonable fit.

Table 3.4 Particle size statistics from APS data.

	GMMD (μm)		MGSD	
Test	Best Fit	Raw Data	Best Fit	Raw Data
1	3.84	3.58	1.78	1.86
2	3.82	3.55	1.75	1.83
3	3.95	3.56	1.78	1.83
4	3.88	3.59	1.76	1.85
5	3.81	3.51	1.76	1.83
Avg.	3.86	3.56	1.77	1.84
Std. Dev.	0.05	0.03	0.01	0.01

What is more concerning is the fact that the GMMD is substantially lower than that previously reported of GMMD of 13.1±0.9 µm (see Section 3.5.1). There should not be this level of discrepancy between the two, since the same dust and equipment was used. The most likely culprit is a combination of poor mixing and poor sampling efficiency. As discussed in Chapter 2, the APS has very poor sampling efficiency for larger particles in moving air. To test this theory, perfect log-normal distribution will be generated using both the fitted data as well as the previously reported data of Demmers et al. (2000). The difference between the two distributions can be seen in Figure 3.15. It obvious that in the reported distribution, most of the particles are above 10 µm, while in the measured distribution, most of the mass will be below 10 µm. This is important because the effects of sampling efficiency are most pronounced above 10 µm.

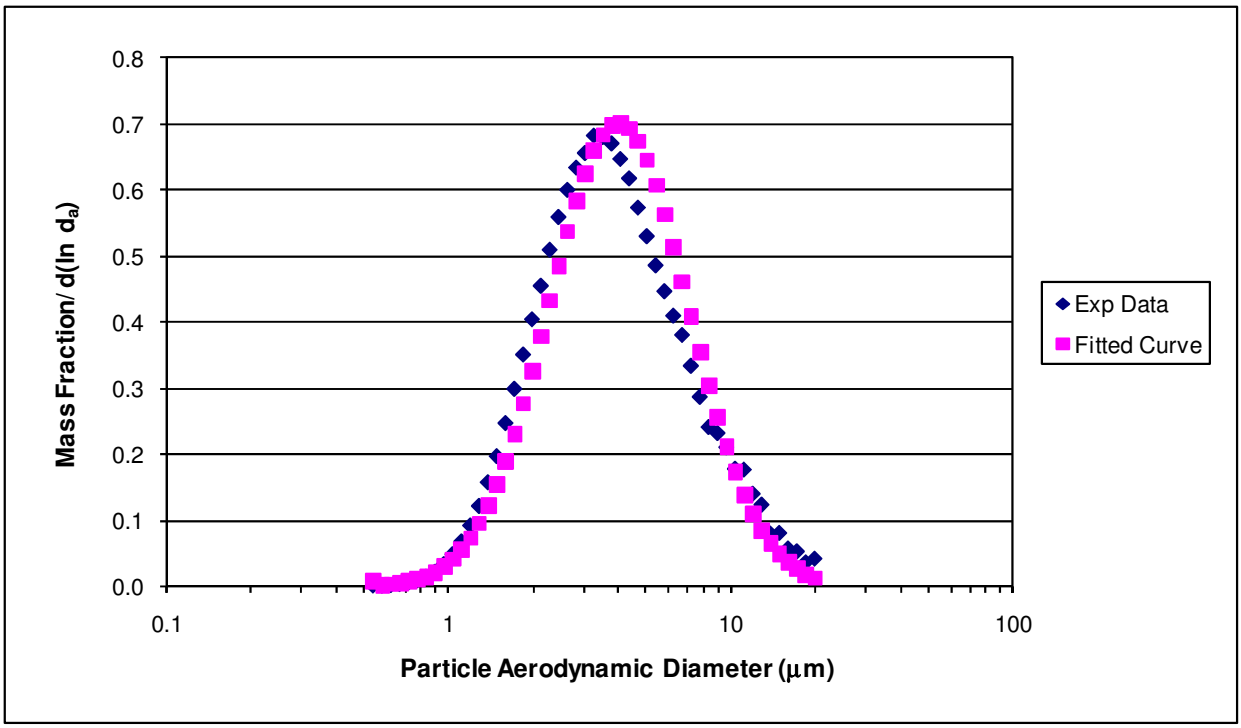

Figure 3.14 Actual and fitted particle size distributions for the artificial swine dust.

3.8.3 Modeled vs. Actual Performance

Due to flow limitation of the fans, all samplers were installed at a point where the average velocity was 2 m/s. This put the 2 m/s nozzle in the isokinetic range, the 3 m/s sampler operated superisokinetically, while the 1 m/s and open faced samplers were subisokinetic. Using

the equations in Chapter 2 and discussed in Section 3.4, Figure 3.16 was created. It shows the expected sampling efficiency at each particle size for the conditions in which the samplers were tested.

To determine the total efficiency these curves must be multiplied by the mass size distribution (not adjusted for bin width). As discussed in the previous section, there is some question as to the accuracy of the APS data acquired during these experiments. To test this, the overall sampler efficiency will be determined using both the particle size statistics measured here as well as those provided by Demmers at al. (2000).

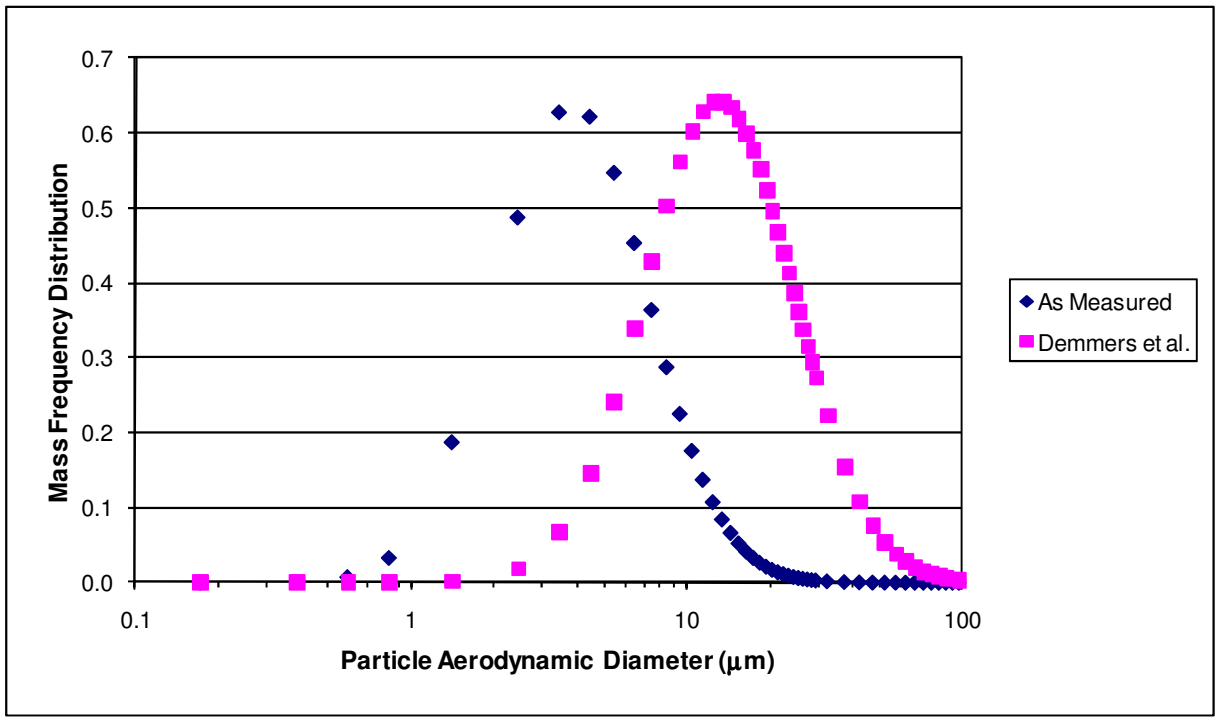

Figure 3.15 Artificial swine dust particle size distribution as measured and as reported by Demmers et al. (2000).

To determine overall efficiency of each nozzle, the mass of particles in each size range must first be determined. This was done by generating a log-normal distribution with the appropriate particle size statistics (APS or Demmers et al.) and multiplying the average dust concentration of 2.93 mg/m^3 (see Table 3.2) by the mass fraction for each bin. This data is then multiplied by the fractional efficiency of each bin as discussed above. Summing this information provides the modeled dust concentration. The results of this analysis are compared alongside the

measured results in Table 3.5. To make it easier to see the relationships, the results are also plotted against the sampling velocity in Figure 3.17, keeping in mind that the air velocity averages 2 m/s.

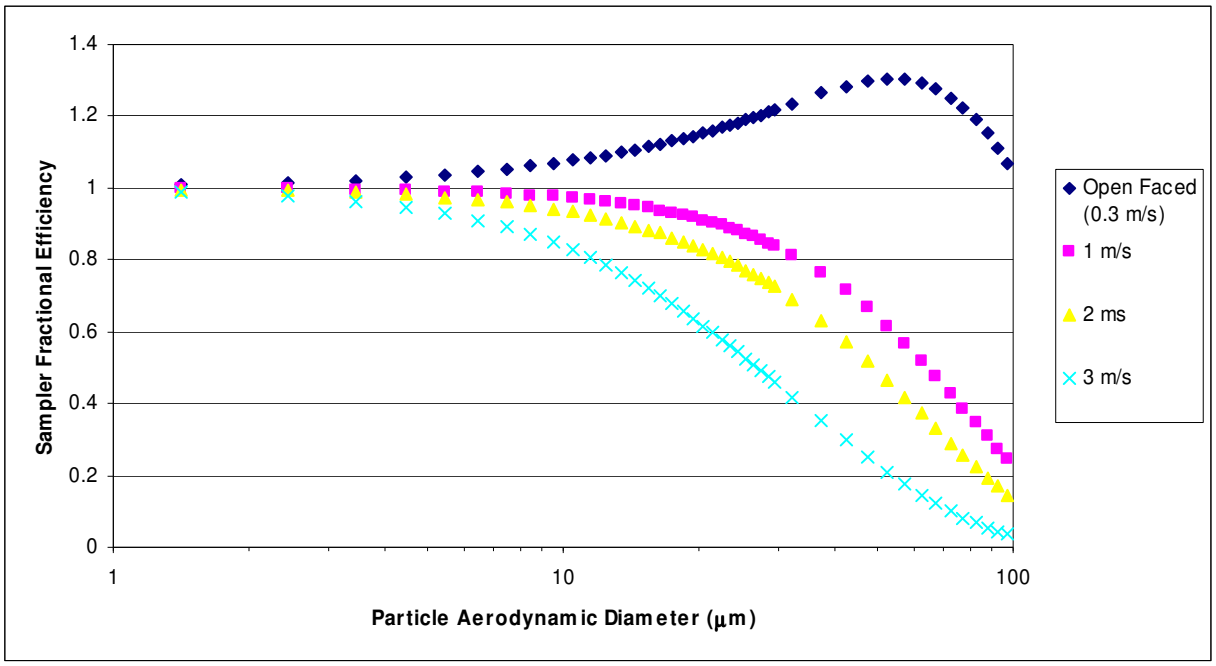

Figure 3.16 Modeled sampler efficiency for each samplers as tested, assuming isoaxial sampling.

Table 3.5 Modeling and sampling results.

Nozzle Velocity (m/s)	Dust Concentration (mg/m^3)			
	Modeled Results		Measured Results	
	APS	Demmers	Average	SD
0.3	3.02	3.28	4.06	0.96
1	2.90	2.70	3.03	0.73
2	2.86	2.52	2.51	0.55
3	2.75	2.07	2.34	0.53

The sampling results show significant variation as indicated by the large standard deviation and wide confidence intervals. This is expected since the samplers were randomly moved around the fan to remove positional bias. In addition, the dust concentration and air velocity were not expected to be perfectly constant. Figure 3.17 makes it clear that the measured results show much greater sensitivity to the sampling velocity than does the APS data. This is expected, because the models indicate that sampling efficiency is fairly steady below 10 µm. The

modeling results that are based the data provided by Demmers et al. (2000), show higher responsiveness. This seems to confirm that the data provided by the APS for this study is not accurate. In all cases the Demmers derived results are within one standard deviation of the sampled results. Statistically, they are the same, although the same could be said of the APS data if you widen the criteria to two standard deviations.

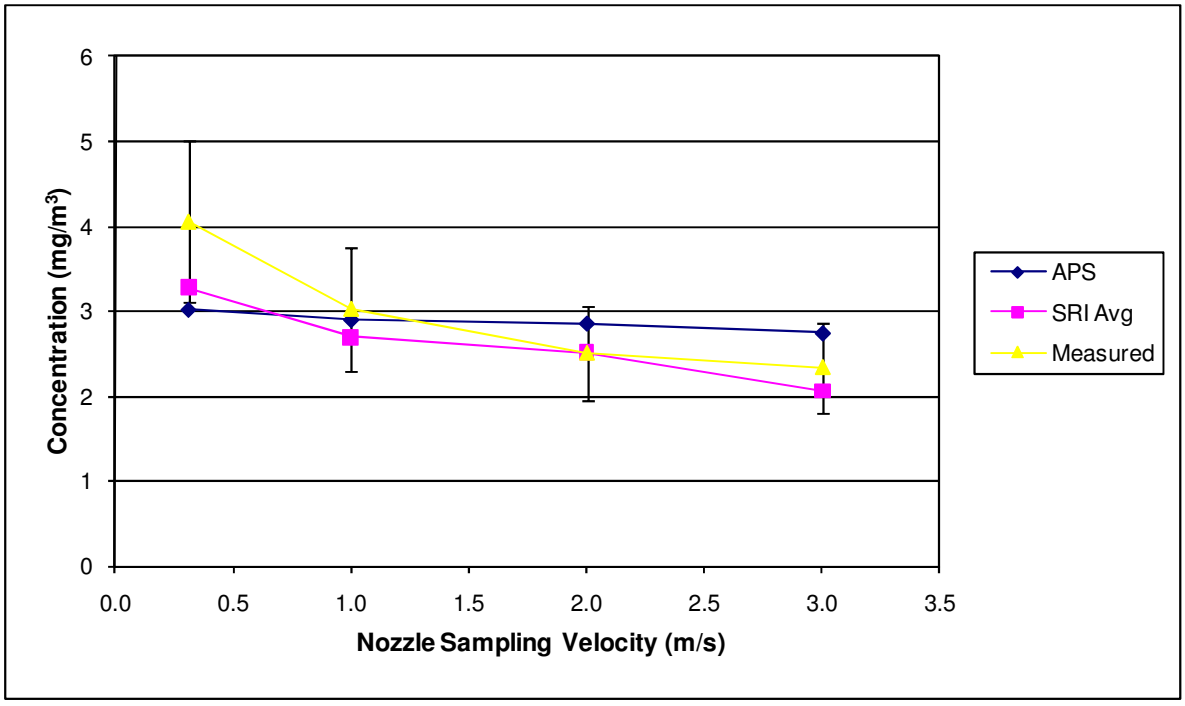

Figure 3.17 Comparison of modeling versus sampling results.

These results seem to indicate that the models perform reasonably well within this velocity range. It is apparent that as the velocities diverge from isokinetic, then the models perform increasing poorly. Baron and Willeke (2001), discuss that there is some debate about the validity of the inertial and vena contracta losses, especially for solid particles such as those used in this study. Figure 3.5 and Figure 3.6 showed the potential magnitude of these losses. If we assume that these losses are minimal, probably due to particle bounce or re-entrainment, then we get the modeled results shown in Table 3.6 and Figure 3.18.

When the inertial and vena contracta efficiencies are set to one, the modeled results are much closer to the actual results for the Demmers particle size. Again, the APS data changed very due to its small size.

Table 3.6 Modeling and sampling results assuming no inertial losses.

Nozzle Velocity (m/s)	Dust Concentration (mg/m^3)			
	Modeled Results		Measured Results	
	APS	Demmers	Average	SD
0.3	3.06	4.15	4.06	0.96
1	2.92	2.93	3.03	0.73
2	2.86	2.52	2.51	0.55
3	2.82	2.31	2.34	0.53

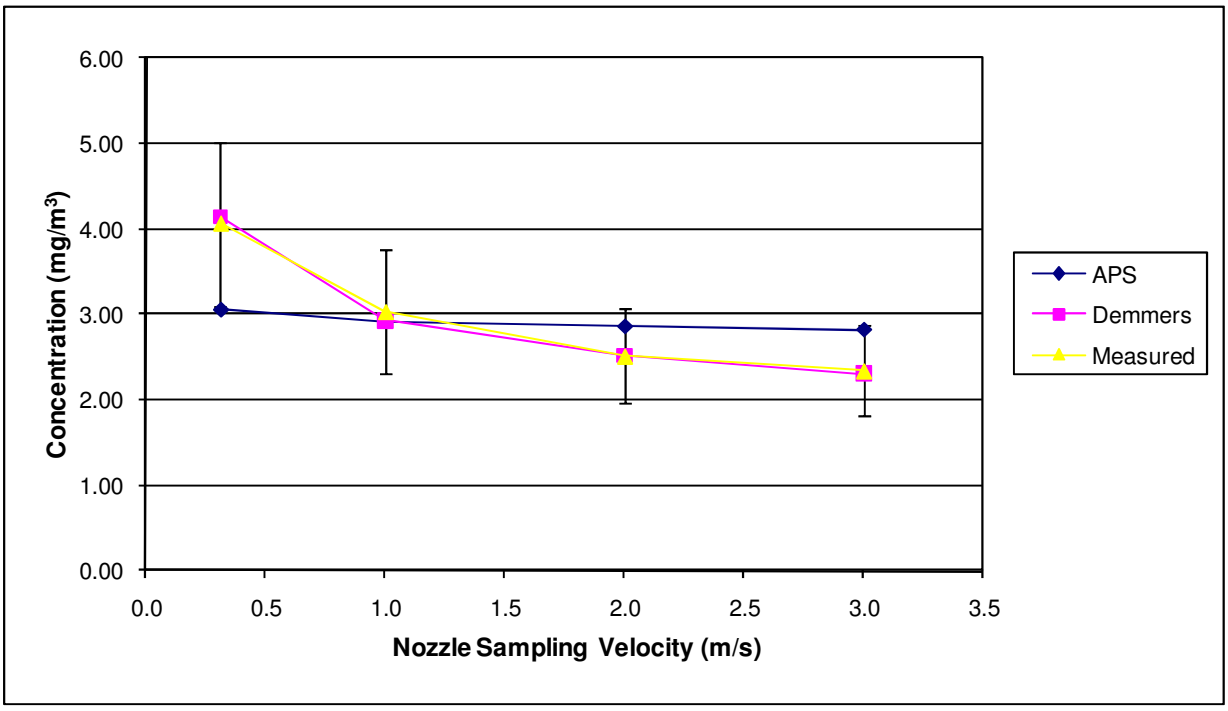

Figure 3.18 Comparison of modeling versus sampling results, assuming no inertial or vena contracta losses.

The models discussed in Chapter 2 appear to predict the nozzle performance very closely, using the following two assumptions: (1) The GMMD is about 13 µm; (2) The inertial and vena contracta losses are negligible. The first assumption certainly appears to be true. There is both evidence in the literature (Demmers at al., 2000) and in the models that indicates that the particle size provided by the APS in these experiments is too small Although there is no hard evidence of why the APS returned such a small particle size range, the literature suggests that it is due to poor sampling efficiency, especially for moving air (Baron and Willeke, 2001; Chen et al., 1998). The second assumption, of no inertial and vena contracta losses, also has some support in

the literature (Baron and Willeke, 2001). It seems reasonable to assume that some of the solid particles are likely to bounce and become re-entrained, especially larger ones. In retrospect, attempts should have been made to quantify deposition in the nozzle.

3.9 Experimental Design – Number of Samplers

The goal of these tests was to determine the number of sampling points needed to obtain an accurate sample for these 45 cm fans. To do this a total of five 2 m/s nozzles were used at the right fan. They were installed as discussed in the previous tests, with the nozzle tip at an average velocity of 2 m/s. A total of three tests were conducted so that statistics could be calculated for each location and an Analysis of Variance (ANOVA) could be conducted on the results. The average of all five points is assumed to be the most accurate concentration. Two arbitrary groupings of points were made as shown in Figure 3.19. The individual points, and grouped results, are then compared against this number to determine if there is any significant difference. All other procedures and materials match those of the previous tests.

3.10 Results – Number of Samplers

Table 3.7 shows the results for these tests. In addition to the individual sampling locations, the samplers were grouped into 3-Horizontal (3H = Left, Middle, and Right), and 3-Vertical (3V = Top, Middle and Bottom).These were compared against the average of all five samples (All). Figure 3.19 shows the layout and groupings of the samplers for these tests.

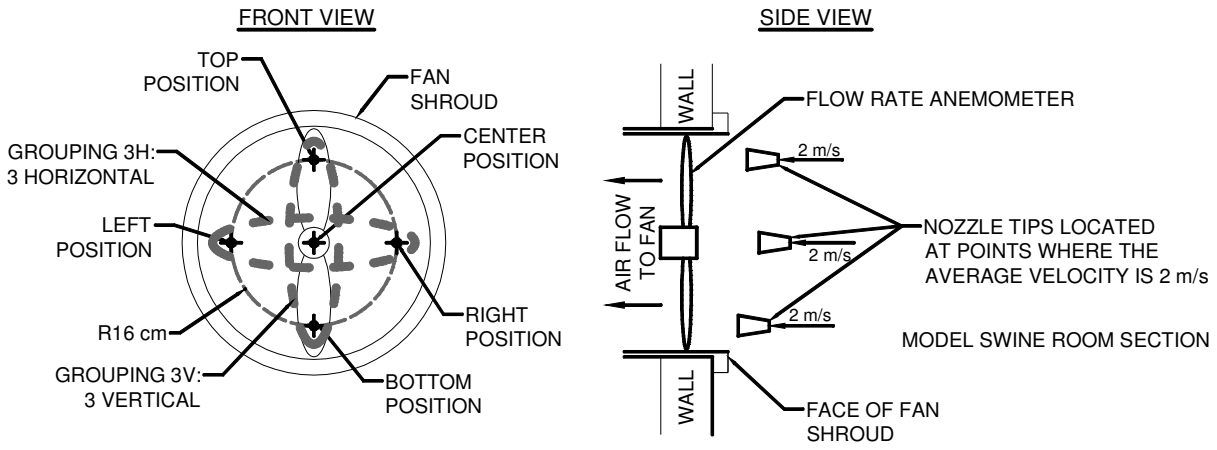

Figure 3.19 General layout of TSP samplers and grouping used for statistical analysis.

Table 3.7 Comparison of the number of samplers used to determine the average concentration.

		Measured Concentration (mg/m^3)					2 Sided
	Location	Rep 1	Rep 2	Rep 3	Average	SD	t-test*
	All	3.131	3.127	3.037	3.099	0.054	1.000
Groupings	3H	3.127	3.108	3.019	3.084	0.058	0.772
	3V	3.182	3.186	3.101	3.157	0.048	0.235
	Top	2.926	2.716	2.811	2.818	0.105	0.026
	Right	3.083	3.029	3.031	3.048	0.031	0.246
Individuals	Bottom	3.352	3.598	3.315	3.422	0.154	0.055
	Left	3.028	3.049	2.848	2.975	0.110	0.183
	Middle	3.269	3.245	3.178	3.230	0.047	0.034

* Relative to the All Grouping, which includes all five locations.

To determine the significance of these differences a two sided unequal variance t-test was conducted. This indicates the probability that the two groups came from the same distribution. Typically a value of 0.1 is used to as a cutoff point. In other words, if the two sided t-test statistic is less than 0.1, then the two groups are different. In this case, a value less than 0.1 means that using only that sampling point or sampling group will not accurately predict the true concentration as represented by the All Grouping.

Both of the groupings of three have t-stats over 0.1, indicating that they could be used with reasonable accuracy. This is certainly more true of the 3-Horizotnal samples than for the 3-Vertical ones. Three of the individual results indicate that they cannot be used, while two possibly could. Although some of the single location gave statistically accurate results, it would not be advisable to use only a single sampler. Especially since the accuracy of each location is likely to change from one fan to another and from one building to another. Based on this, it would be recommended to use at least three samplers for a 45 cm fan. For this particular fan, arranging them horizontally appears to work best, but this may not be the case for all fans. It is likely that larger fans may require more samplers, although this could not be verified during this study.

3.11 Conclusions

The TSP sampling system discussed here was easy to use and relatively inexpensive to assemble. To model the performance of the nozzles, equations from the literature were used to determine the aspiration and transmission efficiency of the each nozzle. These results were tested in an experimental model swine room section using an artificial swine dust. There were apparent

problems with the APS during these tests that caused it to report a much smaller particle size distribution than expected. It was decided to use previously reported data in addition to the measured APS data for all calculations. It was clear that the APS data was too small, since it showed very little difference in measured concentrations between superisokinetic and subisokinetic conditions. The measured data, however, showed large differences in concentration between sampling velocities. By comparison, the literature data for the swine dust particle size distribution showed better tracking with the measured results. Neither set of data matched up particularly well from a qualitative standpoint.

To improve the model performance, each portion of the model was examined. The aspiration efficiency is fairly well established. Although there is some question as to the accuracy of the gravitational losses (Baron and Willeke, 2001), the process certainly occurs. The losses associated with inertial and vena contracta parameters are more debatable (Baron and Willeke, 2001). Both of these assume that a particle that impacts on to the nozzle wall will stick. While this is generally true of liquid particles, it does not always hold true of solid particles. When these factors were removed from the models, the results for the literature data matched the measured data very closely.

Based on this comparison, it appears that the nozzle performed as modeled. This means that the equations summarized in Chapter 2, and by Baron and Willeke (2001), can be used to estimate sampler efficiency in these environments reasonably well. Future studies are recommended in wind tunnels to further confirm these results. Any future studies should also attempt to quantify the amount of dust deposited on the inside of the nozzle. This will help evaluate the transmission losses separately.

A second set of tests were conducted to determine how many samplers were required to obtain an accurate estimate of concentration. Based on these results, at least three samplers are recommended. This will likely only apply for fans of about 45 cm in diameter. Larger fans are likely to require more points. Future studies should seek to determine this for a range of fan sizes and configurations.

CHAPTER FOUR: **PARTICLE SIZING**

4.1 Objectives

The primary objective of this chapter is to assess various particle size measurement methods in CAFB. To accomplish this, the following will need to be completed:

1. Measure particle size with available instruments in a variety of different animal buildings.
2. Compare sampler performance.
3. Determine practical limitations of each instrument in an animal housing environment.
4. Determine what, if any, modifications can be made to increase the effectiveness of the instruments.

In addition to these goals, the data can also be used to obtain general information about the particle size distribution for the different building types and species.

4.2 Sampling Locations

The sampling sites were associated with Air Sampling & Measurement Methodology for Confined Animal Housing Systems (APECAB), which collected emissions measurements at a variety of swine and poultry buildings across the country (Jacobson et al., 2003; Heber et al., 2006a and 2006b). The four sites sampled here were located in Indiana, Texas, Illinois, and Minnesota. A brief description of each site is contained below, details are provided in the papers published for the APECAB project (Jacobson et al., 2003; Heber et al., 2006a and 2006b).

4.2.1 Indiana

In Indiana, emissions from a high-rise poultry layer house were sampled. The building housed about 250,000 birds and was approximately 100 m long and 30 m wide. The exhaust fans and sampling equipment were located in the ground level manure storage pit. These buildings have on the order of 100 exhaust fans. Only a single constantly running fan was sampled. The sampling location was collocated with other gas and particle sampling equipment as well as environmental monitors. This site was sampled in February 2004.

4.2.2 Texas

A swine finishing barn was sampled in Texas. The equipment was located upstream of the constantly running primary exhaust fan in an empty pen. The same additional equipment was already sampling at this location as in Indiana. Samples were collected in early March 2004.

4.2.3 Minnesota

The Minnesota site consisted of a gestation barn, a breeding barn and several farrowing rooms. These samples were collected near the primary constantly running exhaust fan. This site was sampled in early April 2004.

4.2.4 Illinois

The Illinois site consisted of a swine farrowing building with several rooms and a breeding and gestation building. Samples were collected in one of the gestation rooms at the primary running fan in an empty pen. These samples were collected in June 2004.

4.3 Equipment

The operating principle of most of the particle sizing equipment has been discussed in the literature review section so a simple list of the models and modifications will be discussed here.

4.3.1 TSP

At most of the sites, the TSP system described in Chapter 3 was used. The operating methods are essentially the same except that the sampling time was adjusted to match the other samples being collected simultaneously.

Open faced filter holders facing upward were also used to obtain TSP samples. These were generally located in areas of slow moving air upstream of the primary exhaust fan. They consisted of a 37 mm filter holder upstream, with flow controlled by a 21 lpm critical venturi. Two types of filters were used, the first was the basic glass fiber filter and the other was a Teflon membrane filter. The glass fiber was for basic gravimetric analysis while the Teflon filters were for Coulter analysis. Most of the time, two of each filter were collected during each sampling period.

4.3.2 Cascade Impactor

An Andersen Six Stage Viable Impactor (Thermo Fisher Scientific Inc., Waltham, MA) was modified to obtain gravimetric samples. This viable impactor is a multi-stage, multi-orifice impactor that typically uses a petri dish filled with agar to collect viable samples for microbiological studies. The size ranges for the stages in this instrument are from 0.65 μm to 7 μm. For this study, the petri dishes were instead filled with epoxy so that when the substrate was added the jet to plate distance was correct. Thick aluminum foil was used as an impaction substrate. Circles were cut from the foil by hand and each one was coated with a silicone lubricant spray to minimize particle bounce. The spray was allowed to dry for several days to before conditioning and weighing.

4.3.3 Dichotomous Sampler

An Anderson Dichotomous Sampler was used to obtain PM 10/2.5 measurements. Teflon membrane filters with a polypropylene support ring were used for collecting the dust samples.

4.3.4 Real Time Instruments

Two TSI instruments were used, the APS 3321 and the Aerosizer DSP. As discussed previously, it has been shown that the APS has a poor sampling efficiency for particles above 10 μm. Prior experience indicated similarly poor sampling efficiencies for the Aerosizer due to its small sampling inlet. To remedy this, a flow dividing system was constructed to increase the flow rate for each instrument.

Figure 4.1 shows a drawing of the flow divider constructed for the Aerosizer. The total flow rate is approximately 20 lpm. This consists of the 5 lpm for the sample and 15 lpm for sheath air supply for the Aerosizer. The larger tube is sharp edged and the diameter was chosen so that the velocity in the larger tube matched that of the sampling nozzle. This creates an isokinetic situation where particle sampling should be optimal. The isokinetic sheath nozzle was designed to fit onto the existing hardware. The distance between the entrance of the large tube and the small tube was chosen to be larger than two diameters (of the larger tube) to allow for better flow development. About two diameters (of the larger tube) were allowed beyond the entrance of the small tube to help prevent downstream obstacles from affecting the flow field

around the entrance of the smaller tube. The sampling pump pulled air from both sides of the base of the larger tube to even out the flow patterns.

A similar system was created for the APS, but with a larger outer tube to match the sampling velocity of the APS. The sample flow was 5 lpm, as controlled by the APS, while the sheath flow was 21 lpm as controlled by a critical venturi for a total of 26 lpm.

For both instruments these isokinetic flow dividing nozzles increased the number of larger particles substantially. This is expected since increasing the flow rate tends to increase the number of larger particles sampled. The instruments primary nozzle then collects an isokinetic sub-sample. Without the flow splitter most of the larger particles are unable to get into the relatively small openings of the instruments' primary nozzles.

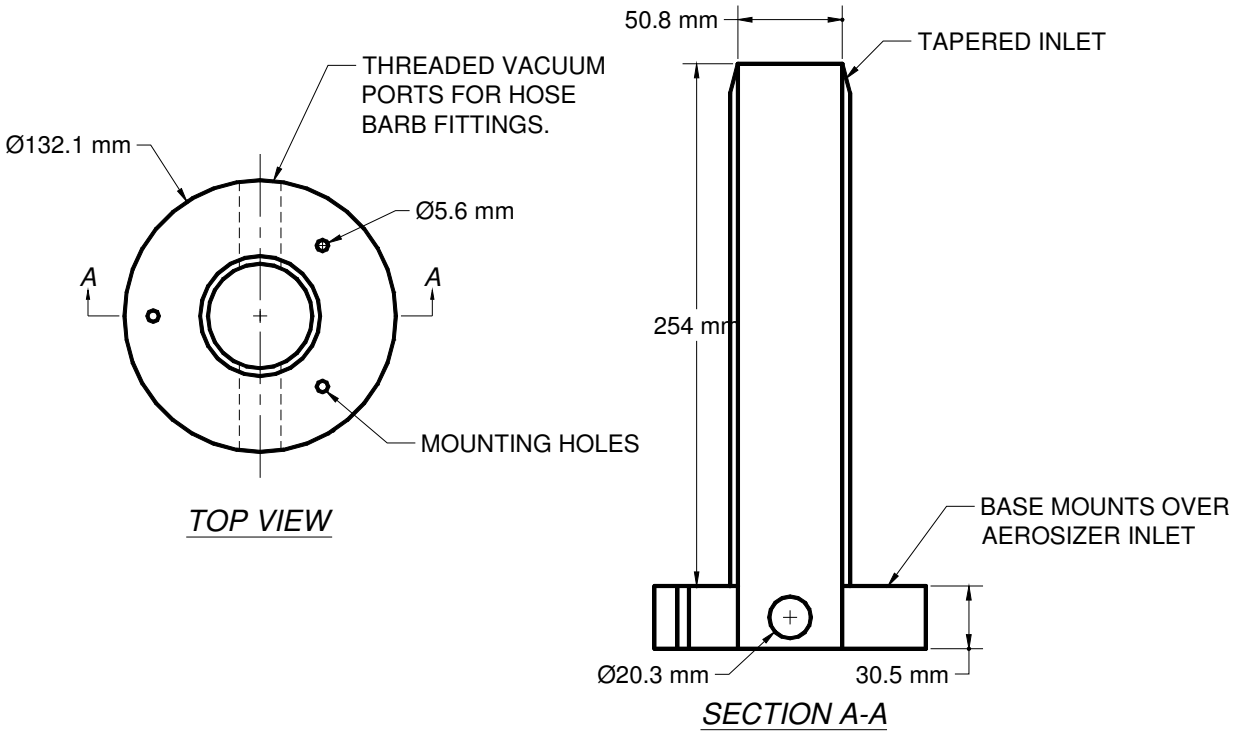

Figure 4.1 DSP flow dividing intake nozzle.

4.3.5 Coulter Multisizer

A Coulter Multisizer 3 was used to analyze the Teflon TSP filters. A 100 μm tube was used to capture most of the range of particles, which yields an effective range of 3 μm to 60 μm. The electrolyte chosen is a lithium chloride salt dissolved in methanol. This electrolyte has been

shown to be effective for sensing agricultural dusts since it does not cause swelling of organic particles. An ultrasonic bath was used to remove particles from the membrane filters and deagglomerate them.

4.4 Methods

4.4.1 Filters

Filters were handled as described in Chapter 3. The dichotomous filters and the cascade impactor substrate were handled in a similar method, except that they were weighed without a container or holder. During storage and transport they were kept in an appropriately sized petri dish. For all filters and substrates a goal of 15% field blanks was used.

4.4.2 Sampling Times

Sampling times were somewhat determined by practical considerations such as having to shower in and out of the buildings, driving distance, etc. It was found that eight hours was the maximum practical limit for sampling before most of the instruments became overloaded. Generally the filters were changed early in the morning, again early in the afternoon and a final time late in the evening. This typically led to sampling times of approximately six to eight hours during the day and about nine to ten hours at night when concentrations were lower. During the early sampling trips, longer sampling times were attempted, but the filters were severely overloaded.

4.4.3 Real Time Data

The Aerosizer and APS were used to collect real time data. The sampling time for each instrument was set to 20 or 30 second. This was thought to be long enough to obtain a fairly smooth representative mass size distribution with few spikes or holes in the data. Typically the Aerosizer was set to collect ten samples while the APS collected five samples.

With the Aerosizer, the data was automatically saved as a mass size distribution with the units of “Percent in Size Range.” The APS data was exported as “Number in Size Range.” The data for each instrument was then manipulated in an Excel spreadsheet with the help of Visual Basic for Applications (VBA). This process was discussed in Chapter 2 and will be further discussed in the results section below.

4.4.4 General Sampling Procedures

After arriving at the sampling site, a couple of hours would be spent setting up the equipment. The majority of the equipment was located near the primary, constantly running exhaust fan, but in an area of "calm" air. Where needed, the flow rates were checked using a BIOS Dry Cal 2 flow calibrator (Bios International Corporation, Butler, NJ). Power was typically supplied by a gasoline generator since most sites could not provide the 30 amps that could be required by the equipment.

The pumps and generator were typically located outside of the building with the tubing and power cords run inside. This was done for biosecurity reasons since all of the wetted surfaces could not be cleaned sufficiently.

Once all of the equipment was set-up and verified, filters would be loaded, including the blanks. Samples would be collected with the real time instruments and then the gravimetric samplers were started and the relevant data recorded. After the allotted sampling time, the gravimetric samplers were stopped and the real time instruments were started. While they were warming up, the filters were changed. The process was then repeated. Generally about three days were allotted for sampling, although actual times varied depending on the quality of data collected and equipment problems.

4.4.5 Methods of Comparison

There are many ways of comparing particle size distributions from different instruments. When the particles follow a standard distribution, they can be described by just a few parameters that can be found using statistics. Unfortunately this is not always the case. Because of the variety of particle sizes, distributions and instruments, this chapter will utilize some simplified versions of the methods discussed in Chapter 2.

The particle size distributions will first be displayed in a standardized form so that their general shape can be examined. A cumulative distribution will follow allowing for a more quantitative comparison of the fraction of particles below each size. Although the particles may not necessarily fit a log-normal distribution, the basic statistics of this distribution will be calculated. These will include some key points in the cumulative distribution, like the D16, D50 and D84. The D50 corresponds to the median diameter and the others can be used to calculate

the GSD as shown in Equation 2-8. If this equation does not hold true then the distribution is likely not log-normal.

Most comparisons of the particle size distributions will be made a composite basis, using all of the data collected at a site to make one sample. This is accomplished by adding all of the particles in each bin (size range) together. This helps average the results and smooth out irregularities in the data. When available, the groups of samples collected at certain times will be compared to evaluate whether there is an apparent trend between particle size and time of day.

4.4.6 Size Ranges

Each instrument has a different size range which makes comparison difficult. The number of data bins shows the general resolution of the data, where the more data bins there are, the finer the detail of the particle size distribution. Generally there are more bins at the smaller particle sizes and fewer as the particle size increases.

The size range is standard for each instrument except the Coulter. The Coulter has various orifices which can be changed out to target certain particle sizes. In this case a 100 μm orifice was chosen because it was likely to capture the larger particles, which were of more interest. The trade off is that you lose the ability to detect particles at the lower end of the spectrum. Although analyzing with a smaller orifice would extend the range down to about 1 μm, it would also likely result in larger particles clogging the orifice. Merging data from two different orifices can also prove problematic. The effects of this decision will be seen in the Results and Discussion sections.

All results will be compared with the full range of data for each instrument. This naturally skews the results lower for instruments that are not able to detect larger particles. A second comparison will be made with the data trimmed so that all instruments will effectively have the same size range. This allows for a more direct comparison of the actual sampler performance in measuring the same particle size.

4.5 Results and Discussion

4.5.1 Practical Performance

A practical evaluation of the instruments is warranted since this can greatly affect their accuracy and general usability in the field environment. Most of the instruments tested were

intended for ambient sampling and/or indoor use where the particle concentrations are expected to be relatively low. In most of the animal buildings tested, the dust concentration was much higher than ambient air. As a result, many of the instruments failed to work properly due to overloaded filters and clogged jets.

4.5.1.1 Dichotomous Sampler

The primary problem with this instrument was overloading of the filter. Because the filter was a Teflon membrane it did not capture and hold the dust, instead the dust simply sits on the filter. Even with our shortest sampling time of five hours there was still so much dust on the coarse filter that the dust cake would easily fall off during handling. This made obtaining an accurate measurement of the dust weight nearly impossible. Shorter sampling times would have solved this problem, but would have reduced the amount of dust on the fine filter to below the detection threshold.

Additionally there were problems with the equipment. During sampling, the capacitor of the sampling pump failed. After replacing the capacitor, water from the condensation jars in the sampling plumbing worked its way into the flow control system. During the next sampling trip we were unable to maintain a consistent flow rate, even after the water appeared to have evaporated. As a result, because of these two factors there is no useful data from this instrument.

4.5.1.2 Cascade Impactor

As discussed in the Equipment Section, a viable cascade impactor was adapted for use as a non-viable gravimetric impactor. Several problems arose with this instrument. Initially the petri dishes used to hold the impaction substrate had to be modified to hold the substrate at the proper height. This was done using an epoxy, but filling to the proper height proved to be difficult, but probably not much more difficult than normally experienced with the agar.

A suitable impaction substrate was difficult to find since the literature has indicated that the filters offered by the manufacturer are not suitable (ACGIH, 2001; Baron and Willeke, 2001). As a result, most authors – including this one – have attempted to make their own. In this case, a thick aluminum craft foil was used since it remained rigid when handling but was relatively easy to work with. A silicone spray was used to prevent particle bounce. It proved difficult to keep the foil completely flat since it came in rolls and tended to wrinkle during cutting. It was also difficult to apply an even coating of the silicone oil spray.

The primary problem with the cascade impactor was overloading of the upper stages. The first couple of stages of the impactor quickly became overloaded because of the larger size of the agricultural dust. As a result, it was impossible to obtain measurable quantities of dust on the lower stage without overloading the top stages. In the Indiana poultry layer building the jets of the first stage also clogged with fine feather material, thus throwing off the entire stage calibration.

4.5.1.3 Open Faced TSP

These samplers seemed to work fine, except for the possibility of being contaminated by larger objects such as feathers and insects, but this was not a noticeable problem during these sampling trips. Similar problems as those of the dichotomous sampler were experienced with relation to the Teflon membrane filters. The dust cake could easily fall off during handling. Because of this, the gravimetric results from the Teflon filters were not considered. Coulter analysis of these filters will be included since the size analysis should not be significantly affected if some of the dust cake is lost. The TSP sampler has a 30% higher sampling efficiency compared with the TEOM TSP samplers in field tests (Jerez et al., 2006). And in the controlled laboratory wind tunnel conditions, the TSP samplers had a 92% sampling efficiency compared with 60% sampling efficiency using coarse testing dust (Arizona Road Dust A4) under typical animal building exhaust fan flow conditions (Brem and Zhang, 2008).

4.5.1.4 Real Time Devices

The real time devices such as the Aerosizer DSP and the APS generally performed well, except for one malfunction of the Aerosizer. Despite this these instruments are not well suited for use in the field. They are very expensive and sensitive electronic devices. Great care had to be taken to protect the instruments from the animal environment. Because of this, it is not recommended that these types of instruments be used for routine monitoring in the field.

4.5.2 Instrumentation Comparison

As discussed previously, the sized data from most of the gravimetric instruments was not reliable and, therefore, will not be discussed here. Instead, comparisons will be made between the Aerosizer, APS, Coulter, and Malvern results as available. Malvern results are only available for the Minnesota site due to problems with sample handling. There was an equipment

malfunction with the Aerosizer during the Indiana sampling trip so no data will available from it at this site. All other sites have results for the Aerosizer, APS and Coulter. The results from each site will be discussed individually.

4.5.2.1 Illinois Results

The results from the sampling at the swine farrowing room in Illinois can be seen in Figure 4.2. At first glance it is clear that the distributions are not log-normal. With the exception of the Coulter, the distribution appears to have two or three modes. This could likely be due to multiple particle sources, such as skin cells and feed particles. Each of these may follow a log-normal distribution, but when added together the resulting distribution is not easily described. This makes simple comparisons of statistics difficult and dictates a more qualitative approach. One thing that is clear is that the Coulter reported the largest particle size distribution, while the APS reported the smallest distribution. This can be confirmed more easily in the cumulative particle size distribution shown in Figure 4.3.

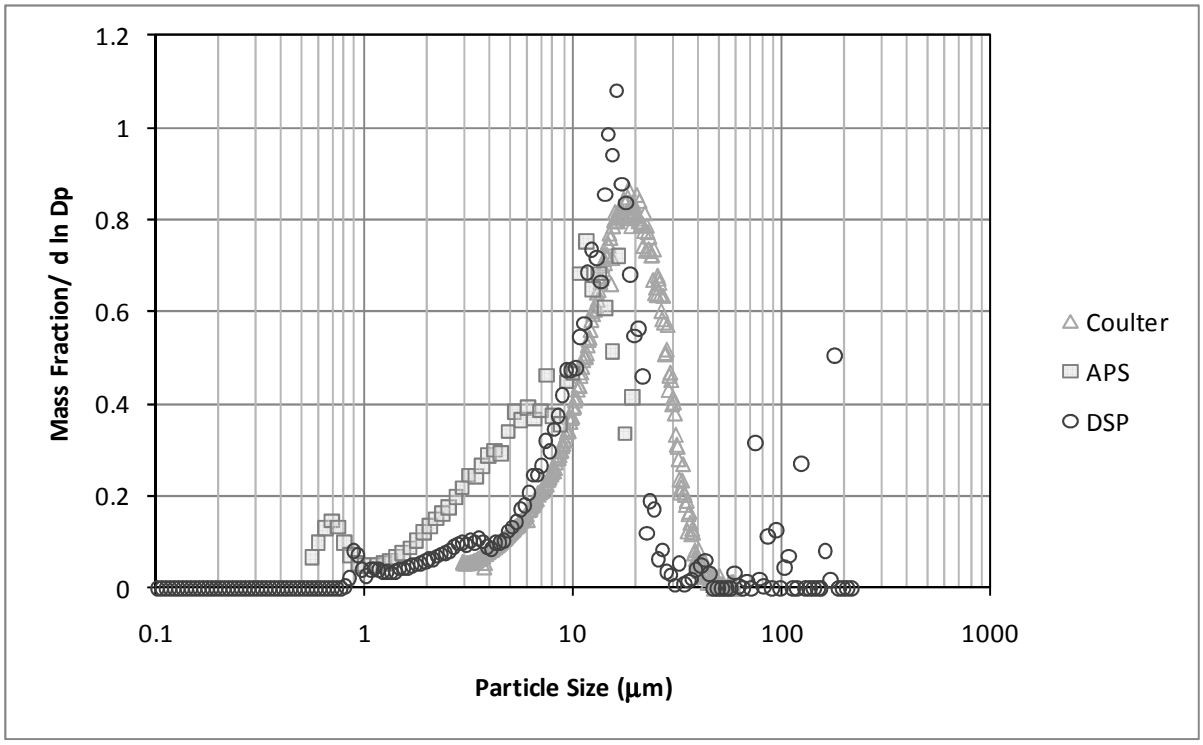

Figure 4.2 Particle size results for a swine farrowing room in Illinois.

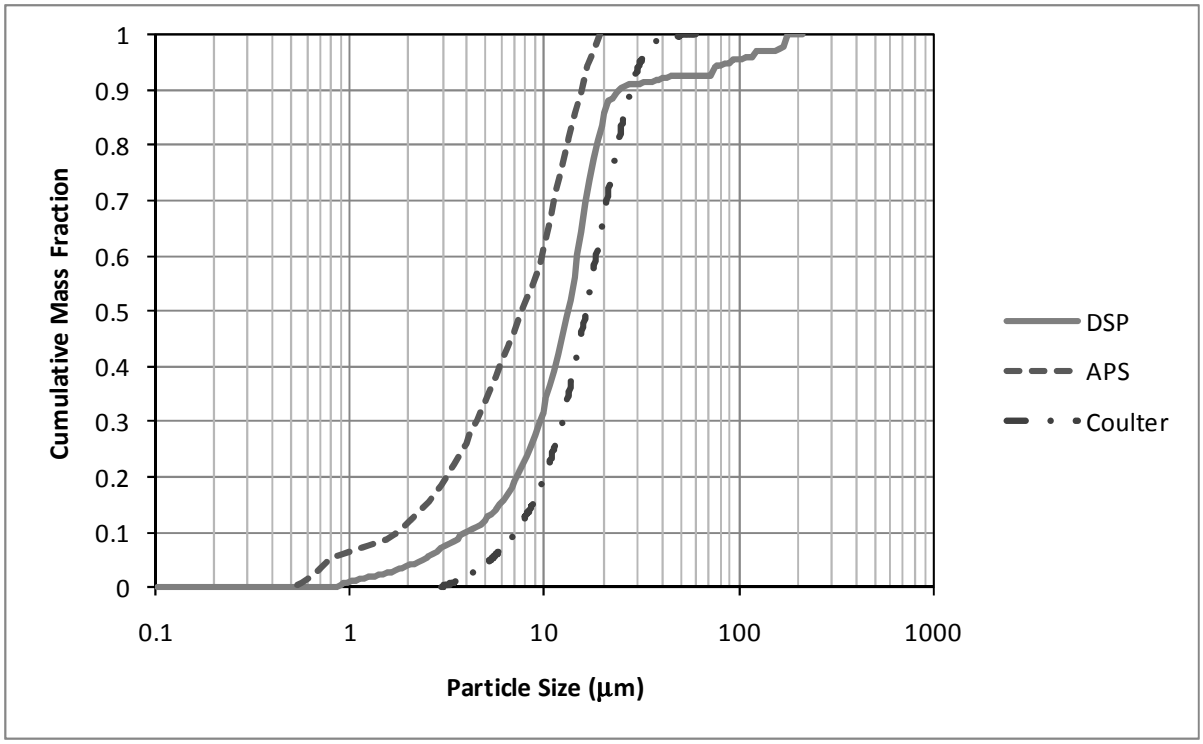

Figure 4.3 Cumulative particle size distribution for the swine farrowing room in Illinois.

The cumulative distribution confirms the general trend that the APS reports the smallest distribution and that the Coulter reports the largest. There is a small exception at the upper end of the DSP distribution. This appears to be more related to the noise at the upper end of the DSP distribution. These points do not appear to be part of a greater trend, but are more likely to be random large particles, which because of their relatively large mass, can skew the distribution.

There is also some noise at the upper end of the APS distribution. This is more likely either due to an inadequate sampling time or problems with collecting these larger particles. Even though an attempt was made to improve the sampling efficiency, it is likely that there is still some difficulty in obtaining and measuring particles at the upper end of this instrument's capabilities. The DSP data was trimmed of the noisy particles above 40 µm, the results of which can be seen in Figure 4.4 and Figure 4.5.

Once the outliers have been removed the cumulative distribution shows clearly that the Coulter distribution is larger than the DSP. The size limits for each instrument are also playing a role. Since the Coulter readings do not start until about 3 µm, it will be skewed higher than the APS and DSP, which both report readings well below this. At the upper end of the range, the fact

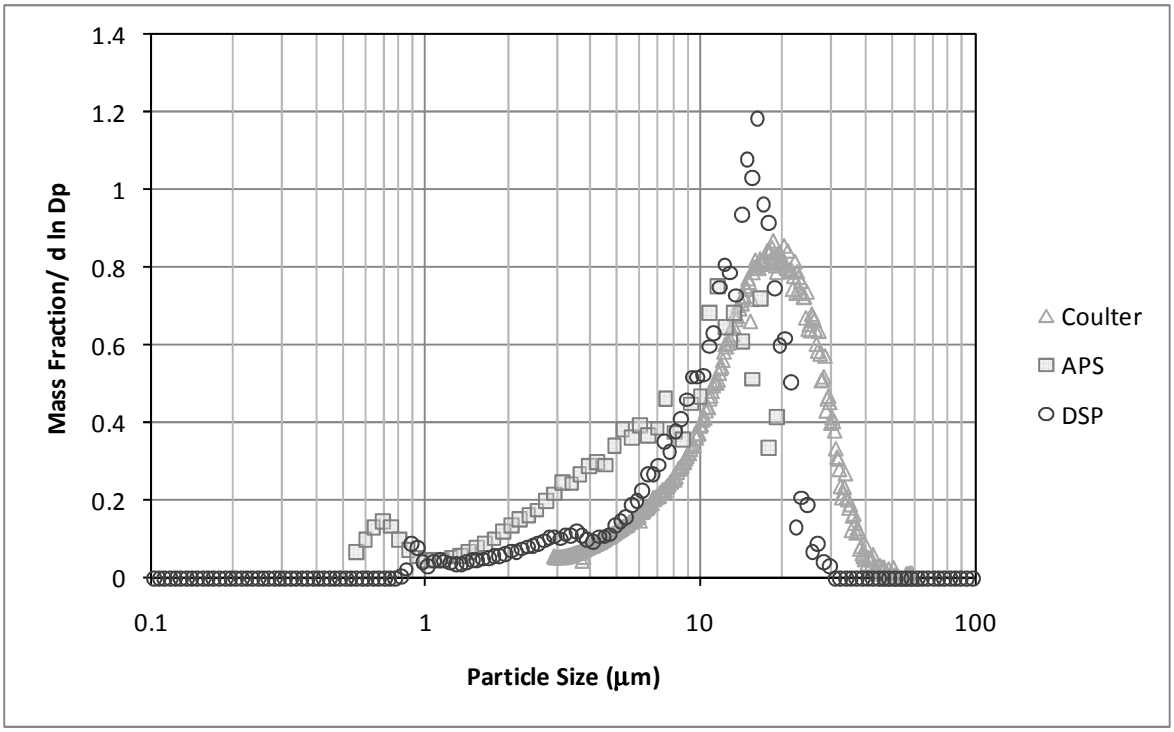

Figure 4.4 Particle size distribution with DSP outliers removed for the Illinois site.

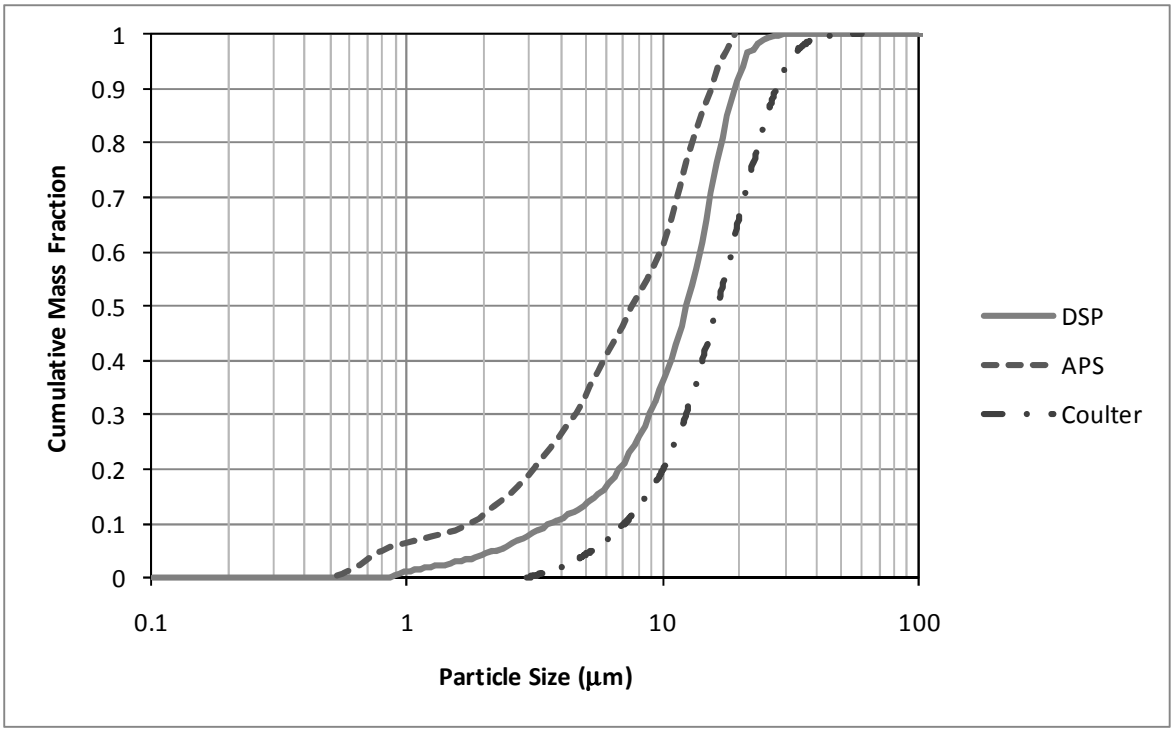

Figure 4.5 Cumulative particle size distribution with DSP outliers removed for the Illinois site.

that the Coulter and DSP can sample larger particles naturally skews them higher than the APS, which must reach 100% by about 20 μm. This is an inherent problem for any instrument whose effective range does not completely cover the particle size range of interest. To compare the actual performance over a given size range, all data below the Coulter range and above the APS range was removed. A new cumulative distribution was generated as shown in Figure 4.6.

By removing the differences due to size limits, the cumulative distribution changed noticeably. While the APS is still clearly lower, due mostly to the second mode around 6 μm, the DSP and Coulter results now closely match each other. The Coulter continues to be slightly larger, but the general performance is very comparable to the DSP. This shows that the effective range of the instrument can significantly impact the perceived results.

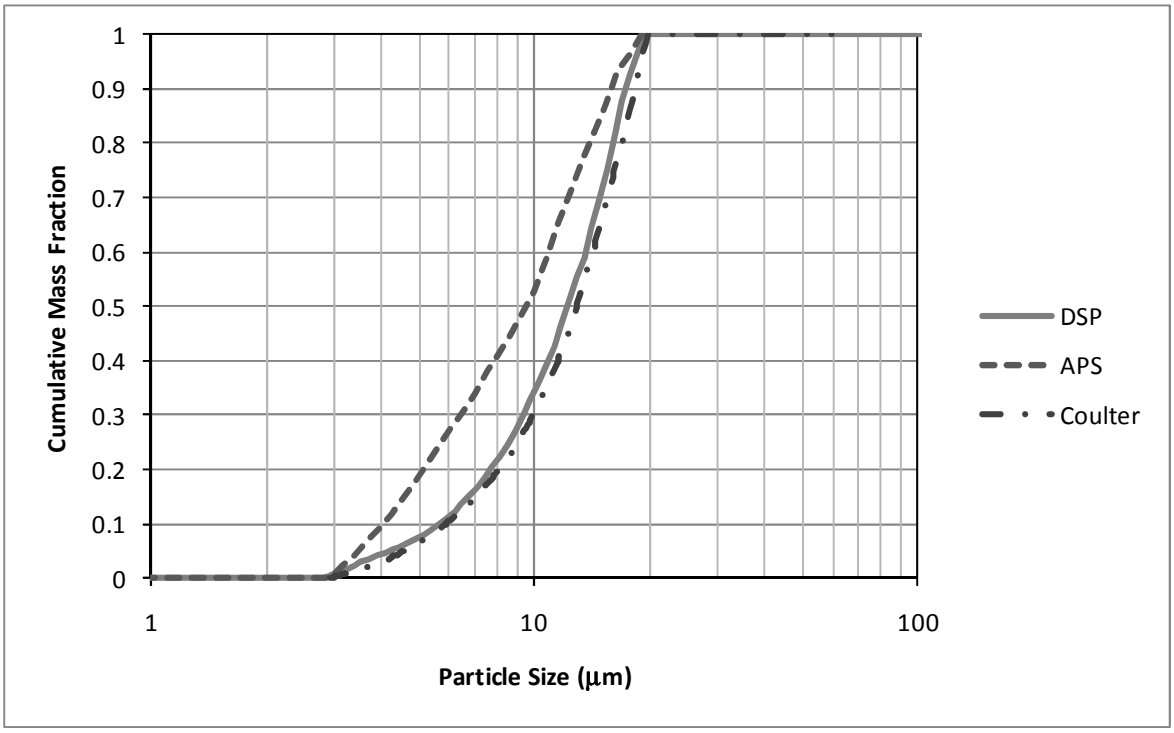

Figure 4.6 Cumulative particle size distribution with all data trimmed the same size range.

A more quantitative view of the results can be found in Table 4.1, which shows the particle size statistics for the data. This table contains all of the data, both combined (each bin summed together), as well as the composite data collected at each time period. Five APS samples and fifteen DSP samples were collected at each time period. Only one composite Coulter value is

reported because of the Coulter samples were collected over several hours and do not necessarily correspond to the grab samples of the real-time instruments.

Table 4.1 Particle size statistics for the Illinois site with all data included.

	Date Time	6/8/2004 2:55:00 PM	6/8/2004 8:59:33 PM	6/9/2004 2:31:44 PM	6/10/2004 10:20:16 AM	Average	Standard Deviation	All Data Combined
APS - All Data	$D_{15.9}$	2.16	1.58	2.51	3.55	2.45	0.83	2.68
	D_{50} (GMMD)	5.82	5.40	8.27	9.27	7.19	1.88	7.85
	$D_{84.1}$	12.98	12.90	14.49	15.16	13.88	1.12	14.48
	$GSD = (D_{84.1}/D_{15.9})^{1/2}$	2.45	2.85	2.40	2.07	2.44	0.32	2.32
	$GSD = D_{84.1}/D_{50}$	2.23	2.39	1.75	1.64	2.00	0.37	1.84
	$GSD = D_{50}/D_{15.9}$	2.69	3.41	3.30	2.61	3.00	0.41	2.93
DSP - All Data	$D_{15.9}$	6.46	3.68	6.54	8.31	6.24	1.91	6.30
	D_{50} (GMMD)	12.87	10.87	14.72	16.36	13.71	2.37	13.39
	$D_{84.1}$	17.63	15.97	21.49	120.38	43.87	51.06	20.23
	$GSD = (D_{84.1}/D_{15.9})^{1/2}$	1.65	2.08	1.81	3.81	2.34	0.99	1.79
	$GSD = D_{84.1}/D_{50}$	1.37	1.47	1.46	7.36	2.91	2.96	1.51
	$GSD = D_{50}/D_{15.9}$	1.99	2.96	2.25	1.97	2.29	0.46	2.13
DSP - Outliers Removed	$D_{15.9}$	6.41	3.68	6.13	6.94	5.79	1.45	5.87
	D_{50} (GMMD)	12.77	10.87	13.82	13.90	12.84	1.41	12.58
	$D_{84.1}$	17.41	15.97	19.38	19.40	18.04	1.67	18.00
	$GSD = (D_{84.1}/D_{15.9})^{1/2}$	1.65	2.08	1.78	1.67	1.80	0.20	1.75
	$GSD = D_{84.1}/D_{50}$	1.36	1.47	1.40	1.40	1.41	0.04	1.43
	$GSD = D_{50}/D_{15.9}$	1.99	2.96	2.25	2.00	2.30	0.45	2.14
Coulter - All Data as One Composite Sample	$D_{15.9}$	--	--	--	--	--	--	8.92
	D_{50} (GMMD)	--	--	--	--	--	--	16.39
	$D_{84.1}$	--	--	--	--	--	--	25.31
	$GSD = (D_{84.1}/D_{15.9})^{1/2}$	--	--	--	--	--	--	1.68
	$GSD = D_{84.1}/D_{50}$	--	--	--	--	--	--	1.54
	$GSD = D_{50}/D_{15.9}$	--	--	--	--	--	--	1.84

It is generally recognized that the time of flight instruments (APS and DSP) will generally yield lower particle size results because they tend to overcompensate for particle drag (Baron and Willeke, 2001). This is because both instruments operate outside of the Stokes region, thus skewing the definition of the aerodynamic diameter. It is also recognized that the Coulter is expected to report undersized particles since it cannot account for particle shape (Baron and Willeke, 2001). At least one study has been published that has confirmed these trends, showing that the Coulter reported larger particle sizes than the APS (Chung and Thompson, 1989).

The performance difference between the APS and DSP is more difficult to decipher. Due to the difference in flow regimes in the two instruments (APS is subsonic while the DSP is

supersonic), it is expected that each instrument will perform differently with irregularly shaped particles. The extent of these differences is not well documented (Baron and Willeke, 2001). Some of these differences could be in the way each instrument detects particles and handles noise in the detection system. The APS uses a single clock system, so that any false signals tend to be concentrated. On the other hand, the DSP uses four different detectors so that the noise is fairly even throughout its detection range (Baron and Willeke, 2001). This might also explain why there is much more noise at the upper end of the DSP particle size range, where even a single phantom particle can show up in the mass distribution.

There is not enough data to spot any real trends in the data with time. It appears that the data collected in the late evening, after the lights were turned out, showed lower particle sizes than the daytime data. This is expected considering that the animal activity would be lower at night, thus generating less dust and allowing the larger particles to settle.

The statistical data also confirms the general trend of the Coulter reporting the largest particles while the APS reports the smallest. It is also evident that none of the measured distributions are log-normal since the various GSD calculations vary significantly. To evaluate the impacts of trimming the data to the same size range, as seen in Figure 4.6, the statistics were recalculated as shown in Table 4.2.

Forcing the size ranges to be equal brings the statistics much closer together. This is especially true of the Coulter and DSP data which are very similar throughout their range. As expected, the APS data is still substantially lower due to the mid range peak that was not as noticeable in the DSP and Coulter data.

4.5.2.2 Minnesota Results

Data was available from the APS, DSP and Coulter at the Minnesota swine breeding facility. Figure 4.7 shows the particle size distributions measured at the swine gestation barn. The APS and Coulter both show bimodal distributions, although the modes are at different locations. On the other hand, the DSP distribution appears to have only a single mode, generally in line with the Coulter's bimodal distribution. As at the Illinois site, the APS data has a peak near 6 μm that is not present in the data of the other instruments. This, in addition to the APS upper size limit, results in a generally smaller particle size distribution. There is substantial noise at the upper end of the DSP, which again does not appear to be part of a larger mode.

Table 4.2 Particle size statistics for the Illinois site trimmed to equal size ranges.

	Date	6/8/2004	6/8/2004	6/9/2004	6/10/2004		Standard	All Data
	Time	2:55:00 PM	8:59:33 PM	2:31:44 PM	10:20:16 AM	Average	Deviation	Combined
APS	$D_{15.9}$	4.29	4.21	4.87	5.24	4.65	0.49	4.87
	D_{50} (GMMD)	7.88	8.23	10.66	10.41	9.30	1.44	9.89
	$D_{84.1}$	13.81	15.66	15.22	15.94	15.16	0.95	15.26
	$GSD = (D_{84.1}/D_{15.9})^{1/2}$	1.79	1.93	1.77	1.74	1.81	0.08	1.77
	$GSD = D_{84.1}/D_{50}$	1.75	1.90	1.43	1.53	1.65	0.21	1.54
	$GSD = D_{50}/D_{15.9}$	1.84	1.95	2.19	1.99	1.99	0.15	2.03
DSP	$D_{15.9}$	7.69	7.01	6.45	7.10	7.07	0.51	7.08
	D_{50} (GMMD)	12.71	11.69	13.00	13.10	12.63	0.64	12.48
	$D_{84.1}$	16.40	16.15	17.46	17.80	16.95	0.80	16.88
	$GSD = (D_{84.1}/D_{15.9})^{1/2}$	1.46	1.52	1.64	1.58	1.55	0.08	1.54
	$GSD = D_{84.1}/D_{50}$	1.29	1.38	1.34	1.36	1.34	0.04	1.35
	$GSD = D_{50}/D_{15.9}$	1.65	1.67	2.01	1.84	1.79	0.17	1.76
Coulter	$D_{15.9}$	--	--	--	--	--	--	7.25
	D_{50} (GMMD)	--	--	--	--	--	--	12.96
	$D_{84.1}$	--	--	--	--	--	--	17.52
	$GSD = (D_{84.1}/D_{15.9})^{1/2}$	--	--	--	--	--	--	1.55
	$GSD = D_{84.1}/D_{50}$	--	--	--	--	--	--	1.35
	$GSD = D_{50}/D_{15.9}$	--	--	--	--	--	--	1.79

Figure 4.8 shows the cumulative distribution for the same data. It is clear that the APS is consistently lower than the other instruments. The noise in the DSP distribution is apparent at the upper end, which pushes it above the Coulter. To evaluate this impact the same data was trimmed at 40 μm and the results displayed in Figure 4.9 and Figure 4.10. These figures show a cleaner distribution where the DSP and Coulter criss-cross each other due to the bimodal nature of the Coulter data. This can also be seen in the particle size statistics included in Table 4.3. Here the DSP and Coulter have comparable D50 values, but the ends of the distributions (D16 and D84) are considerably different.

The readings from the three distributions were again trimmed to reduce the impact of the instrument boundaries. Figure 4.11 shows the resulting cumulative distribution. It is clear that the APS still reports the smallest distribution, principally due to the lower first peak. Once trimmed, the Coulter appears to produce a much smaller distribution than the DSP. This is due to the bimodal distribution being effectively split in the middle, while the DSP distribution occurs principally below the 20 μm cutoff.

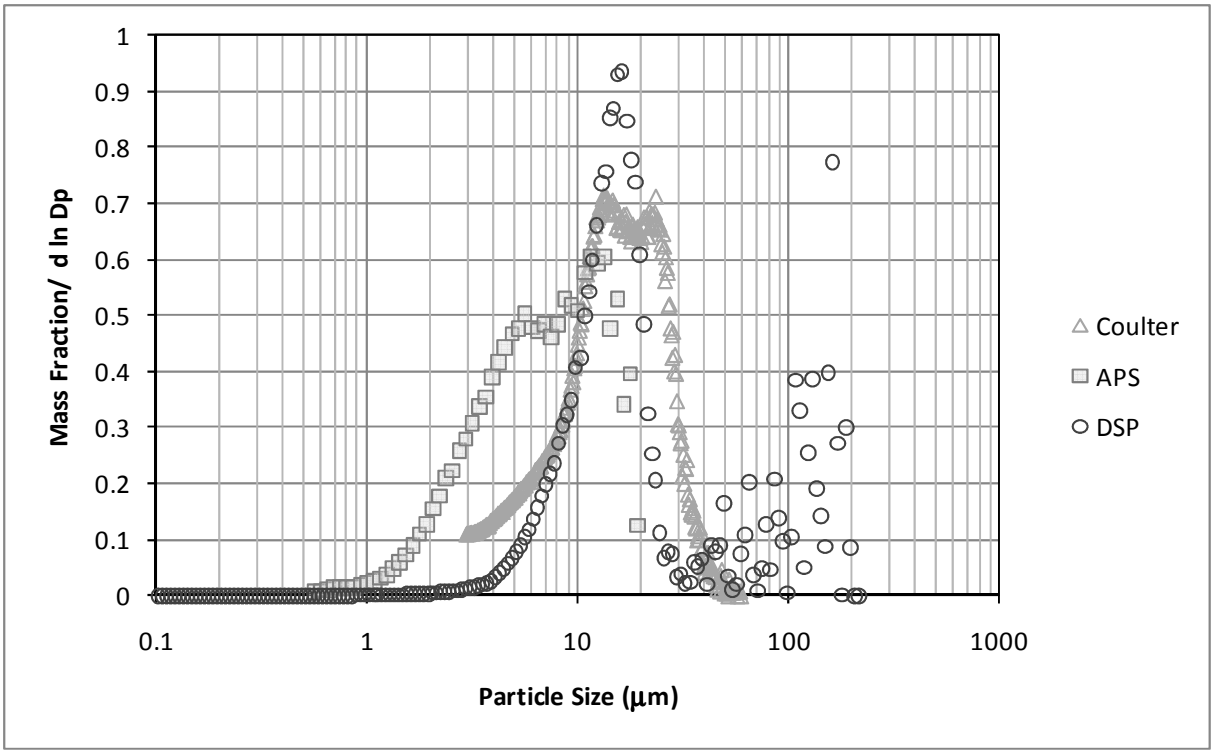

Figure 4.7 Particle size results for a swine gestation barn in Minnesota.

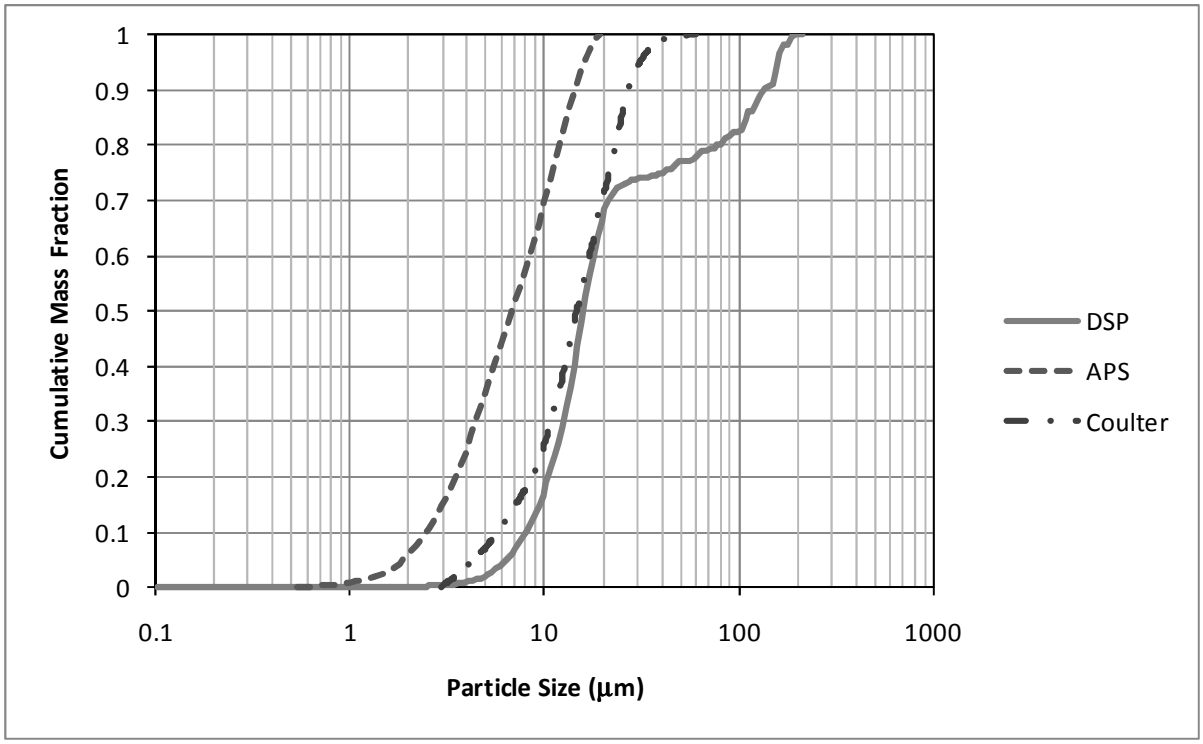

Figure 4.8 Cumulative particle size distribution for the Minnesota site.

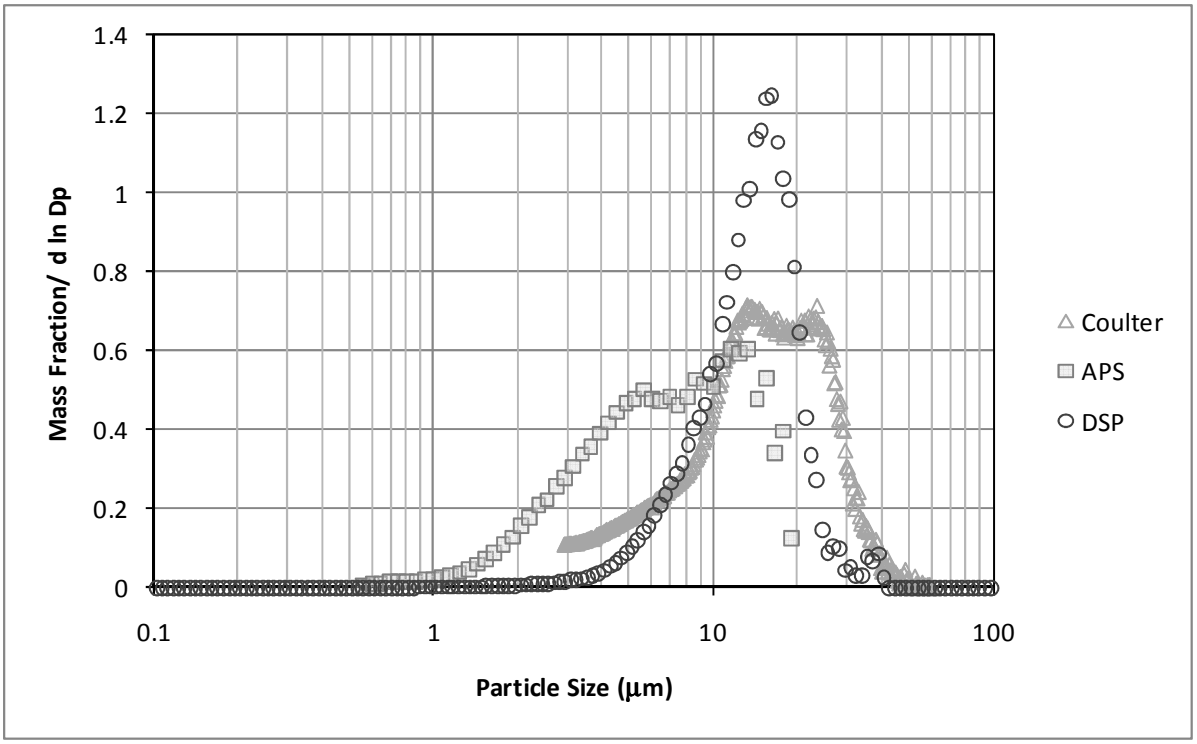

Figure 4.9 Particle size distribution with DSP outliers removed for the Minnesota site.

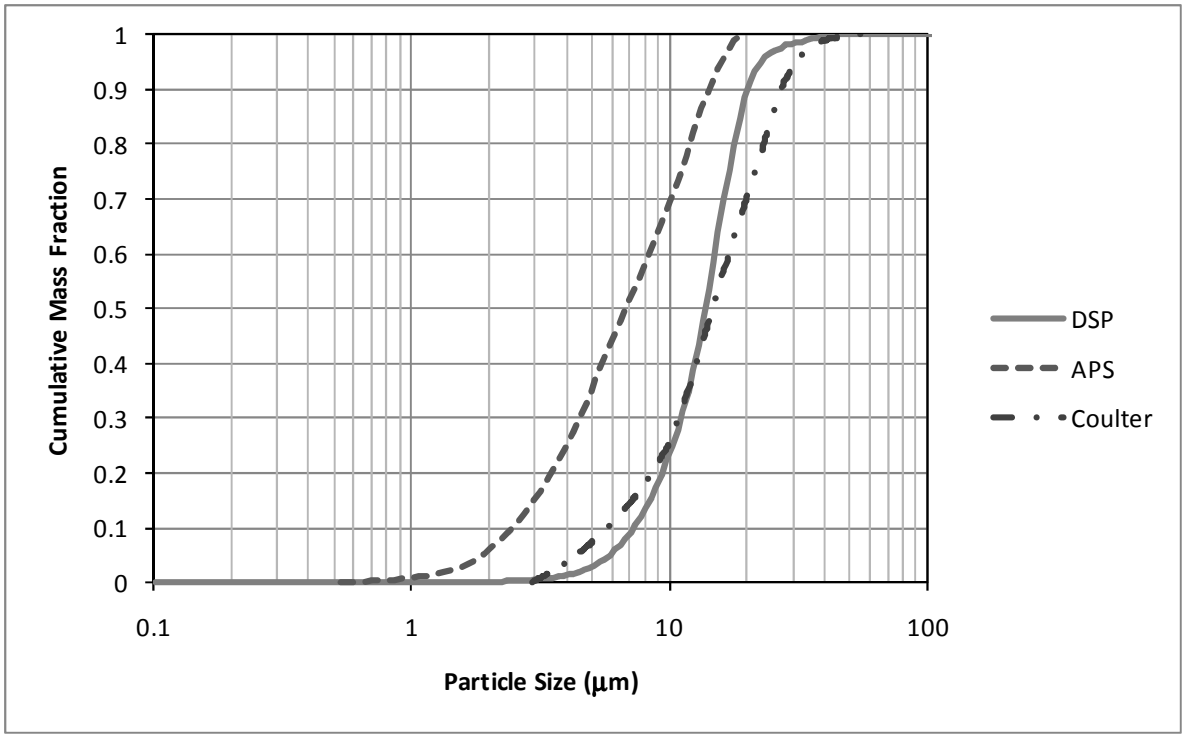

Figure 4.10 Cumulative particle size distribution with DSP outliers removed for the Minnesota site.

Table 4.3 Particle size statistics for the Minnesota site with all data included.

	Date Time	4/13/2004 2:12:00 PM	4/13/2004 10:25:00 PM	4/14/2004 7:10:00 AM	4/14/2004 2:50:00 PM	4/14/2004 9:40:00 PM	4/14/2004 10:21:00 AM	Average	Standard Deviation	All Data Combined
APS - All Data	$D_{15.9}$	3.11	3.00	3.45	3.10	3.19	3.14	3.16	0.15	3.19
	D_{50} (GMMD)	6.73	6.32	8.10	6.73	6.95	6.82	6.94	0.60	7.02
	$D_{84.1}$	12.77	12.42	14.59	12.78	13.09	12.66	13.05	0.78	13.29
	$GSD = (D_{84.1}/D_{15.9})^{1/2}$	2.02	2.03	2.06	2.03	2.03	2.01	2.03	0.02	2.04
	$GSD = D_{84.1}/D_{50}$	1.90	1.96	1.80	1.90	1.88	1.86	1.88	0.05	1.89
	$GSD = D_{50}/D_{15.9}$	2.16	2.11	2.35	2.17	2.18	2.17	2.19	0.08	2.20
DSP - All Data	$D_{15.9}$	11.72	8.68	10.75	9.15	9.46	9.95	9.95	1.12	9.82
	D_{50} (GMMD)	46.03	14.44	16.60	15.35	16.06	15.68	20.69	12.43	16.15
	$D_{84.1}$	148.16	20.59	110.93	86.90	151.15	63.06	96.80	50.67	108.58
	$GSD = (D_{84.1}/D_{15.9})^{1/2}$	3.56	1.54	3.21	3.08	4.00	2.52	2.98	0.86	3.33
	$GSD = D_{84.1}/D_{50}$	3.22	1.43	6.68	5.66	9.41	4.02	5.07	2.81	6.72
	$GSD = D_{50}/D_{15.9}$	3.93	1.66	1.54	1.68	1.70	1.58	2.01	0.94	1.65
DSP - Outliers Removed	$D_{15.9}$	8.90	8.47	9.94	8.05	8.49	9.23	8.85	0.67	8.78
	D_{50} (GMMD)	13.94	14.05	15.23	12.82	13.80	14.29	14.02	0.78	14.05
	$D_{84.1}$	18.88	19.32	20.04	17.08	19.25	18.92	18.91	0.99	18.98
	$GSD = (D_{84.1}/D_{15.9})^{1/2}$	1.46	1.51	1.42	1.46	1.51	1.43	1.46	0.04	1.47
	$GSD = D_{84.1}/D_{50}$	1.35	1.38	1.32	1.33	1.39	1.32	1.35	0.03	1.35
	$GSD = D_{50}/D_{15.9}$	1.57	1.66	1.53	1.59	1.63	1.55	1.59	0.05	1.60
Coulter - All Data as One Composite Sample	$D_{15.9}$	--	--	--				--	--	7.43
	D_{50} (GMMD)	--	--	--				--	--	14.72
	$D_{84.1}$	--	--	--				--	--	24.65
	$GSD = (D_{84.1}/D_{15.9})^{1/2}$	--	--	--				--	--	1.82
	$GSD = D_{84.1}/D_{50}$	--	--	--				--	--	1.67
	$GSD = D_{50}/D_{15.9}$	--	--	--				--	--	1.98

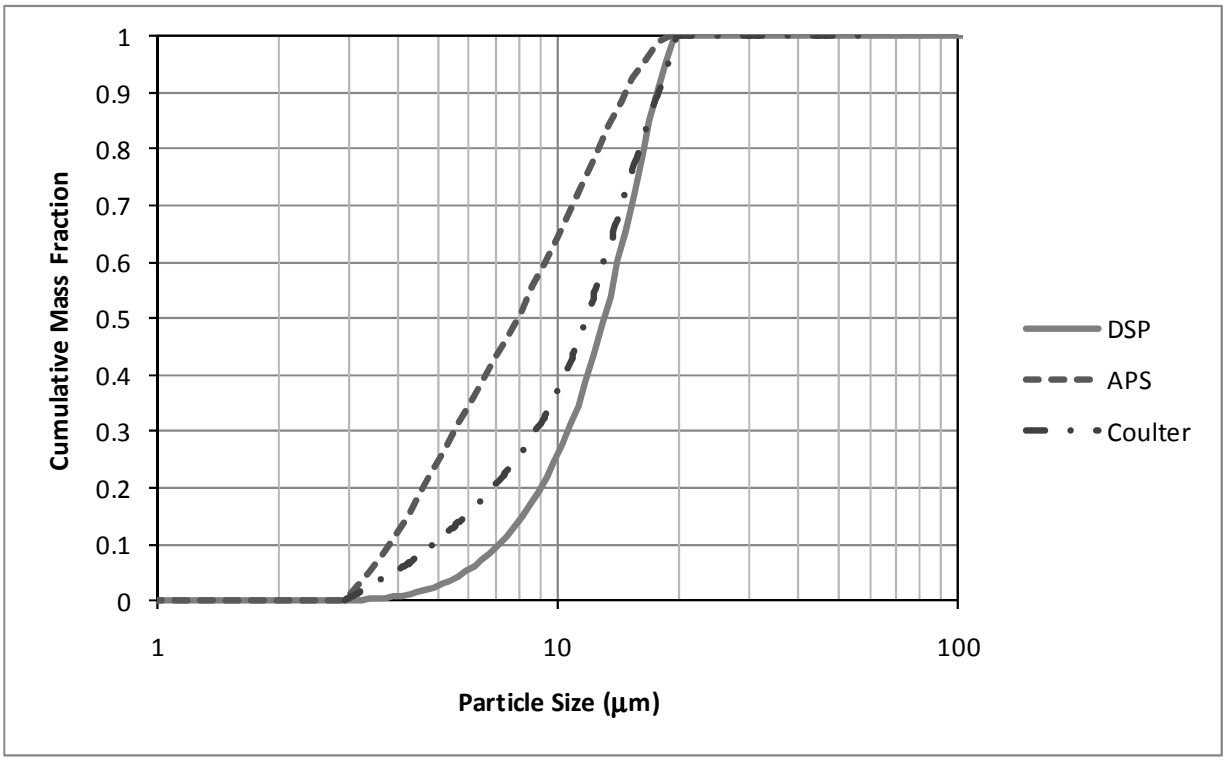

Figure 4.11 Cumulative particle size distribution with all data trimmed the same size range.

Table 4.4 provides the revised statistics for this trimmed data. As expected, the DSP statistics are now all higher than those of the Coulter. Table 4.3 showed these stats to fluctuate with the D50 being nearly equal. This data reiterates what can be missed if an instrument does not have the proper size range for particles in question.

Table 4.4 Particle size statistics for the Minnesota site trimmed to equal size ranges.

	Date	4/13/2004	4/13/2004	4/14/2004	4/14/2004	4/14/2004	4/14/2004		Standard	All Data
	Time	2:12:00 PM	10:25:00 PM	7:10:00 AM	2:50:00 PM	9:40:00 PM	10:21:00 AM	Average	Deviation	Combined
APS	$D_{15.9}$	4.39	4.24	4.69	4.38	4.42	4.35	4.41	0.15	4.43
	D_{50} (GMMD)	7.80	7.48	9.25	7.80	8.06	7.93	8.05	0.62	8.19
	$D_{84.1}$	13.29	13.02	15.09	13.26	13.52	13.19	13.56	0.77	13.80
	$GSD = (D_{84.1}/D_{15.9})^{1/2}$	1.74	1.75	1.79	1.74	1.75	1.74	1.75	0.02	1.77
	$GSD = D_{84.1}/D_{50}$	1.70	1.74	1.63	1.70	1.68	1.66	1.69	0.04	1.68
	$GSD = D_{50}/D_{15.9}$	1.78	1.76	1.97	1.78	1.82	1.82	1.82	0.08	1.85
DSP	$D_{15.9}$	8.58	8.36	9.41	7.97	8.11	8.91	8.56	0.54	8.50
	D_{50} (GMMD)	13.27	13.30	14.28	12.59	12.85	13.68	13.33	0.60	13.34
	$D_{84.1}$	17.25	17.34	17.80	16.50	16.96	17.53	17.23	0.45	17.27
	$GSD = (D_{84.1}/D_{15.9})^{1/2}$	1.42	1.44	1.38	1.44	1.45	1.40	1.42	0.03	1.43
	$GSD = D_{84.1}/D_{50}$	1.30	1.30	1.25	1.31	1.32	1.28	1.29	0.03	1.30
	$GSD = D_{50}/D_{15.9}$	1.55	1.59	1.52	1.58	1.58	1.53	1.56	0.03	1.57
Coulter	$D_{15.9}$	--	--	--	--	--	--	--	--	6.08
	D_{50} (GMMD)	--	--	--	--	--	--	--	--	11.82
	$D_{84.1}$	--	--	--	--	--	--	--	--	16.77
	$GSD = (D_{84.1}/D_{15.9})^{1/2}$	--	--	--	--	--	--	--	--	1.66
	$GSD = D_{84.1}/D_{50}$	--	--	--	--	--	--	--	--	1.42
	$GSD = D_{50}/D_{15.9}$	--	--	--	--	--	--	--	--	1.95

4.5.2.3 Texas Results

Particle size sampling results for the swine finishing room in Texas can be seen in Figure 4.12 and Figure 4.13. The APS and DSP both show bimodal distributions, the DSP reporting larger particle sizes than the APS. There is some noise at the upper end of the DSP, although not as severe as the other locations. The Coulter reported only a single mode, but the lower end of the distribution is suspect.

Unlike the other instruments, the Coulter's lower tail never really approaches zero. The same phenomenon existed in the data from the other locations, but not as significantly. This larger tail is partly due to the fact that there are probably still a considerable number of particles in the region below 3 μm. The shape of the Coulter's lower tail suggest that there might be an additional mode below this point or that there is noise in the data. Since the particles are subjected to an ultrasonic bath, it is also possible that larger particles were broken up, thus increasing the number of small particles.

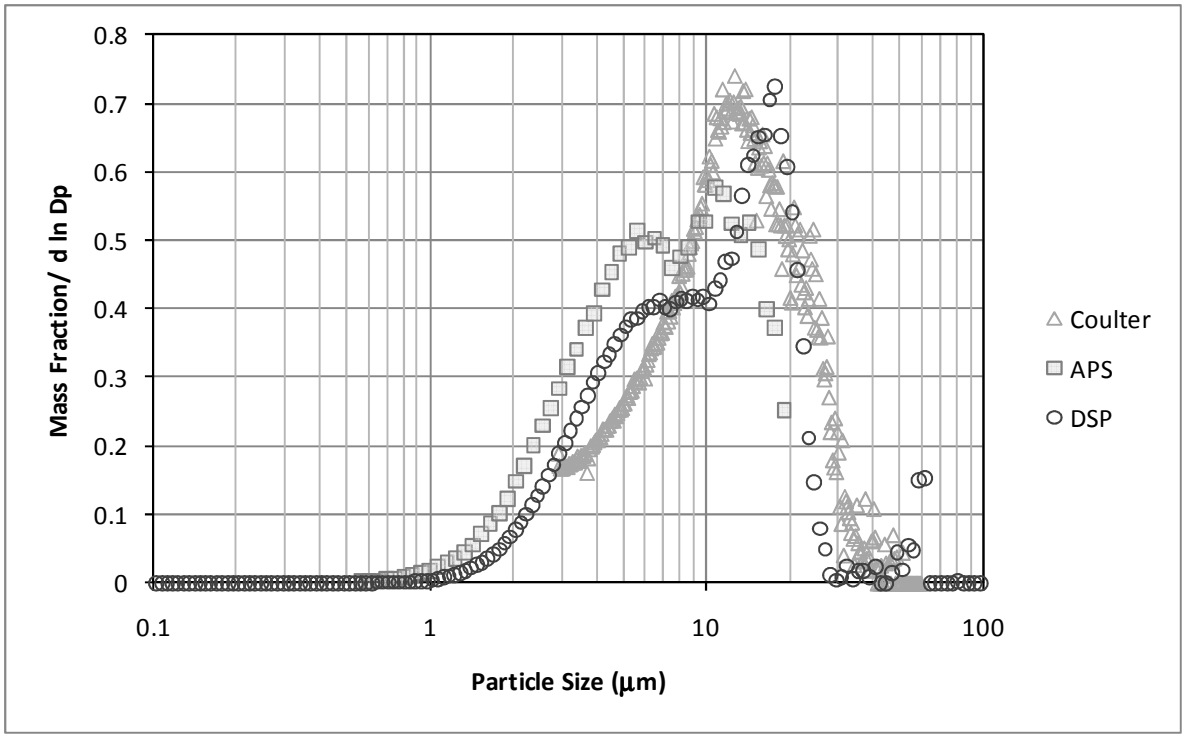

Figure 4.12 Particle size results for a swine finishing room in Texas.

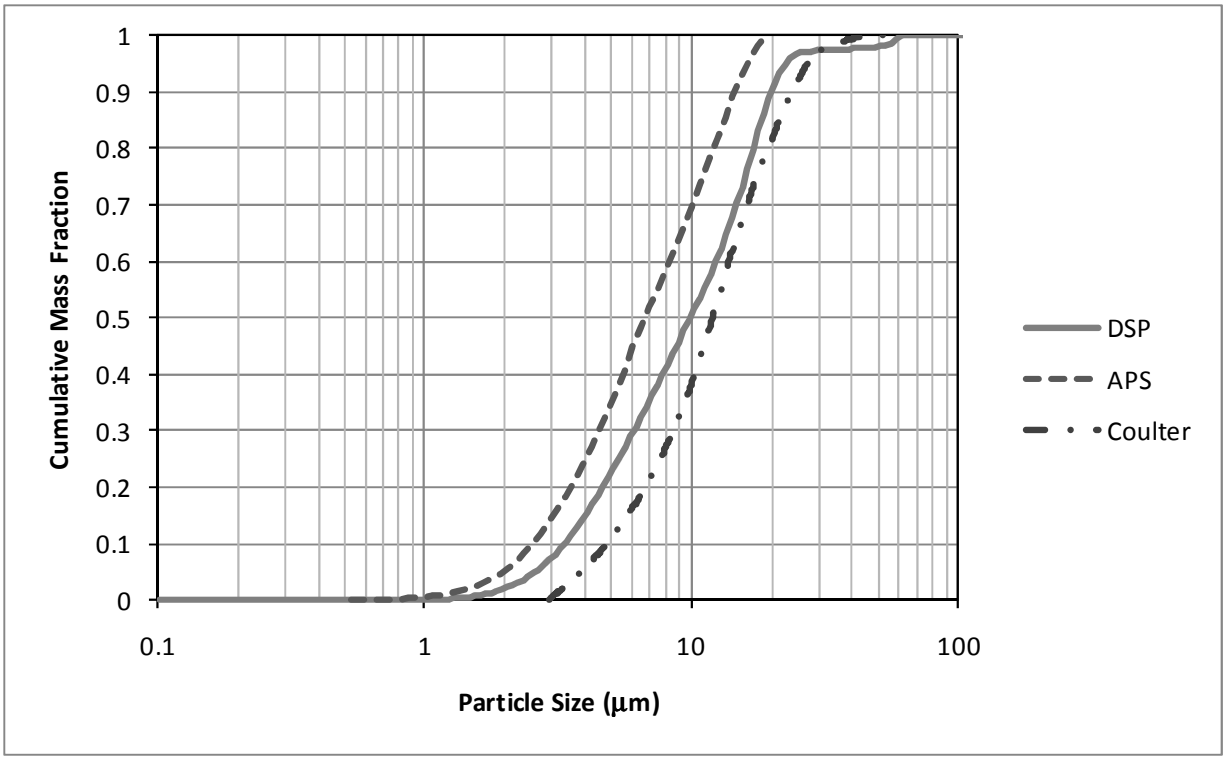

Figure 4.13 Cumulative particle size distribution for the Texas site.

The noise at the upper end of the DSP distribution was removed and the resulting distributions can be seen in Figure 4.14 and Figure 4.15. Once trimmed of outliers, the cumulative distribution clearly shows that the APS reports the smallest distribution, while the Coulter again reports the highest. The particle size statistics in Table 4.5 also confirm this.

Trimming the data so that the size ranges match, produces the distributions shown in Figure 4.16, and the statistics shown in Table 4.6. Modifying the size limits brings the data much closer together, but the general trend of instrument performance still exists with the APS presenting the smallest sizes and Coulter the highest.

4.5.2.4 Indiana Results

As discussed previously, an instrument malfunction meant that only results for the APS and Coulter are available at the Indiana poultry facility. The results from these instruments can be seen in Figure 4.17 and Figure 4.18. Here the APS appears to have a nearly bi-modal distribution, although there is not a clear separation of peaks. Again this smaller peak is near 6 μm. The Coulter distribution has only one mode, and, like at the other sites, its lower tail does not go down to zero. The primary peaks of the two instruments agree very favorably.

Trimming the data to force the instruments size limits to agree results in the distribution shown in Figure 4.19. The resulting cumulative distributions are much closer together, especially at the upper end of each distribution. Evidence of the lower second peak in the APS data is still evident. Statistics for all of the data can be seen in Table 4.7.

4.5.3 Site Comparison

It was expected that the poultry barn would have larger particles due to the feathers and the rapid clogging of some of the impaction instruments. Table 4.8 shows the particle size statistics for all of the sites. The statistics from the APS suggests that this is true, with all of the swine sites having similar stats with D50 values between 7 and 8 μm, while the poultry site's D50 is 11.52 μm. The Coulter data seems to contradict this, with the poultry statistics being in the same area as the swine facilities. Unfortunately there is no data from the DSP at the poultry facility to compare against the swine facilities.

No definitive conclusions can be drawn about the differences between the swine and poultry sites here due to a lack of data for this and other poultry sites. Based on the statistics

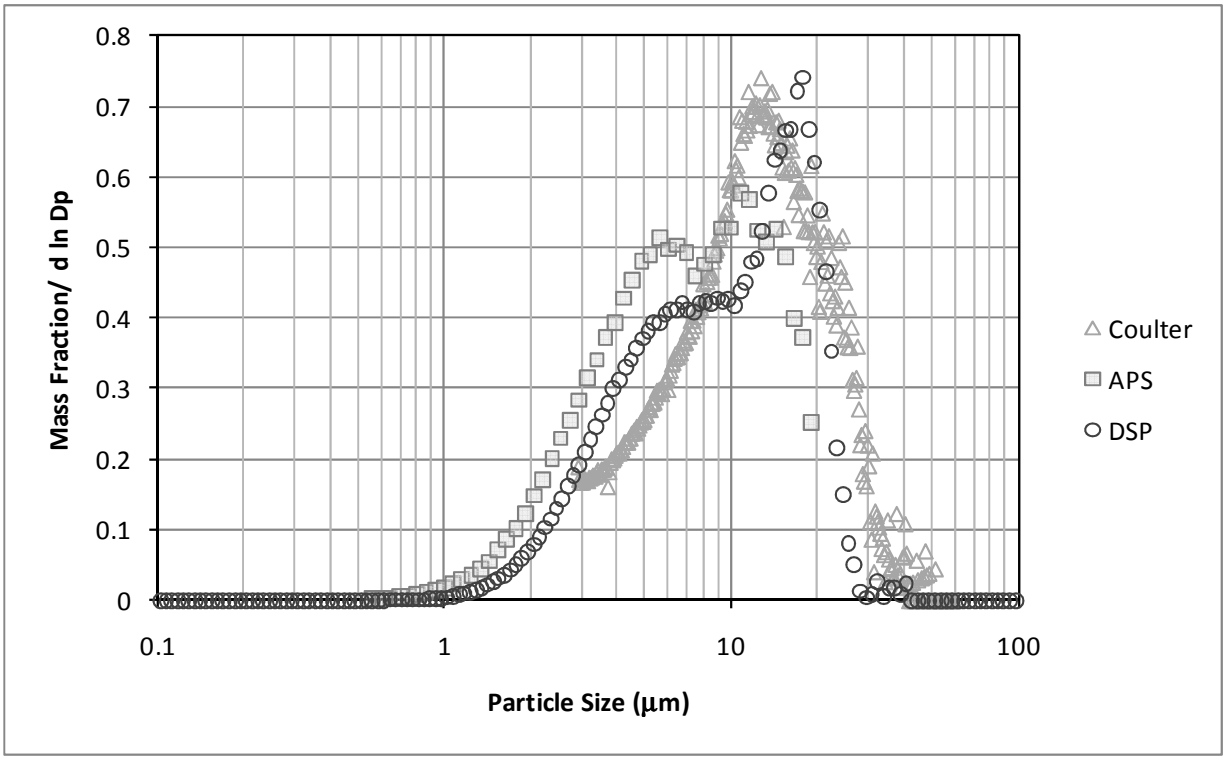

Figure 4.14 Particle size distribution with DSP outliers removed for the Texas site.

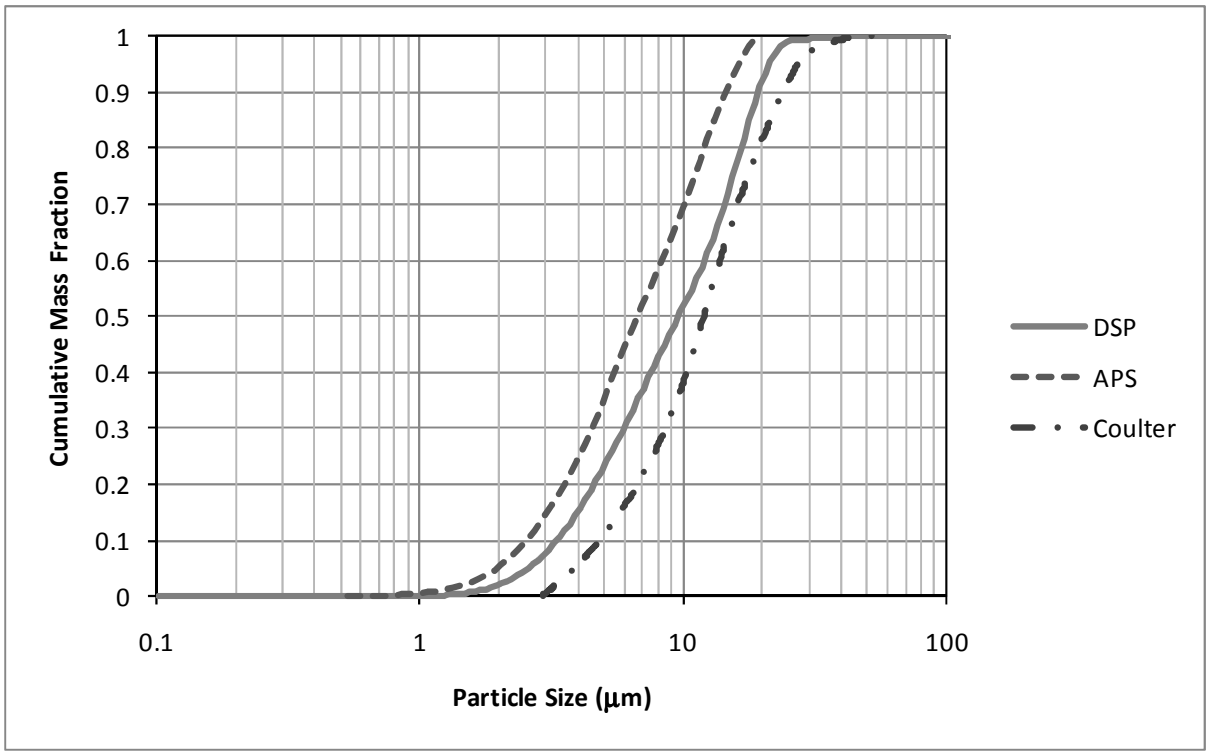

Figure 4.15 Cumulative particle size distribution with DSP outliers removed for the Texas site.

Table 4.5 Particle size statistics for the Texas site with all data included.

	Date Time	3/7/2004 7:50:00 AM	3/7/2004 5:30:00 PM	3/8/2004 7:43:00 AM	Average	Standard Deviation	All Data Combined
APS - All Data	$D_{15.9}$	3.38	3.30	3.13	3.27	0.13	3.25
	D_{50} (GMMD)	7.18	7.18	6.66	7.01	0.30	6.97
	$D_{84.1}$	13.77	13.40	13.33	13.50	0.24	13.50
	GSD = $(D_{84.1}/D_{15.9})^{1/2}$	2.02	2.01	2.06	2.03	0.03	2.04
	GSD = $D_{84.1}/D_{50}$	1.92	1.87	2.00	1.93	0.07	1.94
	GSD = $D_{50}/D_{15.9}$	2.13	2.17	2.13	2.14	0.03	2.14
DSP - All Data	$D_{15.9}$	4.23	4.07	4.36	4.22	0.15	4.22
	D_{50} (GMMD)	10.10	9.92	10.32	10.11	0.20	10.10
	$D_{84.1}$	17.88	19.34	18.60	18.61	0.73	18.52
	GSD = $(D_{84.1}/D_{15.9})^{1/2}$	2.06	2.18	2.06	2.10	0.07	2.09
	GSD = $D_{84.1}/D_{50}$	1.77	1.95	1.80	1.84	0.10	1.83
	GSD = $D_{50}/D_{15.9}$	2.39	2.44	2.37	2.40	0.04	2.39
DSP - Outliers Removed	$D_{15.9}$	4.23	3.96	4.33	4.17	0.19	4.17
	D_{50} (GMMD)	10.10	9.31	10.12	9.84	0.46	9.83
	$D_{84.1}$	17.88	17.85	18.27	18.00	0.23	18.01
	GSD = $(D_{84.1}/D_{15.9})^{1/2}$	2.06	2.12	2.05	2.08	0.04	2.08
	GSD = $D_{84.1}/D_{50}$	1.77	1.92	1.81	1.83	0.08	1.83
	GSD = $D_{50}/D_{15.9}$	2.39	2.35	2.34	2.36	0.03	2.36
Coulter - All Data as One Composite Sample	$D_{15.9}$	--	--	--	--	--	5.95
	D_{50} (GMMD)	--	--	--	--	--	12.02
	$D_{84.1}$	--	--	--	--	--	21.09
	GSD = $(D_{84.1}/D_{15.9})^{1/2}$	--	--	--	--	--	1.88
	GSD = $D_{84.1}/D_{50}$	--	--	--	--	--	1.75
	GSD = $D_{50}/D_{15.9}$	--	--	--	--	--	2.02

compiled here and the graphs in the preceding sections, most of the poultry particles occur in the 10 to 20 μm range, with very few above and below this range. The swine particle size distributions seem more spread out. This results in the APS reporting smaller statistics because it can't detect the larger particles. The Coulter can detect most of the particles throughout the size range and therefore shows comparable statistics since it seems that the bulk, but not as great a fraction, of the swine particles also occur in this same 10 to 20 μm range.

4.6 Conclusions and Recommendations

As previously discussed, the particle size data varied significantly between each instrument and between each site. Only general qualitative conclusions can be drawn as there is no standard

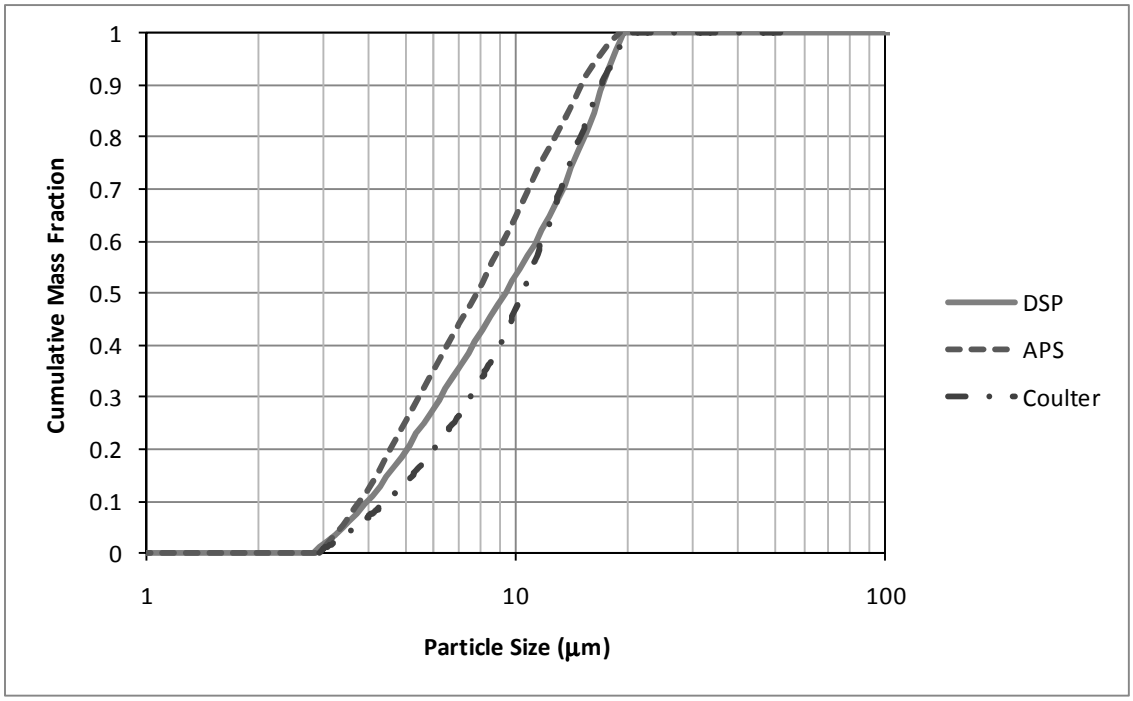

Figure 4.16 Cumulative particle size distribution for the Texas site with all data trimmed the same size range.

Table 4.6 Particle size statistics for the Texas site trimmed to equal size ranges.

	Date Time	3/7/2004 7:50:00 AM	3/7/2004 5:30:00 PM	3/8/2004 7:43:00 AM	Average	Standard Deviation	All Data Combined
APS	$D_{15.9}$	4.49	4.46	4.32	4.42	0.09	4.41
	D_{50} (GMMD)	8.20	8.31	7.80	8.10	0.27	8.07
	$D_{84.1}$	14.30	13.88	14.09	14.09	0.21	14.09
	$GSD = (D_{84.1}/D_{15.9})^{1/2}$	1.78	1.76	1.81	1.79	0.02	1.79
	$GSD = D_{84.1}/D_{50}$	1.74	1.67	1.81	1.74	0.07	1.75
	$GSD = D_{50}/D_{15.9}$	1.83	1.86	1.81	1.83	0.03	1.83
DSP	$D_{15.9}$	4.76	4.56	4.77	4.69	0.12	4.70
	D_{50} (GMMD)	9.87	9.09	9.68	9.55	0.41	9.54
	$D_{84.1}$	16.60	15.96	16.70	16.42	0.40	16.45
	$GSD = (D_{84.1}/D_{15.9})^{1/2}$	1.87	1.87	1.87	1.87	0.00	1.87
	$GSD = D_{84.1}/D_{50}$	1.68	1.76	1.73	1.72	0.04	1.72
	$GSD = D_{50}/D_{15.9}$	2.07	1.99	2.03	2.03	0.04	2.03
Coulter	$D_{15.9}$	--	--	--	--	--	5.39
	D_{50} (GMMD)	--	--	--	--	--	10.45
	$D_{84.1}$	--	--	--	--	--	15.82
	$GSD = (D_{84.1}/D_{15.9})^{1/2}$	--	--	--	--	--	1.71
	$GSD = D_{84.1}/D_{50}$	--	--	--	--	--	1.51
	$GSD = D_{50}/D_{15.9}$	--	--	--	--	--	1.94

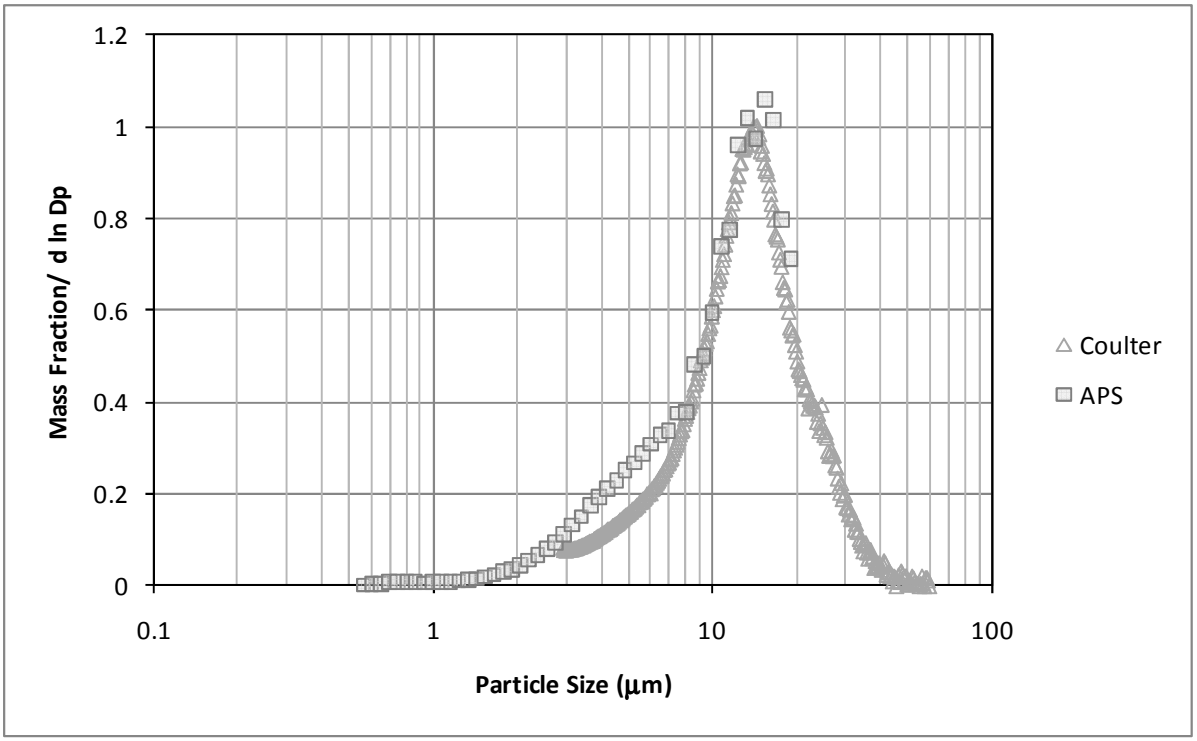

Figure 4.17 Particle size results for a poultry layer building in Indiana.

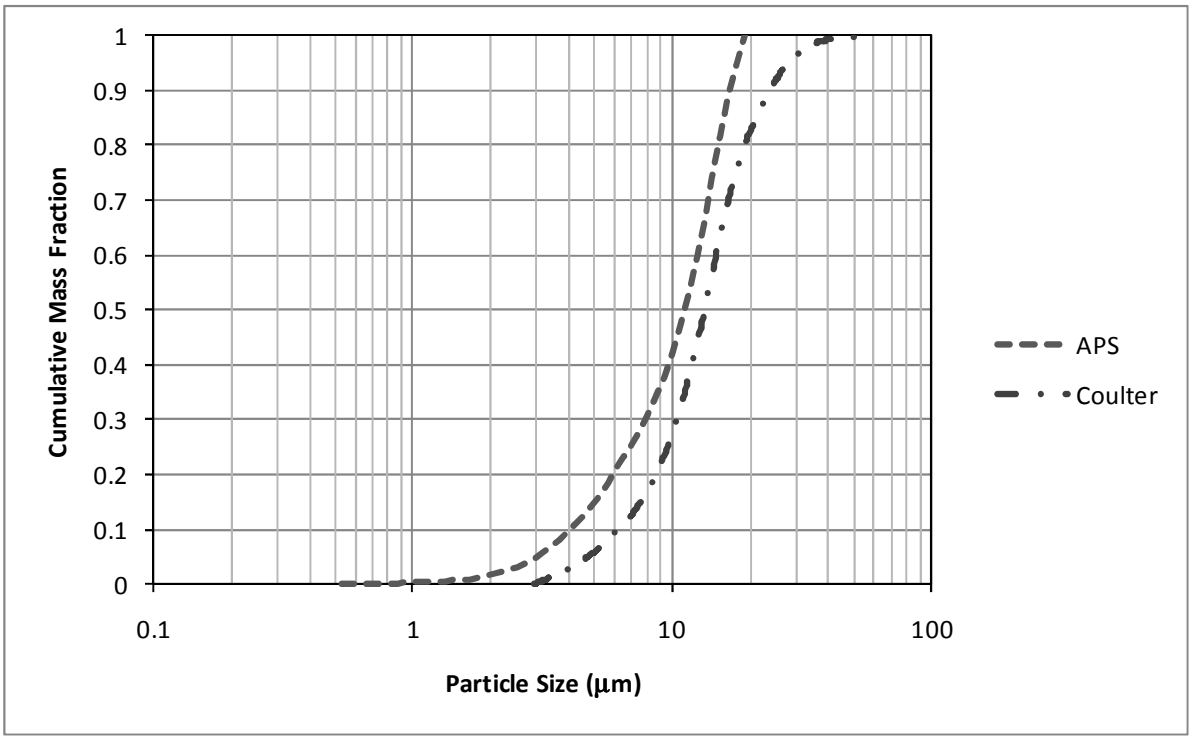

Figure 4.18 Cumulative particle size distribution for the Indiana site.

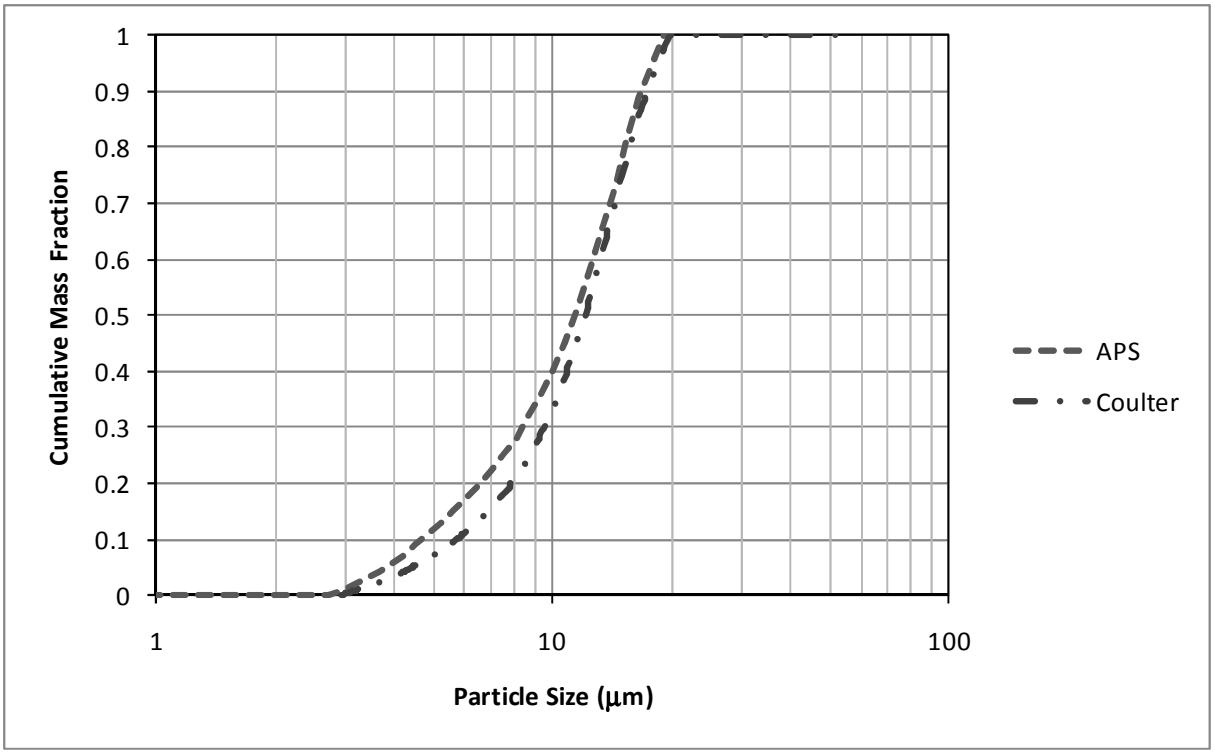

Figure 4.19 Cumulative particle size distribution with all data trimmed the same size range.

method against which to compare. As a result, the general performance and the applicability of each instrument for animal housing environments will be discussed.

4.6.1 APS

The APS functioned in the animal environment but great care was taken to protect it from the high dust and humidity levels. It would not be appropriate for long term measurements and is really not designed to be frequently transported.

In addition to the practical considerations, the instrument consistently reported lower particle sizes than any of the other instruments. This is at least in part due to an upper size limit of 19.8 µm. Although attempts were made to improve the sampling efficiency at larger particle sizes, it appears that there was still some inefficiency at the upper range which may have skewed the particles toward smaller sizes.

It seems the APS would not be a good choice for general use in animal buildings due to its low particle size range and sensitivity to extreme environments. It can be very useful for

laboratory environments although more work needs to be done to investigate and improve the sampling efficiency at larger particle sizes.

Table 4.7 Particle size statistics for the Indiana site.

APS - All Data	$D_{15.9}$	5.34
	D_{50} (GMMD)	11.52
	$D_{84.1}$	16.34
	$GSD = (D_{84.1}/D_{15.9})^{1/2}$	1.75
	$GSD = D_{84.1}/D_{50}$	1.42
	$GSD = D_{50}/D_{15.9}$	2.16
APS - Trimmed to Coulter Size Range	$D_{15.9}$	5.99
	D_{50} (GMMD)	11.82
	$D_{84.1}$	16.44
	$GSD = (D_{84.1}/D_{15.9})^{1/2}$	1.66
	$GSD = D_{84.1}/D_{50}$	1.39
	$GSD = D_{50}/D_{15.9}$	1.97
Coulter - All Data	$D_{15.9}$	7.80
	D_{50} (GMMD)	13.35
	$D_{84.1}$	20.70
	$GSD = (D_{84.1}/D_{15.9})^{1/2}$	1.63
	$GSD = D_{84.1}/D_{50}$	1.55
	$GSD = D_{50}/D_{15.9}$	1.71
Coulter - Trimmed to APS Size Range	$D_{15.9}$	7.11
	D_{50} (GMMD)	12.12
	$D_{84.1}$	16.34
	$GSD = (D_{84.1}/D_{15.9})^{1/2}$	1.52
	$GSD = D_{84.1}/D_{50}$	1.35
	$GSD = D_{50}/D_{15.9}$	1.71

4.6.2 Aerosizer DSP

The Aerosizer DSP suffers from some of the same physical limitations as the APS. In addition, this model is large and requires a large external pump. All of this helps makes its use for routine field sampling in animal buildings impractical.

Despite its practical limitations, the instrument seemed to perform reasonably well. The size range is adequate to report all of the particles of interest, although there was consistent "noise" in the upper end of the distribution. This noise could have been due to inadequate sample times, but seems more likely to have been caused by either poor sampling efficiency of larger

particles or very low number concentrations of these particles. These could combine to result in a few large particles being sampled and spiking the mass distribution. This is always a potential problem when sampling large particles as you approach the limits of the definition of a "suspended" particle.

Table 4.8 Comparison of particle size statistics for each location.

	Animal	Swine			Poultry
	Location	Illinois	Minnesota	Texas	Indiana
APS	$D_{15.9}$	2.68	3.19	3.25	5.34
	D_{50} (GMMD)	7.85	7.02	6.97	11.52
	$D_{84.1}$	14.48	13.29	13.50	16.34
	$GSD = (D_{84.1}/D_{15.9})^{1/2}$	2.32	2.04	2.04	1.75
	$GSD = D_{84.1}/D_{50}$	1.84	1.89	1.94	1.42
	$GSD = D_{50}/D_{15.9}$	2.93	2.20	2.14	2.16
DSP	$D_{15.9}$	6.30	9.82	4.22	--
	D_{50} (GMMD)	13.39	16.15	10.10	--
	$D_{84.1}$	20.23	108.58	18.52	--
	$GSD = (D_{84.1}/D_{15.9})^{1/2}$	1.79	3.33	2.09	--
	$GSD = D_{84.1}/D_{50}$	1.51	6.72	1.83	--
	$GSD = D_{50}/D_{15.9}$	2.13	1.65	2.39	--
DSP - Outliers Removed	$D_{15.9}$	5.87	8.78	4.17	--
	D_{50} (GMMD)	12.58	14.05	9.83	--
	$D_{84.1}$	18.00	18.98	18.01	--
	$GSD = (D_{84.1}/D_{15.9})^{1/2}$	1.75	1.47	2.08	--
	$GSD = D_{84.1}/D_{50}$	1.43	1.35	1.83	--
	$GSD = D_{50}/D_{15.9}$	2.14	1.60	2.36	--
Coulter	$D_{15.9}$	8.92	7.43	5.95	7.80
	D_{50} (GMMD)	16.39	14.72	12.02	13.35
	$D_{84.1}$	25.31	24.65	21.09	20.70
	$GSD = (D_{84.1}/D_{15.9})^{1/2}$	1.68	1.82	1.88	1.63
	$GSD = D_{84.1}/D_{50}$	1.54	1.67	1.75	1.55
	$GSD = D_{50}/D_{15.9}$	1.84	1.98	2.02	1.71

4.6.3 Coulter

The Coulter has the practical advantage that it remains in the laboratory and the filters are collected in the field and brought back for analysis. This allows for many samples to be collected

at multiple locations simultaneously and analyzed later. The disadvantage is that you cannot get real time results and there could be contamination or losses in the samples during transport.

The Coulter seemed to perform reasonably well toward the upper end of the distribution. It seemed to miss detail at the lower end of the distribution. This could be due to the lower limit being around 3 µm, whereas 1 µm would be more appropriate. There may also be issues with the electrolyte solution and ultrasonic bath having some effect on the particles tested here. It is also possible that coincidence error may be impacting the lower end of the distribution, thus causing the distribution to go back toward zero. This error comes into play when concentrations are high and two or more particles enter the system simultaneously, thus appearing as one larger particle (Baron and Willeke, 2001). This would be more prone to happen with small particles. More research is needed in this area to fully document the appropriateness of this preparation method and hot to determine the appropriate level of dilution for dust samples from animal buildings.

Overall the Coulter combined with cheap simple TSP samplers is a very efficient system for determining particle size in animal environments. Questions of accuracy still need to be fully addressed since it has not been fully accepted in the literature.

4.6.4 Instrument Comparison

As discussed in Section 4.5.2.1 (Page 68), there is evidence in the literature to help explain why the Coulter generally reported larger particles while the APS and DSP generally reported smaller particles (Baron and Willeke, 2001; Chung and Thompson, 1989). This is in part because the Coulter cannot take into account particle shape, thus ignoring an important component of settling velocity. On the other hand the APS and DSP can overcompensate for this by working outside of the Stokes region, thus skewing the definition of the aerodynamic diameter. The differences between the APS and DSP are not as well documented, but could be caused in part by noise in the system which is evenly spread throughout the DSP range, but concentrated at the lower end of the APS range (Baron and Willeke, 2001).

4.6.5 Summary

For large scale sampling, the Coulter appears to be the most promising choice. When feasible the Aerosizer is also useful, especially for real time data. The APS is limited in its

particle size range and, thus, may be of limited usefulness when needing to analyze the entire particle size distribution.

This raises the question of the purpose of sampling and the need to know particle size above a certain point. EPA generally only considers TSP, PM10 and PM2.5. Whether these points of interest are adequate will depend on the purpose of the study. There have also been a number of questions raised about the actual performance of the EPA approved instruments and what bias this could cause in agricultural settings (Wang et al., 2005). It seems that detailed knowledge of the particle size distribution for animal environments is needed to evaluate applicability of and compliance with regulations as well as the need for and effectiveness of various control methods. What direction this should take will be discussed in more detail in Chapter 6.

CHAPTER FIVE: **FLOW RATE MEASUREMENT**

5.1 Experimental Facilities and Procedures

5.1.1 Objective

The objective of this chapter is to determine whether a single vane anemometer can be used to accurately measure total flow through a vane axial, wall mounted fan, typical of those used in confined animal buildings. To accomplish this task, measurements will be collected using a vane anemometer on three different sized fans in a laboratory environment. The linearity of the anemometer response will be determined as well as the effects of anemometer placement. This will help assess the need for field calibration.

5.1.2 Anemometer Description and Setup

The anemometer chosen for use is a RM Young model 27106RS with model 08234 propeller (R.M. Young Company, Traverse City, Michigan). It consists of an 18 cm diameter vane attached to a sealed bearing DC generator that produces a 0 to 1 VDC output. The total package was about 45 cm in length. This anemometer was selected because it was readily available, affordable and easy to use and the signal could be read by most common data loggers.

Depending on the nature of the fan in question, the anemometer can either be located upstream or downstream of the fan. In this study, three fan sizes were considered: 45, 76 and 91 cm. The two smaller fans had flaps on the exhaust side of the fan as well as a hood directing the airflow downward. This required the anemometers to be located on the inlet side of the fan. For the largest fan the flaps were on the inlet side and there was only a conical shaped shroud on the outlet allowing the anemometer to be positioned on the downstream side of the fan. The exact location of the anemometer in front of the fan depended on the size of the fan and the airflow pattern. For the two smaller fans, the anemometer was positioned as close to the fan as possible and faced upstream. With the larger fan the anemometer was placed just inside the cage of the cone facing into the exhaust stream.

The exact fan models are not provided here, so as to prevent this data being improperly used for calibration by others. This will be discussed in more detail in later sections.

5.1.3 Test Facility

To test the anemometer's ability to measure the flow rate of agricultural fans the Air Movement and Control Association (AMCA, 1999) standard test facility at the University of Illinois BESS Laboratory was used. This facility is the industry standard test site for agricultural fans. It has the capacity to test all typical fans sizes at static pressures ranging from zero to 5 kPa, well above any typical operating pressures.

5.1.4 Experimental Design

For the 45 cm fan, several positions at the same radius around the fan were taken corresponding to each axis facing the fan: Top, Right, Bottom and Left (0, 90, 180, 270º from the top respectively). A radius of 14 cm was chosen due to the physical constraints caused by the motor and the fan shroud. This allowed for determination of flow rate variability around the fan. Due to the relatively small opening between the motor and fan housing, there was very little room to maneuver the anemometer. This only allowed testing at a single radius. Figure 5.1 shows the layout of the 45 cm fan for one anemometer position. The anemometer positions for all tests on the 45 cm fan are shown in Figure 5.2.

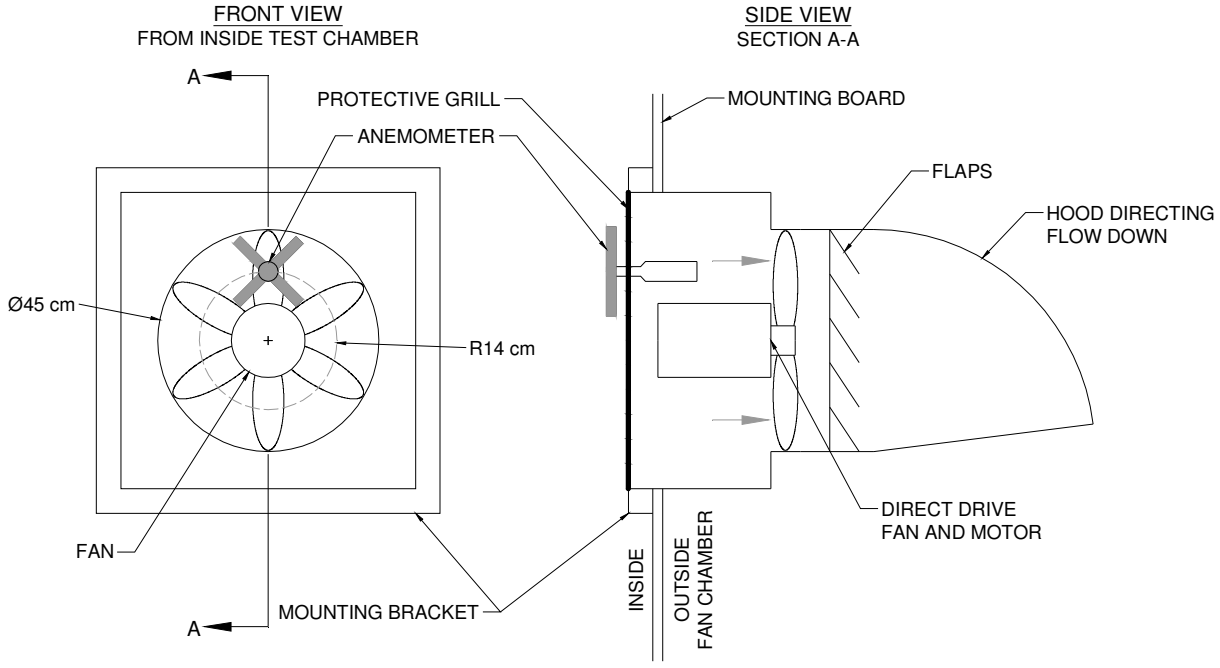

Figure 5.1 Anemometer and 45 cm fan layout.

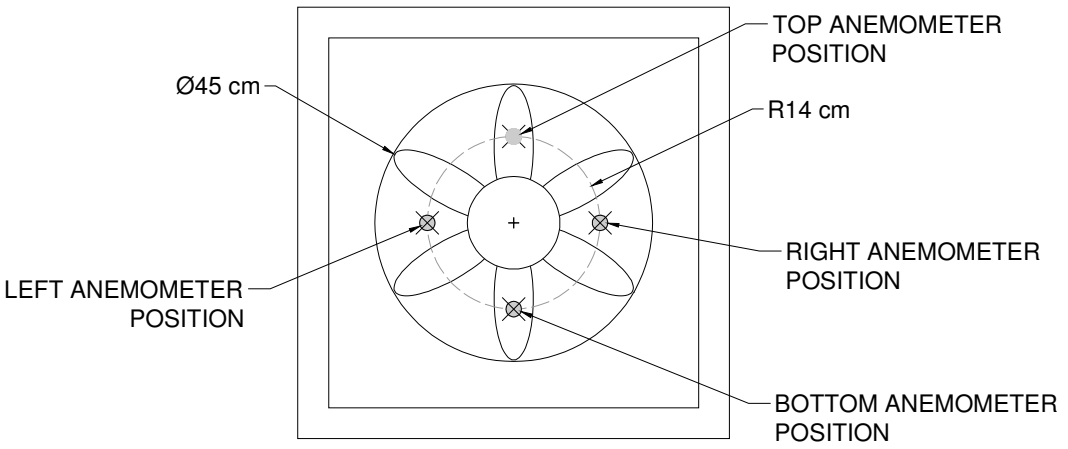

Figure 5.2 Anemometer positions for 45 cm fan tests, viewed from inside the fan test chamber.

The 76 cm fan had a layout for the tests as the 45 cm fan. There was more space to place the anemometer, so the radius was increased to 18.5 cm. The same four basic positions were tested around the fan. An additional group of tests were conducted to assess how small variations in the position of the anemometer would impact the calibration curves. These tests were conducted by moving the anemometer 2 cm in each principal direction around the right side of the fan. Figure 5.3 shows all of the anemometer locations for the 76 cm fan.

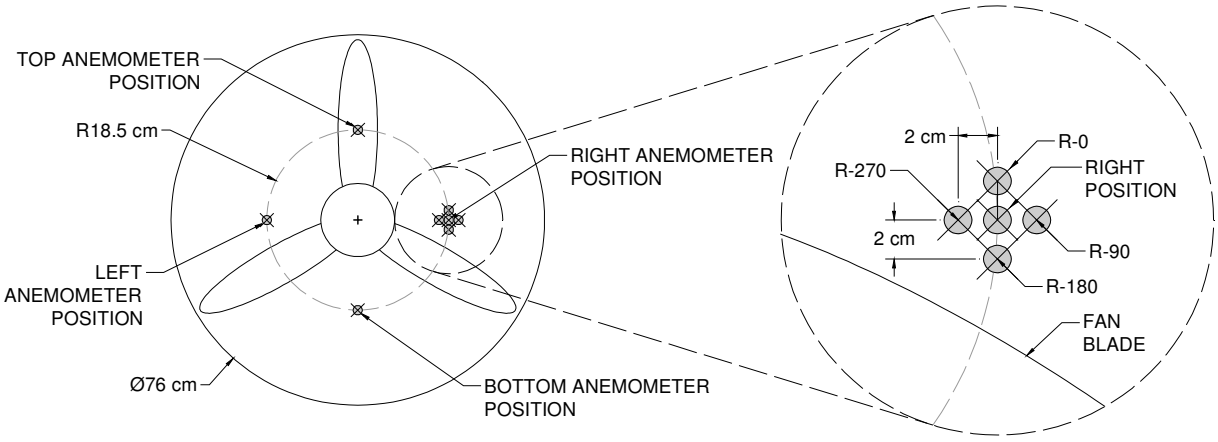

Figure 5.3 Anemometer positions for the 76 cm fan tests, viewed from inside fan test chamber.

With the 91 cm fan, it was necessary to locate the anemometer on the exhaust side of the fan just inside the protective grill of the cone. On the exhaust side of these fans there is an area downstream of the motor that can experience very low velocities or even reverse flows. This area was avoided which limited the effective measurement area of the cone from about 50 to 100% of the radius. A radius of 30.5 cm was chosen to be in the section of highest velocity, thus extending the useful lower range of the sensor as much as possible. The anemometer was located at several angles ranging from 0 to 180º from the top of the cone in 45º increments. Smaller radii were tested but were quickly shown not to be useful due to the expanding dead space as the flow rate dropped. Figure 5.4 shows the general layout for the tests on the 91 cm fan and Figure 5.5 shows the anemometer positions for all of the 91 cm fan tests.

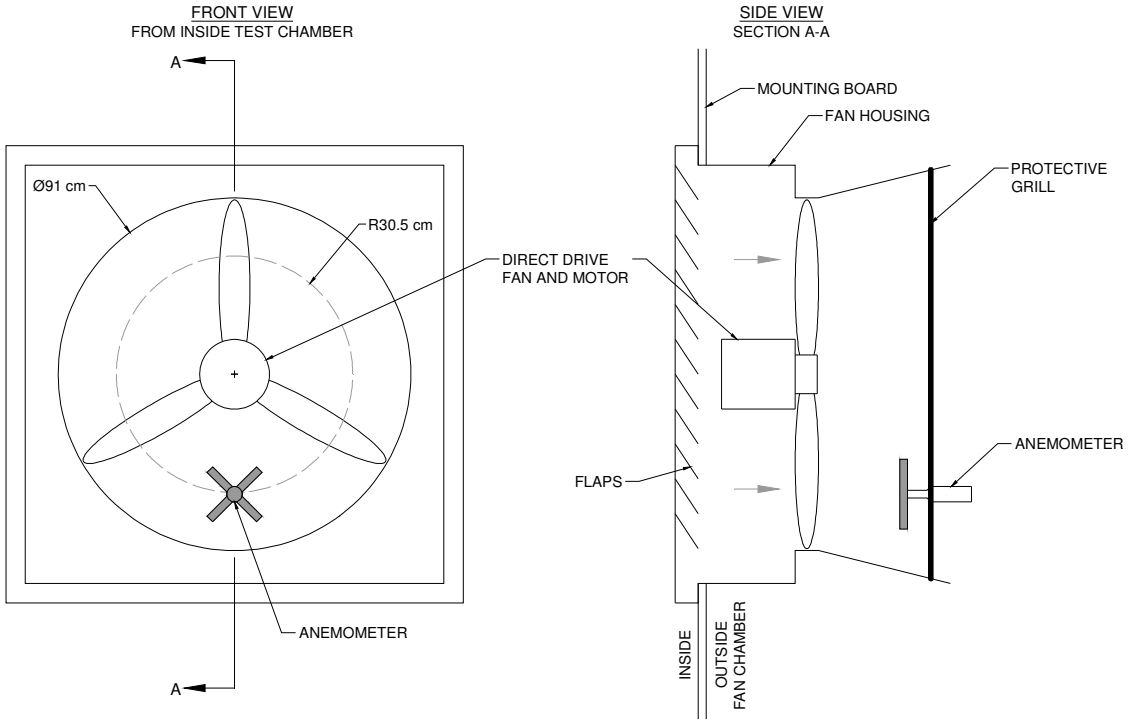

Figure 5.4 Anemometer and 91 cm diameter fan test layout.

5.1.5 Test Procedure

Before each group of tests, the appropriate fan was mounted on the fan test chamber and the anemometer placed in the appropriate location. The chamber was sealed and the basic AMCA fan test procedure was followed. After each test, the flow rate was recorded and the

corresponding anemometer voltages were recorded. The flow rate of the fan was generally taken to well below where it would normally be operated in order to give an idea of the overall linearity and the useful range of the sensor.

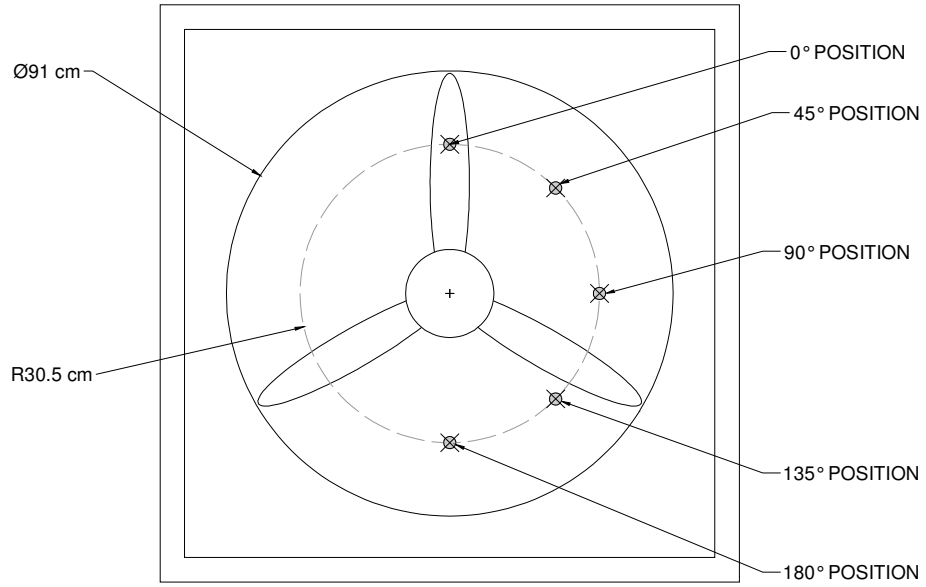

Figure 5.5 Anemometer locations for the 91 cm fan tests viewed from inside test chamber.

5.1.6 Data Analysis

An ideal sensor will have a linear response over the measurement range and with little noise in the response. A linear regression will be performed on the data to determine the sensor response to changes in flow rate. The data and the regression line will be visually examined to qualitatively determine whether the data is indeed linear. The R^2 value will be calculated to provide a more quantitative measure of both the linearity and level of noise in the data.

This regression analysis provide an measure of the variability of the data compared to the line, but not a quantitative measure of how well it can predict future values. To do this the prediction interval (PI) will be calculated. This is a measure of confidence in the predicted flow rate (y) at a given anemometer voltage (x). The following formula is used to determine the prediction interval (Devore, 2004):

$$PI = \pm t_{\alpha/2,n-2} \cdot SE\sqrt{1 + \frac{1}{n} + \frac{(x-\bar{x})^2}{S_{xx}}} \quad (5.1)$$

Where:

SE = standard error

$S_{xx} = \sum_1^n (x_n - \bar{x})$ = the sum of the square of deviations, and

$t_{\alpha/2,n-2}$ = is the t-statistic for the prediction interval, $100(1-\alpha)\%$.

For the following analyses the 95% prediction interval will be used such that α is 0.95.

Calculating the prediction interval will indicate the range of predicted flows for a given anemometer voltage. This will be examined absolutely (i.e. in m^3/min) and as a percentage of the predicted flow rate at that voltage.

Performing this analysis for each anemometer location will provide useful information about the accuracy and precision for that specific calibration scenario, but not about how sensitive the anemometer calibration is to location. To determine this all of the calibration locations will be combined and a new regression analysis performed. This will be compared to the individual locations to determine how significant the location is to the accuracy of the anemometer.

5.2 Results and Discussion

5.2.1 45 cm Fan

The measurements and corresponding regression analysis for the 45 cm fan can be seen in Figure 5.6. The left and top positions appear to have very good linearity and fairly low noise. This is confirmed with their high R^2 values. The right and bottom locations appear to have some slight curvature to them, but appear to be adequately represented by a linear regression. While the R^2 value is still fairly high for both, there is much more noise at the bottom location. This is also confirmed by the wide prediction intervals compared to the other three locations.

Figure 5.7 shows all of the 45 cm fan calibration data together, along with the linear regression based on all of this data. The lumped data still shows good linearity and the regression line seems to reasonably represent all of the data with no obvious deviations for a single anemometer location. The prediction interval is fairly wide, with a few noticeable outliers, mainly from the bottom position.

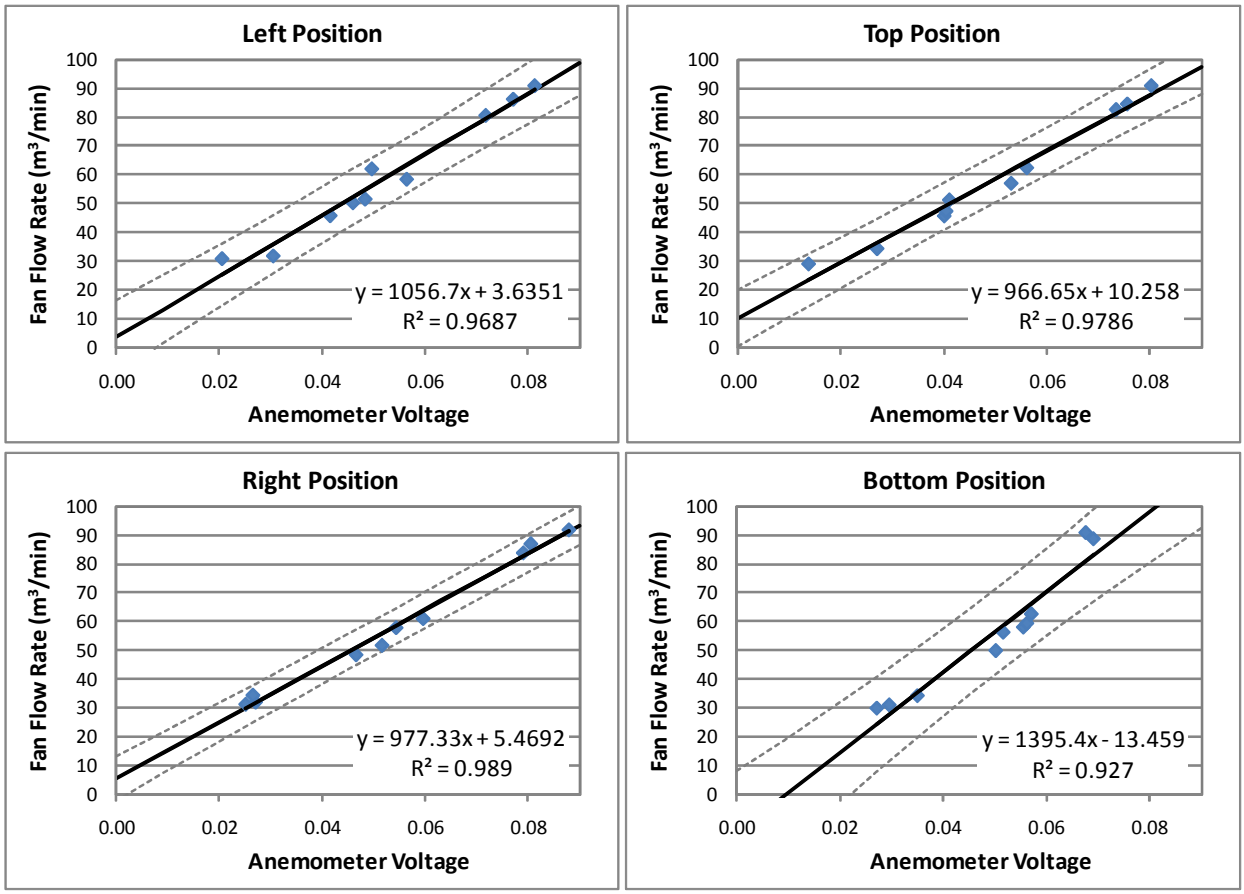

Figure 5.6 Linear regression calibration curves with 95% prediction intervals for the 45 cm fan.

To better evaluate the magnitude of the prediction intervals

Table 5.1 has been created. This table shows the predicted flow rate and prediction interval at various anemometer voltages. The anemometer voltages were chosen to represent certain ranges for the 45 cm fan. It is clear that the prediction interval, as a percentage of the predicted flow rate, is largest at the lower end of the range and decreases as the predicted flow rate goes up. At these lower ranges the prediction interval is worse than 20% in all locations and nearly 100% at the Bottom location. At 100% of the fan's range, the prediction interval becomes more reasonable, averaging around 10%. The Bottom location still shows a fairly large prediction interval of 17.5%.

The prediction intervals at each location vary significantly, indicating that placement of the anemometer could be significant. In particular, the bottom position shows much more uncertainty. This can be verified when Figure 5.6 and Figure 5.7 are re-examined. It is clear that

the bottom position exhibits some curvature. Although it still has a reasonably high R^2 value, it is noticeably lower than the other positions which seem to have better linearity.

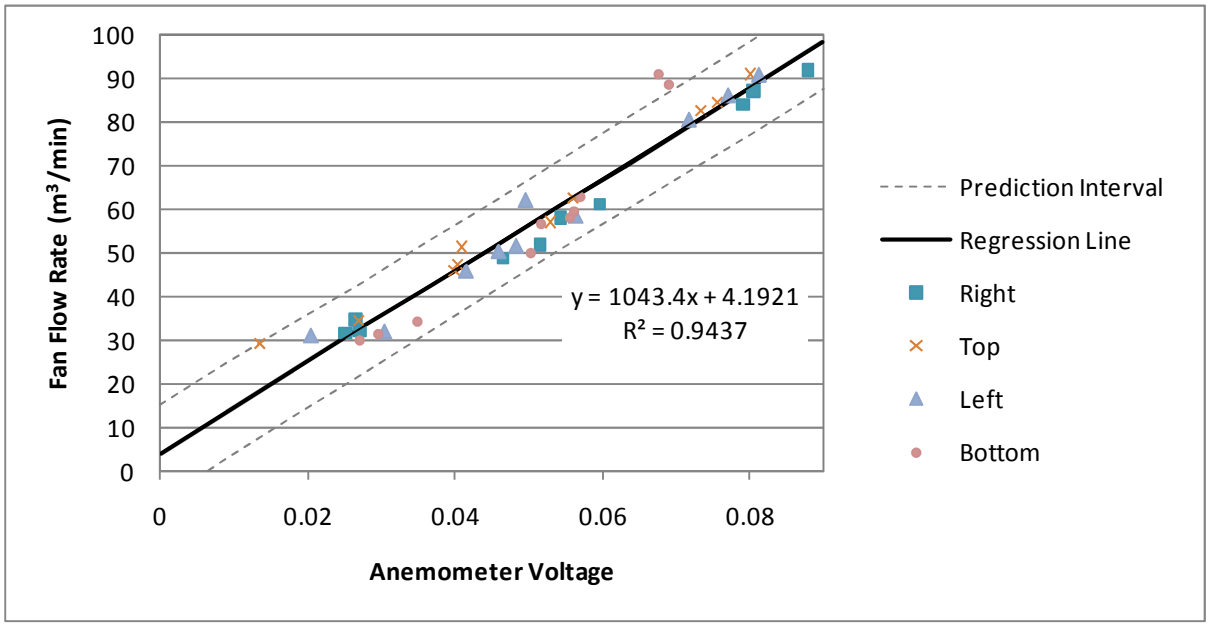

Figure 5.7 Regression analysis with 95% prediction intervals for all locations around the 45 cm fan.

Table 5.1 Estimates of flow and the corresponding prediction intervals throughout the 45 cm fan's range.

Position	Approximate % of Fan Range Anemometer Voltage	25 0.0225	50 0.0450	75 0.0675	100 0.0900
Right	Predicted Flow (m^3/min)	27.5	49.4	71.4	93.4
	Prediction Interval (m^3/min)	6.7	6.2	6.3	6.9
	Prediction Interval (%)	24.3	12.5	8.8	7.3
Top	Predicted Flow (m^3/min)	32.0	53.8	75.5	97.3
	Prediction Interval (m^3/min)	8.6	8.0	8.3	9.3
	Prediction Interval (%)	27.0	14.9	10.9	9.5
Left	Predicted Flow (m^3/min)	27.4	51.2	75.0	98.7
	Prediction Interval (m^3/min)	10.7	9.7	9.9	11.3
	Prediction Interval (%)	39.0	18.9	13.2	11.4
Bottom	Predicted Flow (m^3/min)	17.9	49.3	80.7	112.1
	Prediction Interval (m^3/min)	17.2	14.9	15.9	19.6
	Prediction Interval (%)	96.0	30.2	19.7	17.5
All 4 Combined	Predicted Flow (m^3/min)	27.7	51.1	74.6	98.1
	Prediction Interval (m^3/min)	10.6	10.3	10.4	10.8
	Prediction Interval (%)	38.2	20.2	13.9	11.0

As discussed above, the combined calibration data showed good linearity with a fairly good R^2 value of 0.943. Despite this, the spread of the data is fairly wide with the prediction interval ranging from 11.0% to 38.2%. The likely cause of this is the Bottom dataset. To test this theory, the Bottom dataset was removed from the combined data and the regression re-analyzed. These results can be found in Figure 5.8 and Table 5.2. The quality of the fit improved, with the R^2 increasing from 0.943 to 0.970. Maybe more importantly, the prediction interval narrowed noticeably, with the prediction interval dropping from 11% to 8.4% at the upper end and 38.2% to 27% at the lower end.

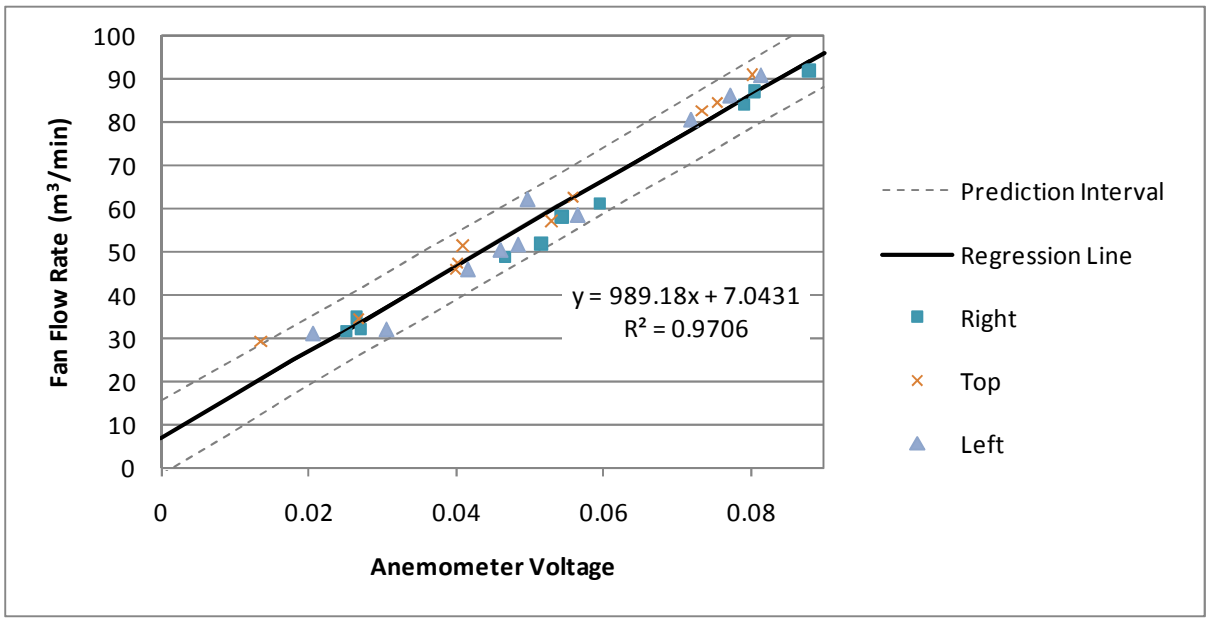

Figure 5.8 Regression analysis with 95% prediction intervals for the Left, Top and Right positions combined around the 45 cm fan.

Table 5.2 Estimates of flow and the corresponding prediction intervals throughout the 45 cm fan's range.

Position	Approximate % of Fan Range	25	50	75	100
	Anemometer Voltage	0.0225	0.0450	0.0675	0.0900
All 4 Combined	Predicted Flow (m^3/min)	27.7	51.1	74.6	98.1
	Prediction Interval (m^3/min)	10.6	10.3	10.4	10.8
	Prediction Interval (%)	38.2	20.2	13.9	11.0
Left, Top and Right Combined	Predicted Flow (m^3/min)	29.3	51.6	73.8	96.1
	Prediction Interval (m^3/min)	7.9	7.7	7.7	8.1
	Prediction Interval (%)	27.0	14.9	10.5	8.4

This analysis suggests that a single calibration curve for this fan would not be adequate when higher accuracies are warranted. In general, the uncertainties at the lower end of the fan's range are large, which suggests that caution should be used with smaller fan sizes that may be operating at their lower limits. Fortunately this is less common for small fan sizes, but needs to be considered.

5.2.2 76 cm Fan

The data for the 76 cm fan at the same radius at different angles around the fan is shown in Figure 5.9 and Table 5.3. Each dataset is very linear with R^2 values in excess of 0.99 and narrow prediction intervals. The prediction intervals are all less than 15% and in some locations less than 10% throughout the 76 cm fan's range. At the upper end of the fan's range the prediction intervals is better than 5% for all locations.

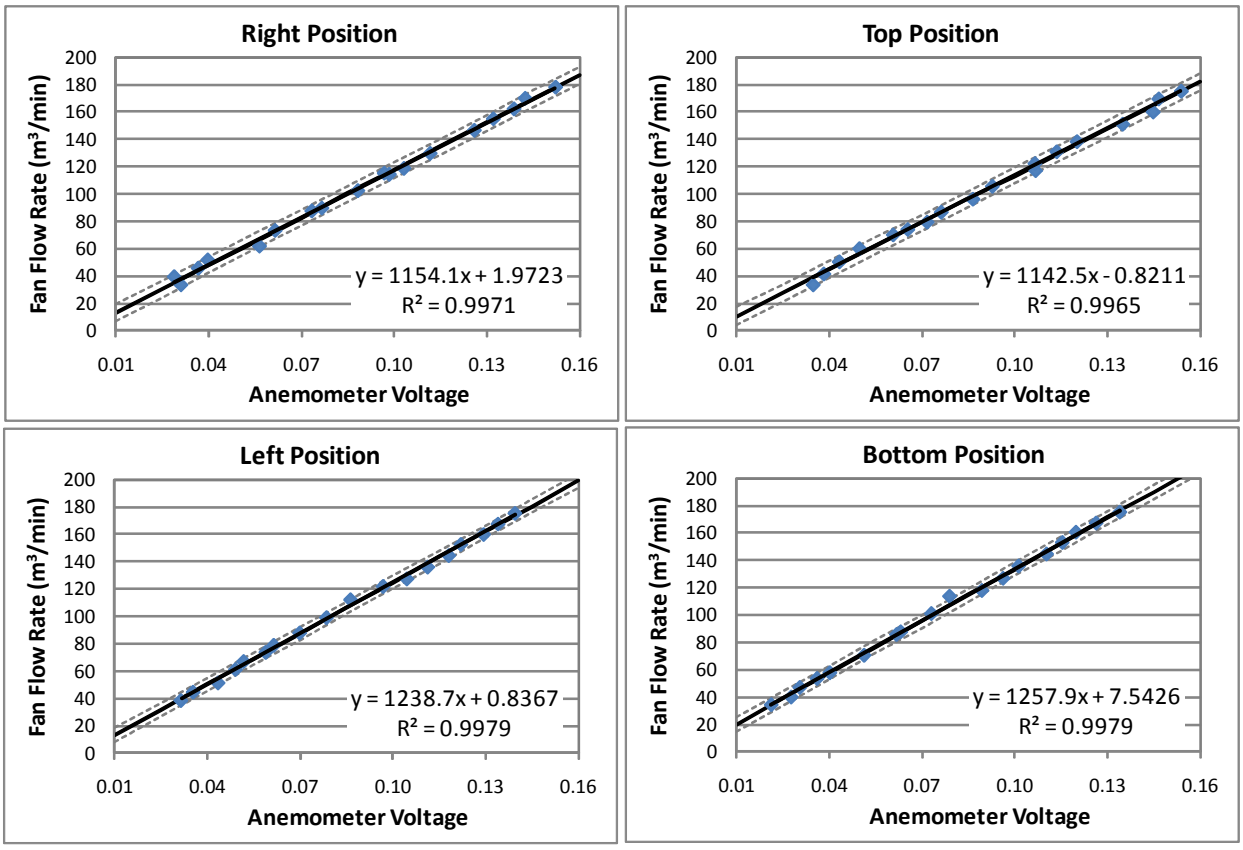

Figure 5.9 Linear regression calibration curves with 95% prediction intervals for the 76 cm fan at each axis.

Table 5.3 Estimates of flow and the corresponding prediction intervals throughout the 76 cm fan's range at each axis.

Position	% of Fan Range / Anemometer Voltage	25 / 0.04	50 / 0.08	75 / 0.12	100 / 0.16
Right	Predicted Flow (m^3/min)	48.1	94.3	140.5	186.6
	Prediction Interval (m^3/min)	5.9	5.7	5.7	6.1
	Prediction Interval (%)	12.2	6.0	4.1	3.3
Top	Predicted Flow (m^3/min)	44.9	90.6	136.3	182.0
	Prediction Interval (m^3/min)	6.2	5.9	6.0	6.4
	Prediction Interval (%)	13.8	6.5	4.4	3.5
Left	Predicted Flow (m^3/min)	50.4	99.9	149.5	199.0
	Prediction Interval (m^3/min)	4.7	4.5	4.7	5.1
	Prediction Interval (%)	9.4	4.5	3.1	2.5
Bottom	Predicted Flow (m^3/min)	57.9	108.2	158.5	208.8
	Prediction Interval (m^3/min)	4.9	4.8	5.0	5.4
	Prediction Interval (%)	8.5	4.4	3.1	2.6
All 4 Combined	Predicted Flow (m^3/min)	51.4	98.2	144.9	191.6
	Prediction Interval (m^3/min)	15.1	14.9	15.0	15.3
	Prediction Interval (%)	29.3	15.2	10.4	8.0

Figure 5.10 shows the datasets for each axis around the 76 cm fan combined into one regression analysis. It is clear that combining the datasets creates a much wider confidence interval that now ranges from 8% at the higher end of the fan's range to nearly 30% at the lower end. The reason is that the datasets doe not overlap well. Particularly the Top and Bottom locations appear to have distinctly different calibrations curves. To verify this, these two regression analysis are overlaid in Figure 5.11. It is clear that the two regression lines are different and, in fact, their prediction intervals do not overlap. This indicates that using data from one location to predict values at another will introduce significant error. This was also shown in Table 5.3, where the combined regression analysis introduced significant uncertainty into the predictions compared to the individual anemometer locations.

The analysis above shows the impact of moving the anemometer around the fan at the same radius, which suggests that significant error could be introduced if the anemometer was installed in a location other than where it was calibrated. The following analysis will study the impact of a small error in placement of the anemometer by moving the anemometer 2 cm in each principal direction around the right side location.

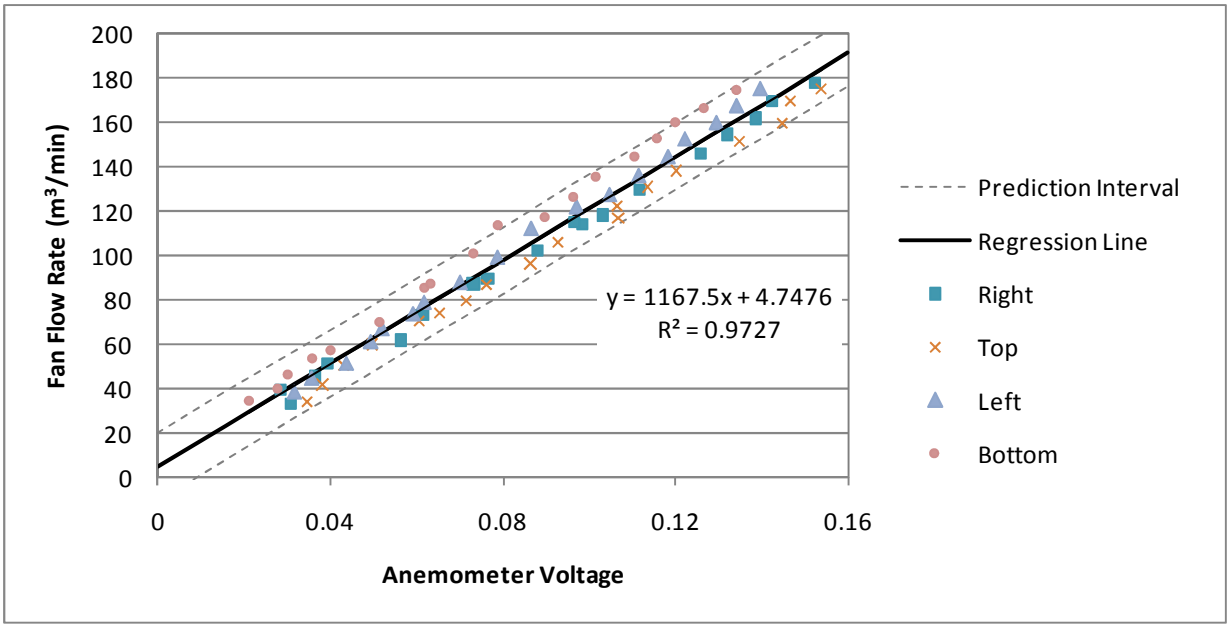

Figure 5.10 Combined regression analysis with 95% prediction intervals for all axes around the 76 cm fan.

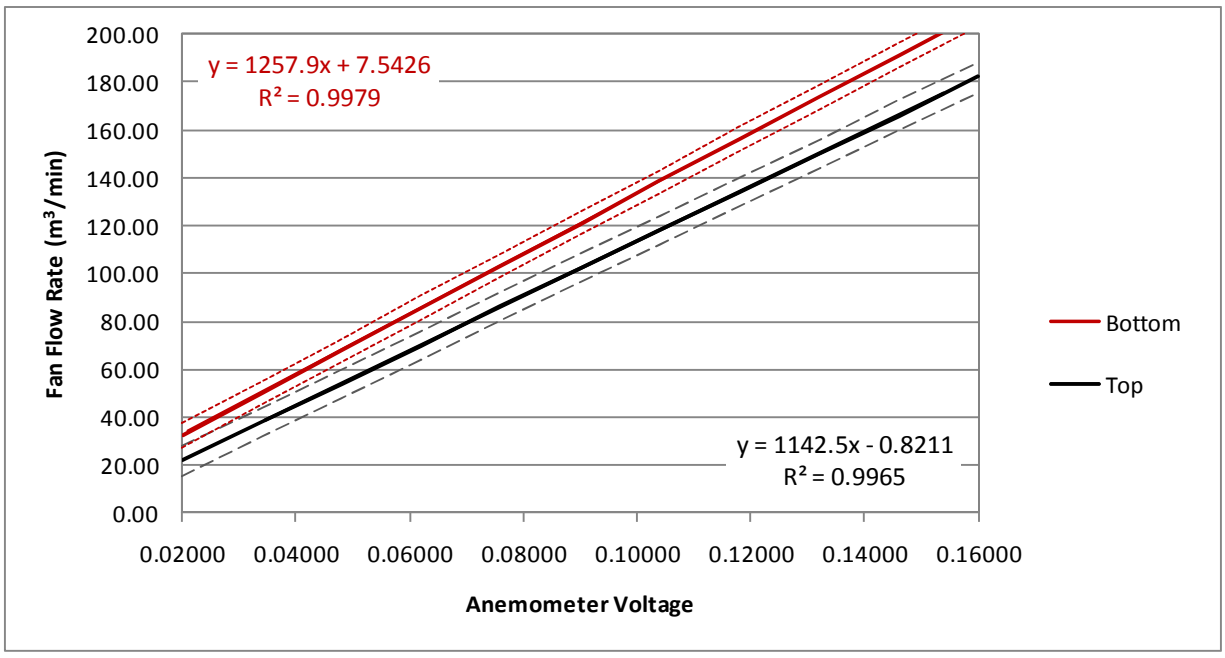

Figure 5.11 Comparison of linear regression curves with 95% prediction intervals for the 76 cm fan at the Top and Bottom Position.

The regression analysis for each variation around the right side can be seen in Figure 5.12 and Table 5.4. Again, each location shows god linearity with R^2 values above 0.99 and narrow prediction intervals. In some cases the prediction intervals are very narrow. All of the anemometer positions show prediction intervals generally less than 15% at the lower end of the fan's capacity and less than 10% at the upper end. Some locations have prediction intervals less than 10% throughout and one had less than 5% throughout. This indicates that the anemometer location could be optimized to obtain the best accuracy.

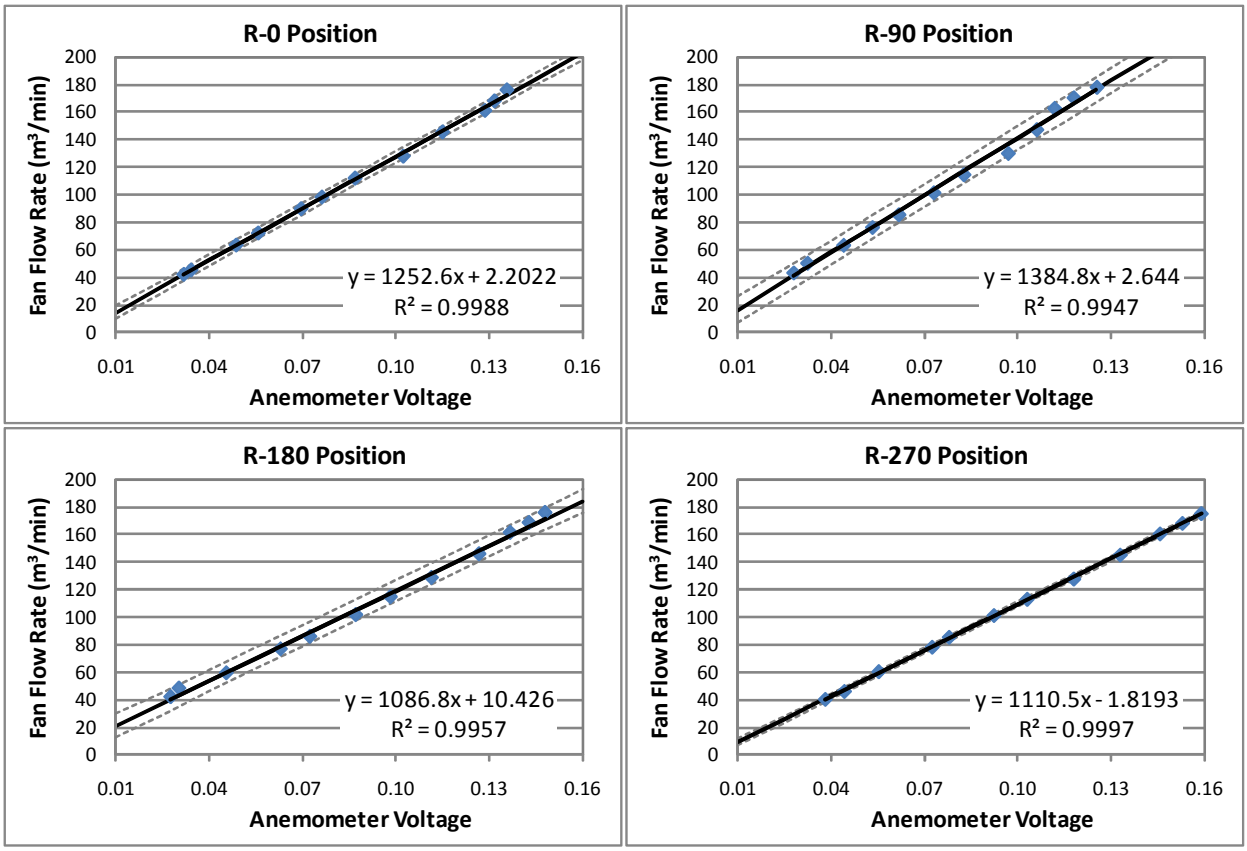

Figure 5.12 Linear regression calibration curves with 95% prediction intervals for the 76 cm fan at with small variations around the Right position.

When the data from each location is combined into a single dataset, the uncertainty increases noticeably, as can be seen in Figure 5.13 and Table 5.4. The prediction interval is now above 10% throughout and reaches nearly 40% at the lower end of the fan's range. Again this is due to each location appearing to have a different calibration curve. This is most noticeable with

the R-90 and R-270 locations. These essentially represent two different radii to the right side of the fan. The R-0, R-180 and Right location have much more overlap. Figure 5.14 shows a comparison of the R-90 and R-180 location regression analyses. It is clear that these two datasets represent different curves, since their prediction intervals only overlap at the lower end of the fan's range.

From this analysis, it would appear that even small variations in placement of the anemometer could introduce significant error into the flow rates predicted by the anemometer. This would indicate that great care is needed in placement of the anemometer or that field calibrations would be required.

Table 5.4 Estimates of flow and the corresponding prediction intervals throughout the 76 cm fan's range.

Position	% of Fan Range / Anemometer Voltage	25 / 0.04	50 / 0.08	75 / 0.12	100 / 0.16
Right	Predicted Flow (m^3/min)	48.9	94.8	140.7	186.5
	Prediction Interval (m^3/min)	6.8	6.4	6.5	7.1
	Prediction Interval (%)	14.0	6.8	4.6	3.8
R-0	Predicted Flow (m^3/min)	52.3	102.4	152.5	202.6
	Prediction Interval (m^3/min)	4.2	4.0	4.1	4.6
	Prediction Interval (%)	8.0	3.9	2.7	2.3
R-90	Predicted Flow (m^3/min)	58.0	113.4	168.8	224.2
	Prediction Interval (m^3/min)	8.8	8.4	8.9	10.2
	Prediction Interval (%)	15.1	7.4	5.3	4.6
R-180	Predicted Flow (m^3/min)	53.9	97.4	140.8	184.3
	Prediction Interval (m^3/min)	8.0	7.6	7.7	8.3
	Prediction Interval (%)	14.8	7.8	5.5	4.5
R-270	Predicted Flow (m^3/min)	42.6	87.0	131.4	175.9
	Prediction Interval (m^3/min)	2.0	1.9	1.9	2.0
	Prediction Interval (%)	4.7	2.2	1.4	1.1
All 5 Variations	Predicted Flow (m^3/min)	53.5	98.8	144.2	189.5
	Prediction Interval (m^3/min)	20.8	20.6	20.7	21.1
	Prediction Interval (%)	39.0	20.8	14.3	11.1

5.2.3 91 cm Fan

Results for the 91 cm fan can be seen in Figure 5.15. There is more variation in this data than with the 76 cm fan data, although the R^2 values are still above 0.95. The variability shows up more in the prediction intervals, which are quite wide for some of the anemometer locations. Table 5.5 shows the magnitude of this variation. Some locations have prediction intervals of over

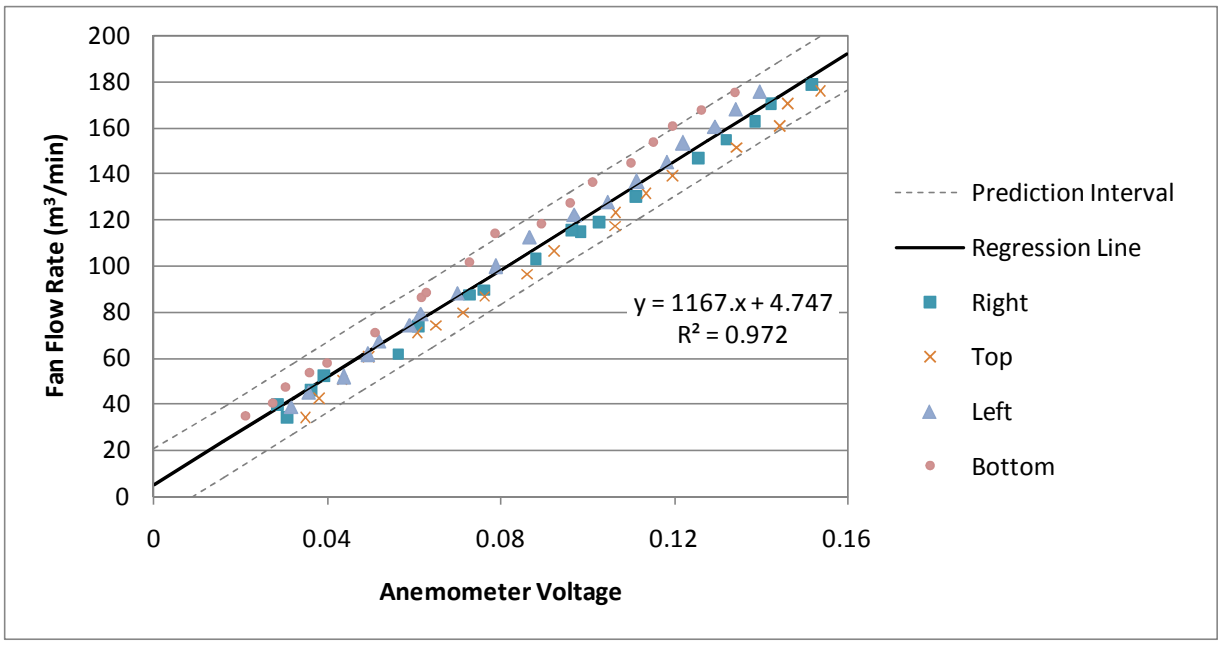

Figure 5.13 Combined regression analysis with 95% prediction intervals for all variations around the 76 cm fan.

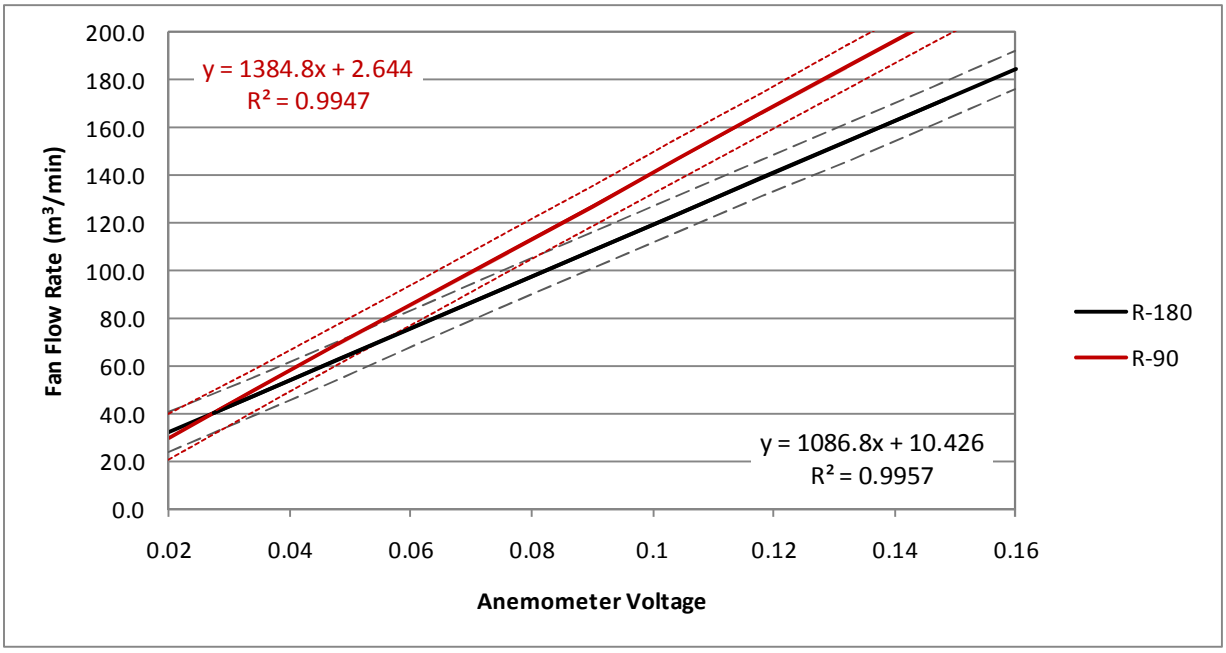

Figure 5.14 Comparison of linear regression curves with 95% prediction intervals for the 76 cm fan at two positions around the right side of the fan.

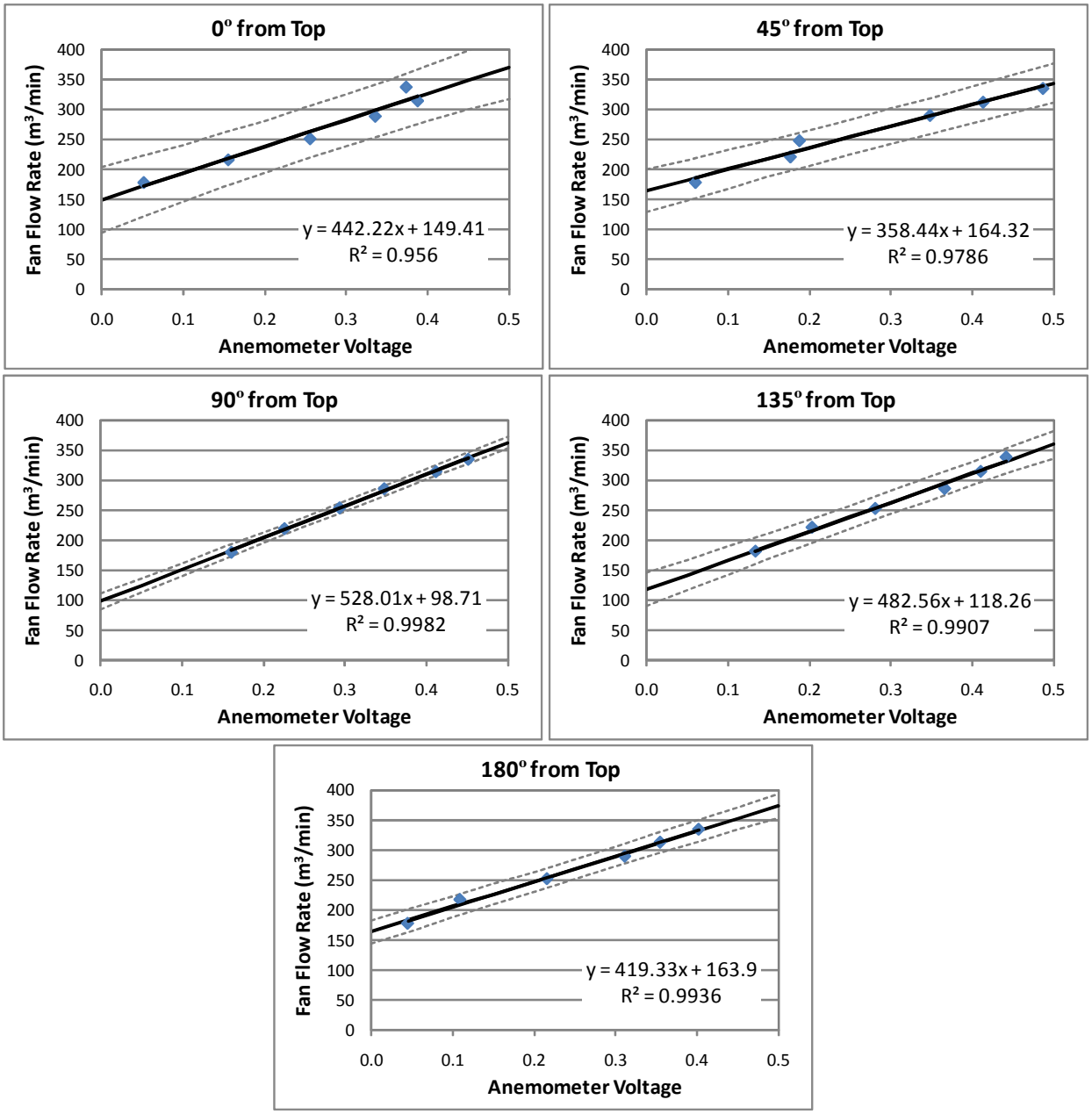

Figure 5.15 Linear regression calibration curves with 95% prediction intervals for the 91 cm fan at various locations.

20%, while others stay below 10% throughout the fan's range. The locations with higher intervals have noticeable outliers which widen the prediction intervals significantly. It appears that more data points would greatly improve the regression analysis at these locations. This spread in the data is also likely due to the fact that this anemometer installation was on the

exhaust side of the fan where there is more turbulence and greater likelihood of interference from external air movement and pressure changes.

The effects of combining the datasets into a single calibration curve can be seen in Figure 5.16 and Table 5.5. Combining the data drops the R^2 values to 0.922 with prediction intervals of 9.6% to 16.6%. Compared to some of the individual locations, this is a significant increase in the level of uncertainty. More importantly, the single regression line will noticeably over predict or under predict certain anemometer locations. Again, this indicates that the anemometer calibration is indeed sensitive to anemometer location.

Table 5.5 Estimates of flow and the corresponding prediction intervals throughout the 91 cm fan's range at various locations.

Position	% of Fan Range / Anemometer Voltage	25 / 0.125	50 / 0.250	75 / 0.375	100 / 0.500
0º From Top	Predicted Flow (m^3/min)	204.7	260.0	315.2	370.5
	Prediction Interval (m^3/min)	46.2	42.7	45.3	53.1
	Prediction Interval (%)	22.6	16.4	14.4	14.3
45º From Top	Predicted Flow (m^3/min)	209.1	253.9	298.7	343.5
	Prediction Interval (m^3/min)	31.1	29.0	29.8	33.2
	Prediction Interval (%)	14.9	11.4	10.0	9.7
90º From Top	Predicted Flow (m^3/min)	164.7	230.7	296.7	362.7
	Prediction Interval (m^3/min)	10.1	8.5	8.5	10.1
	Prediction Interval (%)	6.2	3.7	2.9	2.8
135º From Top	Predicted Flow (m^3/min)	178.6	238.9	299.2	359.5
	Prediction Interval (m^3/min)	22.4	19.4	19.6	22.9
	Prediction Interval (%)	12.5	8.1	6.5	6.4
180º From Top	Predicted Flow (m^3/min)	216.3	268.7	321.1	373.6
	Prediction Interval (m^3/min)	16.9	16.1	17.3	20.2
	Prediction Interval (%)	7.8	6.0	5.4	5.4
All Positions	Predicted Flow (m^3/min)	201.2	252.5	303.9	355.2
	Prediction Interval (m^3/min)	33.4	32.6	32.9	34.1
	Prediction Interval (%)	16.6	12.9	10.8	9.6

5.3 Conclusions

The results discussed above, show that a single vane anemometer can be used to accurately predict fan flow rates for a variety of fan ranges. When properly installed and calibrated the accuracy can be better than 5%. However, the validity of the calibration is highly sensitive to location. It should be assumed that using lab derived calibration curves for field installations is likely to introduce potentially significant errors. In this study the uncertainty introduced by even

small variations in installation could be three to four times as much as when properly installed and calibrated.

Generally speaking, the prediction intervals were widest at lower flow rates and decreased as the flows increased. At best, the accuracy could be brought to within 5 to 10% with proper installation and calibration. This was most difficult for the 45 cm fan, which consistently showed the widest prediction intervals. Most likely, this was due to relatively low flow rate of the fan, although the physical limitations of the installation may have contributed as well.

This study did not seek to conduct field tests to verify performance. Nor did it seek to simulate interferences often encountered in the field. Dust, moisture and other environmental variables are likely to alter the performance and calibration of these anemometers. This will be especially true for situations that require installation outside of the barn on the exhaust side of the fan. Here ice and rain can impact, if not prevent, performance. It is also possible that ambient air movement is likely to have some impact. These issues need to be studied further to determine the long term usefulness of these anemometers for field use.

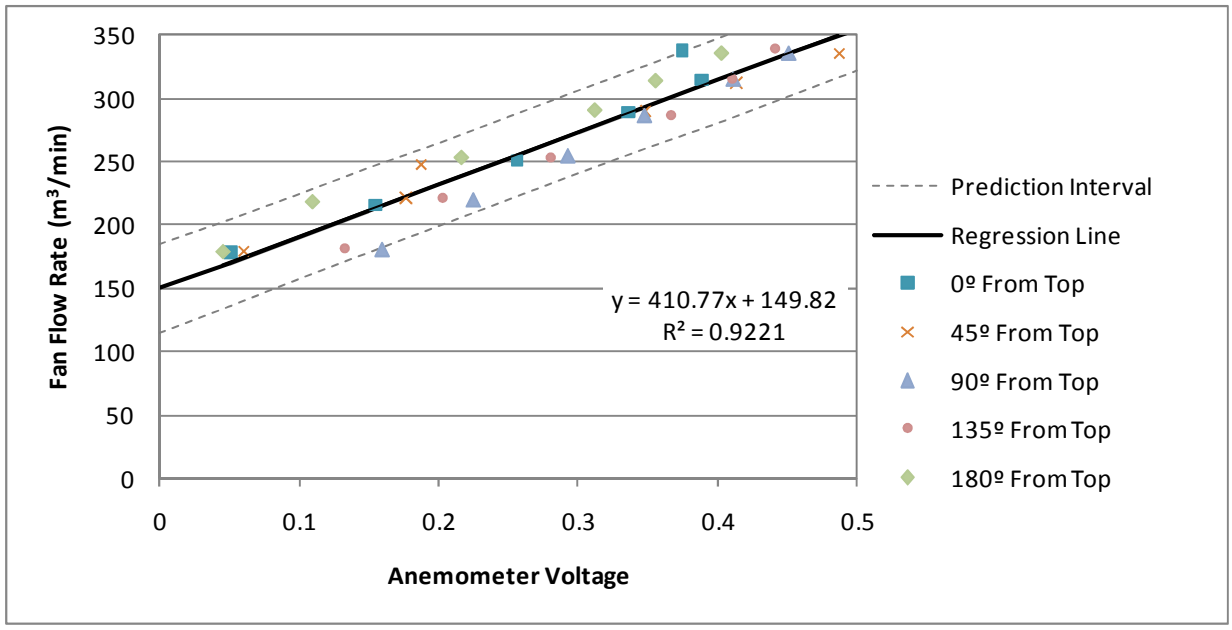

Figure 5.16 Combined regression analysis with 95% prediction intervals for various locations around the 91 cm fan.

Regardless of long term durability, field calibration should be used to obtain maximum accuracy. Even under the laboratory conditions used in this study, the location of the anemometer was critical to its calibration and accuracy. Although general curves could be developed for a fan, the accuracy will be substantially reduced. Without field verification, the accuracy will not be known with confidence. This field calibration would likely be conducted using an instrument like the FAN, which could be used to conduct an entire calibration, or at least make adjustments to the laboratory calibration curve. Determining a reliable field calibration procedure should be completed before relying on these instruments for flow measurement.

CHAPTER SIX: **CONCLUSIONS AND RECOMMENDATIONS**

The studies conducted here sought to answer a number of questions concerning the methodologies used to determine particulate emission rates from animal buildings. While a number of questions were answered, many more were raised. This is common in research and is a necessary step in the process. The following sections summarize the findings of each study and where to go from this point considering what was learned during this research.

6.1 TSP Sampling

As shown in Chapters 2 and 3, sampling of TSP can be difficult. In fact, the very definition of "Total Suspended Particulates," is at best vague. The isokinetic sampling nozzles appeared to function well and matched modeled results well, once a number of potential errors and biases were removed. The results only highlighted the difficulty of sampling larger particles. Even under isokinetic conditions, the gravitational and other losses quickly dropped the efficiency of particles over 10 μm, making it very difficult to capture a representative sample of the larger particles. Considering the size of the particles measured in Chapter 4, these errors could substantially misrepresent what is considered TSP. Chapter 3 also highlighted potential problems with misalignment and improper matching of velocities.

Considering these results, we should ask: Do we really care about TSP, or should we focus our efforts on a more easily defined set of particles? This is a question that is not easily answered since each researcher and agency has a different interest and agenda.

The USEPA has already shifted away from TSP for most industries. It is generally mentioned but not actively pursued. For over 20 years now PM-10 has been of greater interest and for about a decade PM-2.5. The EPA is actively studying particles even smaller. The reason for this is that the smaller particles are responsible for the majority of health effects since they are more easily inhaled and can penetrate further into the respiratory system.

Although from a health effects and regulatory perspective the emphasis should be on PM-10 and smaller, there will undoubtedly continue to be reasons for sampling TSP, or at least particles larger than PM-10. This can be particularly true when considering transport of odors and disease as well as general nuisance conditions that can be caused by larger particles. As shown in Chapters 2 and 3, in the real world the sampling efficiency deviates significantly as the

particle size increases above PM-10. This makes development of samplers very difficult in this range.

Chapters 2 and 3 detail the modeling that could be used to design and optimize a sampling method for collecting TSP or at least larger particles. The easiest method may be to design a sampler with a known cutpoint. Based on the results of the particle size measurements in Chapter 4, it would appear that a cutpoint of 30 μm would allow for the capture of over 90% of the particles in the buildings tested here.

The modeling results in Chapter 3 showed that such a cutpoint would be very shallow. This means a considerable number of larger particles would end up being sampled. Maybe more importantly, it also means that a considerable number of smaller particles would not be sampled. This error can be significant for particles with a distribution centered near the cutpoint of the sampler.

Another potential use of the models could be to design a sampling system that can correct for the inherent sampling errors. This process would be similar to the process used for studying the sampler performance in Chapter 3. Measurements of a number of parameters could be used to estimate the sampling efficiency at each particle size and then adjust the mass concentration accordingly. Such a method would rely on many measurements and models, each with their own inaccuracies.

6.2 Particle Size

Although parameters such as TSP, PM-10 and PM-2.5 are useful for regulatory and reporting purposes, they are fairly limiting from a scientific and design perspective. As discussed in Chapter 2 there are a number of methods for measuring particle size. Several of the more promising and available methods were tested and the results discussed in Chapter 4.

Again, there are few definitive answers because the actual particle sizes and sampler performance are fairly complex. Generally speaking the samplers performed as expected and the relative performance of one sampler compared to another could generally be explained by the literature and a theoretical analysis. Despite this, it could not be said that any of the samplers gave the “correct” answer.

One thing that was very evident is that the time of flight instruments (TOF), such as the APS and the Aerosizer, performed generally well but were not suited for field use. They are very

sensitive electronic devices that should not be routinely used in animal environments. Although it may be possible to make the electronics more robust, there is an additional issue associated with the sampling efficiency. Both devices had problems with sampling particles more than about 10 μm. This problem was improved with the addition of a higher flow inlet and flow splitting device. More testing is needed to determine the effectiveness of this method.

The Coulter has shown great promise in that it is able to quickly and easily analyze large quantities of samples that could be collected simultaneously. It can be left in the lab while fairly inexpensive samplers collect samples from numerous locations. There are questions of its accuracy since it is unable to account for particle shape and resistance to fluid flow.

Future research should focus on a sampler or sampling method that allows for the capture of samples that can be brought back to the lab and analyzed with almost a number of particle sizing devices. This is essentially what was done with the Coulter samples. They were collected on Teflon membrane filters and then brought back to the lab for analysis.

By developing a method to re-aerosolize the samples it would then be possible to analyze the samples with TOF and other *in situ* methods in a more controlled laboratory environment. Some instruments currently exist that do this, but research is needed to ensure that they perform well and provide a representative sample. Of course, in-situ measurement with the real-time instruments discussed here could continue for occasional use, but not routine sampling.

6.3 Flow Rate Measurement

The single vane anemometer tested in Chapter 5 performed quite well in a laboratory setting. It is clear that field calibration would be required using an instrument such as the FANS discussed in Chapter 2. This is likely to be true of any single point continuous measure of air flow. In addition, field testing is needed to fully evaluate the effect of environmental variables on the accuracy of the anemometers. This method does have potential when continuous measurement is needed due to variable flow scenarios or verification of fan operation.

6.4 Summary of Recommendations

As discussed in Section 6.1, the agricultural community needs to establish a functional definition of TSP. With this, a proper sampler can be developed. This sampling method is likely to include a sampler with a well defined cut-point, possibly near that of the traditional, albeit

poorly defined, EPA high volume TSP samplers. A process may need to be included for correcting for poor particle sampling efficiency that is inherent in sampling particles above 10 to 15 μm.

None of the instruments used in this study performed exceptionally well in animal buildings, either due to physical limitations, restrictive size range limits or questionable performance. Some of these issues could be addressed through the development of system that allows collection of the particles in the field for analysis in the laboratory. This would be similar to the Coulter system, but flexible enough to use other instruments for particle size analysis. With such a system it would become feasible to collect many samples simultaneously and to be analyzed by multiple instruments. This could lead to a much better understanding of particle size, shape and make-up. To do this, a sampling media and matching laboratory equipment will be needed that will allow for aerosolisation of the collected particulate matter. Future research should focus on the existing techniques and their effectiveness as well as development of new methods.

As discussed in Chapter 1, obtaining a measurement of particle concentration and size is not sufficient for determining emission rates. A single vane anemometer, field calibrated with the FANS analyzer, shows potential for use in continuous measurement of fan flow rate. This is especially true for variable speed fans where the FANS method may not be adequate. Future research should focus on the accuracy and durability of these anemometers in various environments over extended periods of time as well as developing a field calibration procedure using the FANS.

REFERENCES

ACGIH. 2001. *Air Sampling Instruments, for evaluation of atmospheric contaminants*. 9th ed. Cincinnati, OH: ACGIH

AMCA. 1999. Laboratory Methods of Testing Fans for Aerodynamic Performance Rating. *ANSI/AMCA Standard 210-99*.

Baron, P.A. 2001. *Aerosol Calculator*. Excel spreadsheets.

Baron, P.A., and K. Willeke. 2001. *Aerosol Measurement: Principle, Techniques, and Applications*. New York, NY: John Wiley and Sons.

Berckmans, D., P.Vandenbroeck, and V. Goedseels. 1991. Sensor for Continuous Measurement of the Ventilation Rate in Livestock Buildings. *Indoor Air* 1(3): 323-336.

Bottcher, R.W. 2001. An Environmental Nuisance: Odor Concentrated and Transported by Dust. *Chem. Senses* 26: 327-331.

Brem, B., and Y. Zhang (2008). Development of an Isokinetic Sampler for Variable Flow Velocities. ASABE International Livestock Environment VIII, 31 August – 4 September 2008, Iguassu Falls, Brazil. Paper 701P0408.

Burns, R.T., H. Xin, R. Gates and S. Hoff. 2005. *Total Suspended Particulate, PM10, PM2.5, Hydrogen Sulfide and Hydrocarbon National Consent Agreement Emissions Determination from Broiler Production Systems*. Ongoing research funded by Tyson Foods. 2005 -2007.

Burns, R., H. Xin, R. Gates, H. Li, S. Hoff, L. Moody, D. Overhults and J. Earnest. 2007. *Ammonia Emissions Determination from Broiler Production Systems: Final Report*. Funded by Tyson Foods.

Casey, K.D., S.E. Ford, J.W. McClure, Y. Zhang, and R.S. Gates. 2007. Determining fan performance using FANS: an investigation of performance impacts. *Applied Eng. in Agric.* 23(3): 333-338.

Casey, K.D., R.S. Gates, E.F. Wheeler, H. Xin, Y. Liang, A. Pescatore, and M. Ford. 2008. On-farm fan performance: implications for ventilation and operating cost. *Journal of Applied Poultry Research* 17(2): 283-295.

Chang, C.W., H. Chung, and C.F. Huang, J. Su. 2001. Exposure assessment to airborne endotoxin, dust ammonia, hydrogen sulfide and carbon dioxide in open style swine houses. *Ann. Occup. Hyg.* 45: 457-465.

Chen, Y.C., E.M. Barber, and Y.H. Zhang. 1998. Sampling efficiency of the TSI aerodynamic particle sizer. *Instrumentation Science and Technology* 26(4): 363-373.

Cheng, Y.S., E.B. Barr, I.A. Marshall, and J.P. Mitchell. 1993. Calibration and Performance of an API Aerosizer. *J. Aerosol Sci.* 24(4): 501-514.

Chung, K.Y.K., and J. Thompson. 1989. Coulter vs. APS – A Comparative Study. *J. of Aerosol Science* 20(8): 1517-1520.

Cohen, B.S., and C.S. McCammon, Jr. 2001. *Air Sampling Instruments: For evaluation of atmospheric contaminants*. Cincinnati, OH: ACGIH.

Davies, C.N. 1968. The entry of aerosols into sampling tubes and heads. *J. Phys. D: Appl. Phys.* 1(7): 921-932

Demmers, T.G.M., L.R. Burgess, J.L. Short, V.R. Phillips, J.A. Clark and C.M. Wathes. 1998. First experiences with methods to measure ammonia emissions from naturally ventilated cattle buildings in the UK. *Atmospheric Environment* 32(3): 285-293.

Demmers, T.G.M., L.R. Burgess, J.L. Short, V.R. Phillips, J.A. Clark and C.M. Wathes. 1999. Ammonia emissions from two mechanically ventilated UK livestock buildings. *Atmospheric Environment* 33: 217-227.

Demmers, T.G.M., L.R. Burgess, V.R. Phillips, J.A. Clark and C.M. Wathes. 2000. Assessment of techniques for measuring the ventilation rate, using an experimental building section. *Journal of Agricultural Engineering Research* 76: 71-81.

Demmers, T.G.M., V.R. Phillips, L.S. Short, L.R. Burgess, R.P. Hoxey, and C.M. Wathes. 2001. Validation of ventilation rate measurement methods and the ammonia emission from naturally ventilated dairy and beef buildings in the United Kingdom. *Journal of Agricultural Engineering Research* 79: 107-116.

Demmers, T.G.M., C.M. Wathes, P.A. Richards, N. Teer, L.L. Taylor, V. Bland, J. Goodman, D. Armstrong, D. Chennells, S.H. Done, and J. Hartung. 2003. A Facility for controlled exposure of pigs to airborne dusts and gases. *Biosystems Engineering* 84(2): 217-230.

Gates, R.S., H. Xin, and E.F. Wheeler. 2001. *Reducing Ammonia Emissions from Poultry Houses by Enhanced Manure and Diet Management*. USDA IFAFS.

Gates, R.S., K. D. Casey, H. Xin, E.F. Wheeler, and J.D. Simmons. 2004. Fan assessment numeration system (FANS) design and calibration specifications. *Transactions of the ASAE* 47(5): 1709-1715.

Görner, P., R. Wrobel, V. Micka, V. Skoda, J. Denis, and J.-F. Fabriés. 2001. Study of fifteen respirable aerosol samplers used in occupational hygiene. *Ann Occup Hyg.* 45(1): 43-54.

Grinshpun, S., K. Willeke, and S. Kalatoor. 1993. A General Equation for Aerosol Aspiration by Thin-Walled Sampling Probes in Calm and Moving Air. *Atmospheric Environment*. 27(A): 1459-1470.

Grinshpun, S., K. Willeke, and S. Kalatoor. 1994. Corrigendum. *Atmospheric Environment* 28: 375.

Harral, B.B., and C.R. Boone. 1997. Comparison of Predicted and Measured Air Flow Patterns in a Mechanically Ventilated Livestock Building without Animals. *Journal of Agricultural Engineering Research* 66(3): 221-228.

Heber, A.J. 2003. Air emission measurements at livestock houses. *Resource* 10(4): 7-8.

Heber, A.J., J.-Q. Ni, T.-T. Lim, A.M. Schmidt, J.A. Koziel, P.C. Tao, D.B. Beasley, S.J. Hoff, R.E. Nicolai, L.D. Jacobson, and Y. Zhang. 2006a. Quality Assured Measurements of

Animal Building Emissions: Gas Concentrations. *J. Air & Waste Manage. Assoc.* 56: 1472-1483.

Heber, A.J., T.-T. Lim, J.-Q. Ni, P.C. Tao, A.M. Schmidt, J.A. Koziel, S.J. Hoff, L.D. Jacobson, Y. Zhang, and G.B. Baughman. 2006b. Quality Assured Measurements of Animal Building Emissions: Particulate Matter Concentrations. *J. Air & Waste Manage. Assoc.* 56: 1642-1648.

Hinds, W.C. 1999 *Aerosol Technology: Properties, Behavior, and Measurement of Airborne Particles*. New York, NY: John Wiley and Sons.

Hinz, T., and S. Linke. 1998. A Comprehensive Experimental Study of Aerial Pollutants in and Emissions from Livestock Buildings. Part 1: Methods. *J. Agric. Engng Res.* 70**:** 111-118.

Hinz, T., and S. Linke. 1998. A Comprehensive Experimental Study of Aerial Pollutants in and Emissions from Livestock Buildings. Part 2: Results. *J. Agric. Engng Res.* 70**:** 119-129.

Jacobson, L.D., D.R. Schmidt, J.K. Lake, and V.J. Johnson. 2003. Ammonia, Hydrogen Sulfide, Odor, and PM0 Emissions From Deep-Bedded Hoop And Curtain-Sided Pig Finishing Barns In Minnesota. *Air Pollution from Agricultural Operations III, Proceedings of the 12-15 October 2003 Conference.* St. Joseph, MI: ASAE.

Jerez, S.B., Y. Zhang, Y., J. McClure, L. Jacobson, A. Heber, S. Hoff, J. Koziel, and D.B. Beasley. 2006. Comparison of measured total suspended particulate matter concentration using tapered element oscillating microbalance and a TSP sampler. *J. Air & Waste Management Association* 56: 261-270.

Lacey, R.E., J.S. Redwine, and C.B. Parnell. 2003. Particulate matter and ammonia emission factors for tunnel-ventilated broiler production houses in the Southern US. *Transactions of the ASAE* 46(4): 1203-1214.

Li, S.N., D.A. Lundgren, and D. Rovell-Rixx. 2000. Evaluation of six inhalable aerosol samplers. *Am Ind Hyg Assoc J.* 61: 506-16.

Maghirang, R.G., Y. Liu, and D.S. Chung. 1998. Evaluation of a Freely Rotating Impeller to Measure Fan Airflow Rates in Livestock Buildings. *Transactions of the ASAE* 41(3): 819-824.

McFarland, A.J., C.A. Ortiz, and C.E. Rodes. 1980. Characterization of Sampling Systems. *Proceedings of the Technical Basis for A Size Specific Particulate Standard*. Pittsburgh, PA: Air Pollution Control Assoc.

National Research Council of the National Academies. 2002. *The Scientific Basis for Estimating Air Emissions from Animal Feeding Operations, Interim Report.* Washington D.C.: National Academy Press.

National Research Council of the National Academies. 2003. *Air Emissions From Animal Feeding Operations: Current Knowledge, Future Needs.* Washington D.C.: National Academy Press.

Parnell, C.B., G.A. Niles, and R.D. Rutherford. 1986. Cotton Dust Concentrations and Particle-Size Distributions Associated with Genotypes. *Environmental Health Perspectives* 66: 167-172.

Parnell, C.B., D.D. Jones, R.D. Rutherford, and K.J. Goforth. 1986. Physical-Properties of 5 Grain Dust Types. *Environmental Health Perspectives* 66: 183-188.

Peters, T.M., and D. Leith. 2003. Concentration measurement and counting efficiency of the aerodynamic particle sizer 3321. *Journal of Aerosol Science* 34(5): 627-634.

Phillips, V.R., M.R. Holden, R.W. Sneath, J.L. Short, R.P. White, J. Hartung, J. Seedorf, M. Schröder, K.H. Linkert, S. Pedersen, H. Takai, J.O. Johnsen, P.W. G. Groot Koerkamp, G.H. Uenk, R. Scholtens, J.H.M. Metz, and C.M. Wathes. 1998. The development of robust methods for measuring concentrations and emission rates of gaseous and particulate air pollutants in livestock buildings. *J. Agric. Eng. Res.* 70: 11-24.

Schneider, F.E., T. Engelhardt, and P.H. Wieser. 2001. Characterization of Aerosol Particles from Animal Husbandry with Single Particle Analytic Techniques. ASAE Paper Number: 01-4010. St. Joseph, MI: ASAE.

Seedorf, J., J. Hartung, M. Schroder, K.H. Linkert, V.R. Phillips, M.R. Holden, R.W. Sneath, J. L. Short, R.P. White, S. Pedersen, H. Takai, J.O. Johnsen, J.H.M. Metz, P.W G. Groot Koerkamp, G.H. Uenk, C.M. Wathes. 1998. Concentrations and emissions of airborne endotoxins and microorganisms in livestock buildings in Northern Europe. *J. Agric. Eng. Res.* 70:97–109.

Shaw, B.W., P.P. Buharivala, C.B. Parnell, and M.A. Demny. 1998. Emission factors for grain receiving and feed loading operations at feed mills. *Transactions of the ASAE* 41(3):757-765.

Sweeten, J.B., C.B. Parnell, R.S. Etheredge, and D. Osborne. 1988. Dust Emissions in Cattle Feedlots (Reprinted from American-Society Agricultural Engineers. *Veterinary Clinics of North America-Food Animal Practice* 4(3): 557-578.

Sweeten, J.M., C.B. Parnell, B.W. Shaw, and B.W. Auvermann. 1998. Particle size distribution of cattle feedlot dust emission. *Transactions of the ASAE* 41(5): 1477-1481.

H. Takai, S. Pedersen, J.O. Johnsen, J.H.M. Metz, P.W.G. Groot Koerkamp, G.H. Uenk, V.R. Phillips, M.R. Holden, R.W. Sneath, J.L. Short, R.P. White, J. Hartung, J. Seedorf, M. Schroder, K.H. Linkert, and C.M. Wathes. 1998. Concentrations and emissions of airborne dust in livestock buildings in northern. *Europe. J. agric. Engng Res.* 70: 59-77.

US CFR 1983. *Reference Method for the Determination of Suspended Particulate Matter in the Atmosphere (High-Volume Method)*. 40 CFR. Part 50, Appendix B.

US EPA. Method 201A - Determination of PM10 Emissions (Constant Sampling Procedure). EMTIC TM-201A.

US FR. 2005. *Animal Feeding Operations Consent Agreement and Final Order*. Federal Register Vol 70, No 19, Page 4957-4977, January 31, 2005.

Vincent, J.H. 1989. *Aerosol Sampling Science and Practice*. New York: John Wiley & Sons

Wang, L., C.B. Parnell, B.W. Shaw, R.E. Lacey, M.D. Buser, L.B. Goodrich, and S.C. Capareda. 2005. Correcting PM10 over-sampling problems for agricultural particulate matter emissions: preliminary study. *Trans. ASAE*. 48(2): 749-755.

Wang, X., and Y. Zhang. 1999. Development of a Critical AirFlow Venturi for Air Sampling. *Journal of Agricultural Engineering Research* 73(3): 257-264.

C.M. Wathes, V.R. Phillips, M.R. Holden, R.W. Sneath, J.L. Short, R.P.P. White, J. Hartung, J. Seedorf, M. Schröder, K.H. Linkert, S. Pedersen, H. Takai, J.O. Johnsen, P.W.G. Groot Koerkamp, G.H. Uenk, J.H.M. Metz, T. Hinz, V. Caspary and S. Linke. 1998. Emissions of aerial pollutants in livestock buildings in northern Europe: Overview of a multinational project. *J. Agric. Eng. Res*. 70(1): 3–9.

Wathes, C.M., M.R. Holden, R.W. Sneath, R.P. White, and V.R. Phillips. 1997. Concentrations and Emission Rates of Aerial Ammonia, Nitrous Oxide, Methane, Carbon Dioxide, Dust and Endotoxin in Broiler and Layer Houses. *British Poultry Science* 38(1): 14-28.

Wedding, J.B., A.R. McFarland, and J.E. Cermak. 1977. Large particle collection characteristics of ambient aerosol samplers. *Environmental Science and Technology* 11(4): 387-390.